

ABSTRACT

JIANXUN, CUI. Self-folding of Engineering Materials Actuated by Heat Shrinkable Polymers. (Under the direction of Dr. Yong Zhu).

Shape shifting is an important process for both natural and artificial structures. Animals and plants need to change their shape as a response to environmental stimuli. Some man-made tools also change their shape during the usage. The dissertation focuses on the transformation from 2D sheets into 3D structures. The idea is from origami, an ancient art of paper folding. Various 3D structures can be obtained by folding 2D sheets along pre-designed crease patterns. Besides fabricating 3D structures, origami can be used to design deployable structures and tailor the mechanical behavior of metamaterial structures. In the dissertation, we developed multiple ways to actuate the folding, which are divided into three approaches.

In the first approach, folding is caused by local bending, which is induced by strain gradient across the thickness. We demonstrated the self-folding of a heat shrinkable polymer sheet using a local Joule heater. Strain gradient is induced by unsymmetrical heating. The folding is influenced by thermal force and mechanical force. By modifying the interface between heater and polymer sheet, the folding direction can be changed. We also demonstrated the self-folding of aluminum foil actuated by a local bimorph (heat shrinkable polymer sheet & aluminum foil). For aluminum foil with isotropic stiffness, folding direction is determined by the orientation of the bimorph strip. We used topographical features to enable anisotropic bending stiffness in the aluminum foil, which can be used to tune the folding direction.

In the second approach, folding occurs as a result of compressive buckling, which is localized at the creases due to their lower stiffness. The heat shrinkable polymer sheet was attached to the pre-designed 2D precursor. Upon heating, the polymer sheet shrinks equi-

biaxially. This compresses the 2D precursor and causes the buckling. The buckling deformation is guided by the crease patterns. Various 3D origami structures were folded. Their application in crash energy absorber and thermal insulator were demonstrated.

In the third approach, folding occurs as a result of changing Gaussian curvature. By embedding origami structures into the flat heat shrinkable polymer sheets, the shrinkage of the polymer is constrained and becomes non-uniform. The Gaussian curvature of the composite sheet is changed due to the non-uniform shrinkage, resulting in shape morphing of the composite sheet. The shape morphing is guided by the origami mechanism.

Those geometric rules developed in this dissertation are independent of length scale. The actuating component can be replaced by other materials under other stimuli. The shape transformation model developed in the dissertation can be used to design smart structures which can respond to environmental change. It can also be used to design actuators that can achieve different modes of movements.

© Copyright 2017 by Jianxun Cui

All Rights Reserved

Self-folding of Engineering Materials Actuated by Heat Shrinkable Polymers

by
Jianxun Cui

A dissertation submitted to the Graduate Faculty of
North Carolina State University
in partial fulfillment of the
requirements for the degree of
Doctor of Philosophy

Mechanical Engineering

Raleigh, North Carolina

2017

APPROVED BY:

Yong Zhu
Committee Chair

Jan Genzer

Xiaoning Jiang

Yun Jing

DEDICATION

To my parents, Jiqun Cui and Jiefang Zhang, and my younger brother Jianhua Cui.

BIOGRAPHY

Jianxun Cui is from Henan, China. He obtained his Bachelor's and Master's degree in materials science from Harbin Institute of Technology. After that he joined Dr. Yong Zhu's lab to pursue PhD degree. He is intrigued by the shape shifting phenomenon in plants and motions in animals. His research is about transforming 2D sheets into 3D structures and 2D patterns into 3D patterns.

ACKNOWLEDGMENTS

I would like to thank my PhD advisor, Dr. Yong Zhu, for his guidance and support through my PhD career. I also thank all the colleagues in Dr. Zhu's group: Dr. Guangming Cheng, Dr. Jimmy Chang, Dr. Shanshan Yao, Dr. Qijin Huang, Chengjun Li, Zheng Cui, Felipe Robles Poblete and John Adam. Thank you for the help on my experiments.

Thank Professors Xiaoning Jiang, Yun Jing and Jan Genzer for kindly serving as my Committee members. Thank you for the comments and suggestions, which help greatly to improve the dissertation.

Thank all the members in the EFRI group. Thank Prof. Genzer for organizing the monthly meetings, which are very inspiring and informative. Thanks to Prof. Michael Dickey, Prof. Susan Brandies, Prof. Alan Russell, Sally Van Gorder, Dr. Ying Liu, Dr. Duncan Davis, Dr. Russell Mailen and Amber Hubbard for the helpful discussions. I acknowledge National Science Foundation for supporting this work under the NSF EFRI program (Grant no. 1240438).

Finally, I want to thank my girlfriend, Hongxia, who helps and encourages me a lot.

TABLE OF CONTENTS

LIST OF TABLES	viii
LIST OF FIGURES	ix
CHAPTER 1 Introduction.....	1
1.1 Shape transformation and its applications	1
1.1.1 Shape transformation in soft systems	1
1.1.2 Shape transformation in rigid systems	2
1.2 Different approaches to achieve shape transformation	4
1.2.1 Shape transformation induced by bending.....	5
1.2.2 Shape changing in the form of buckling	5
1.2.3 Shape changing induced by change Gaussian curvature	7
References	9
CHAPTER 2 Controlling the self-folding of a polymer sheet using a local heater.....	14
2.1 Introduction.....	14
2.2 Materials and Methods.....	16
2.2.1 Materials	16
2.2.2 Sample preparation	16
2.2.3 Folding experiment	17
2.3 Results and Discussions	17
2.3.1 Folding mechanism.....	17
2.3.2 Folding without constraint	21
2.3.3 Folding with partial constraint	24
2.3.4 Folding with total constraint	25
2.3.5 Time response of folding	26
2.3.6 Comparison with other folding methods for SMP.....	29
2.3.7 Folded structures	29
2.4 Conclusion	32
Supplementary Information (SI).....	33
2.S1 Failure of AgNW thin film directly coated on PS substrate.....	33
2.S2 Temperature characterization by IR camera.....	34

2.S3 Folding results without constraint	37
2.S4 Geometric calculation of the heater climbing up process.....	38
2.S5 Folding with partial constraint.....	41
2.S6 Finite element modeling	43
2.S7 Folding results in the case of total constraint	46
2.S8 Bimorph model analysis	47
References.....	50
CHAPTER 3 Self-folding of Al foil with local bimorph actuator.....	53
3.1 Introduction.....	53
3.2 Materials and Methods.....	54
3.3 Results and Discussions	55
3.4 Conclusion	66
Supplementary Information (SI).....	67
3.S1 Fold polyimide sheet with a bilayer actuator.....	67
References.....	68
CHAPTER 4 Pop up assembly of 3D structures via compressive buckling.....	70
4.1 Introduction.....	70
4.2 Materials and Methods.....	71
4.2.1 Materials	71
4.2.2 Pop-up by pushing from outside	72
4.2.3 Pop-up by pulling from inside	72
4.3 Results and Discussions	73
4.3.1. Buckling induced by pushing from outside	73
4.3.2. Buckling induced by pulling from inside.....	81
4.3.3. Application of the cellular structures	90
4.4 Conclusion	92
Supplementary Information (SI).....	93
4.S1 Use slits to tailor the size of perforation after shrinking	93
4.S2 The effect of perforation on strain distribution.....	94
4.S3 Geometric models.....	96

4.S4 Distorted shrinkage of PS and defective structures	100
References:.....	101
CHAPTER 5 Folding 2D sheets by changing their Gaussian curvature	104
5.1 Introduction.....	104
5.2 Materials and Methods.....	106
5.3 Results and Discussions.....	106
5.4 Conclusion	120
Supplementary Information (SI).....	121
5.S1 Calculate the dihedral angle from the sector angles	121
References.....	123

LIST OF TABLES

Table 1.S1 Material properties of PS used in finite element model.....	44
---	----

LIST OF FIGURES

- Figure 2.1** (a) Experimental setup showing the pre-strained PS sheet and the flexible AgNW/PI heater on top. Scale bar: 10 mm. The inset shows the AgNW network (scale bar: 10 μm); (b) Schematic of the cross section A-A in panel (a) and the temperature distribution in PS (according to FEA simulation). In the red area the temperature is above the threshold temperature for shrinkage of PS; (c) Schematic showing the folding geometry and related parameters; (d) Schematics showing the three modes of operation for folding a PS sheet: no constraint, partial constraint and total constraint. 20
- Figure 2.2** Folding results in the case of no constraint. (a) Relationship between inward folding angle and heater width. Insets are side views of the folded structures with 0.5 mm and 2 mm wide heaters; (b) Time response and power input during inward folding with a 2 mm wide heater. Insets show several snapshots during the folding. 23
- Figure 2.3** Deformation of heater in the case of no constraint. Top: top view; middle: side view; bottom: schematic of the cross section from side view. Scale bar: 2 mm. Folding was stopped by turning off the power supply. After taking images, folding was resumed by turning on the power supply. 23
- Figure 2.4** Deformation of heater in the case of partial constraint. Top: top view; middle: side view; bottom: schematic of cross section from side view. Scale bar: 2 mm. 28
- Figure 2.5** Folding results in the case of total constraint. (a) Relationship between folding angle and heater width. Insets are side views of the folded structures with 0.5 mm and 2 mm wide heaters; (b) Time response and power input during outward folding with a 2 mm wide heater. Insets show several snapshots during the folding. 28
- Figure 2.6** Structures folded with the AgNW/PI heaters. (a) Digital numbers (black circles indicate complete outward folding); (b) A cube folded by inward folding (heater was peeled off); (c) A simple sailing boat folded by 180 degrees inward folding (heater was peeled off); (d) A crane folded by inward folding (heater was peeled off). 31
- Figure 2.S1** Failure of an AgNW film heater on PS. (b) High magnification image of the highlighted region in (a). Scale bars: (a) 100 μm ; (b) 20 μm 33
- Figure 2.S2** Characterization of the heater using IR camera. (a) Temperature evolution of the heater at different input powers. (b) IR image of the heater at the corresponding input power of (a). The temperatures shown in (a) were the average temperatures in the area highlighted by the black dash line. A piece of PS without pre-strain was attached below the heater in order to replicate the condition for folding. 35
- Figure 2.S3** IR image of a heater during outward folding. The heater is illustrated by yellow dash line and the PS sheet illustrated by blue dash line. PS sheet folded downwards. 36
- Figure 2.S4** Inward folding with a 0.5 mm wide heater. Scale bar: 2 mm. 37

- Figure 2.S5** Heater morphology during inward folding. (a) Schematics of cross sections of the heater on PS during folding. (b) The chord length and gaps between the heater and PS as a function of folding angle..... 40
- Figure 2.S6** Calculation of the arc from the chord length and central angle of the PS sheet. 40
- Figure 2.S7** Calculation of the arc from chord length and arc length of the heater. 40
- Figure 2.S8** Folding results with a 0.5 mm wide heater under partial constraint. Bare tape was applied on both edges to prevent sliding of the heater. Scale bar: 2 mm. 42
- Figure 2.S9** Heater morphology during folding with bare tape on the left side to prevent sliding of the heater from left side. Scale bar: 2 mm. 42
- Figure 2.S10** Temperature distribution across the PS layer under the heater with different widths (FEA steady state analysis). The heater width is indicated by black line. 44
- Figure 2.S11** Temperature evolution across the PS layer (FEA transient state analysis). 45
- Figure 2.S12** Folding results in the case of total constraint. (a) Inward folding with a 0.5 mm wide heater. (b) Complete outward folding with a 2 mm wide heater. The inset in (a) and (b) shows optical microscopic images of the hinge region. Scale bars: 500 μm 46
- Figure 2.S13** Structure and force diagrams of the bilayer structure. Yellow layer: PI; blue layer: PS. 49
- Figure 3.1** The curling behaviors of PS & Al bilayer sheet. (a) Isolated bilayer structure. (b) Bilayer structure embedded in a large passive sheet. Schematics of the curling process are shown below the optical images. Scale bars: 10 mm. 56
- Figure 3.2** Folding angle caused by the actuating hinge. (a) Schematic of the folding. (b) Folding angle (α) as a function of hinge width (L). Fitting lines are included. 58
- Figure 3.3** Flat origami structures. (a) Schematic showing turning a strip by desired angle. (b) Some letters folded from a strip of Al foil. Left is the crease patten (blue: mountain fold; red: valley fold). (c) Deployment of pre-folded structures. Scale bars: 30 mm. 60
- Figure 3.4** Miura-ori structure. (a) Crease patten (blue: mountain fold; red: valley fold). (b) Optical images of Miura-folded Al foil. (c) Using Miura-folded foil as a bridge. Left: two layers of flat Al foil; right: one layer of Miura-folded Al foil. 62
- Figure 3.5** Curling behavior of pleated Al foil. (a) Schematic of the pleating and Curling process. (b) Pleat lines along the transverse direction. (c) Pleat lines at an angle (45 degrees) to the transverse direction. (d) Pleat lines at an angle (-45 degrees) to the transverse direction. Scale bars: 10 mm. 65
- Figure 3.S1** Fold polyimide sheet with a bilayer actuator. Scale bar: 10 mm. 67
- Figure 4.1** Folding along a single crease via the first approach. (a) Schematic of the folding process and geometric parameters; (b) Relationship between folding angle (α) and length ratio (λ); (c) Images of folding results at different length ratios (λ). Scale bars: 50 mm.. 74

- Figure 4.2** Assembling a square prism from its 2D precursor (first approach). (a) Schematic of the buckling process and geometric parameters. (b) Experimental realization of a square prism. Black gridlines were drawn to track the deformation. Scale bars: 30 mm. 76
- Figure 4.3** A number of 3D structures assembled via the first approach. Scale bars: 30 mm. 78
- Figure 4.4** Origami with one degree of freedom. (a) Miura-ori and (b) Insect wing. Scale bars: 30 mm. The 2D precursor is bonded to the polymer sheet at discrete points (highlighted by black circles) with a slit between two points. 80
- Figure 4.5** Folding a single crease via the second approach. (a) Schematic of the buckling process and geometric parameters; (b) Relationship between folding angle and length ratio (λ) /constrained fraction (ρ) for two special conditions; (c) Several folded samples; (d) A wavy structure. 83
- Figure 4.6** Assembling a square prism from its 2D precursor (second approach). Schematic of the buckling process and geometric parameters. 85
- Figure 4.7** A number of 3D structures assembled via the second approach. Scale bars: 30 mm. 87
- Figure 4.8** Combination of prismatic/pyramidal structures. (a) Horizontal tessellation (scale bars: 50 mm); (b) Vertical stack (scale bars: 30 mm)..... 89
- Figure 4.9** Application of cellular structure. (a) Thermal insulator; (b) Crash energy absorber. 91
- Figure 4.S1.** Assembly of a square prism with and without slit. (a) With slits ($\kappa > 0$); (b) Without slits ($\kappa = 0$)..... 93
- Figure 4.S2** Effect of a perforation on thermally induced strain and mechanical strain. (a) Equi-biaxial shrinkage of a PS sheet upon heating (scale bar: 30 mm); (b) FEA simulation of the deformation of a membrane under equi-biaxial tension; (c) Strain distribution (FEA simulation). 95
- Figure 4.S3** Schematic showing the assembly of several (truncated) pyramids (top view). Left: the first approach; right: the second approach. 98
- Figure 4.S4** Schematic showing the assembly of two special structures (top view). Left: house roof via the first approach; right: rhombic prism via the second approach. 99
- Figure 4.S5** Time evolution of the assembly process. 100
- Figure 5.1** Angular shrinkage gadget. (a) Images showing the angular shrinkage. Top: before heating; bottom: after heating. Scale bar: 30 mm. (b) Plot of the shrunk angle as a function of the initial angle. Both experimental results (square dot) and linear fitting line ($y = x/3$) are shown. 108
- Figure 5.2** Folding of a single crease using angular shrinkage gadget. (a) Schematic of the folding and related parameters. Red: paperboard sector; blue: PS sector. (b) Contour plot of

the dihedral angle (θ) as a function of the sector angles (α, β). (c) Images showing folding results with fixed sector angle ($\alpha = \pi$) and varying β , Top: before heating; bottom: after heating (side view). Scale bars: 30 mm. (d) Plot of θ as a function of β (with $\alpha = \pi$). 112

Figure 5.3 Folding truncated pyramids using multiple angular shrinkage gadgets. (a) Schematic of the folding and related parameters. (b) Plot of the dihedral angle (θ) as a function of the sector angle (α). Four cases (triangle, square, pentagon, hexagon) are shown. (c) Images showing folding results. Top: before heating; middle: after heating (top view); bottom: after heating (perspective view). Scale bars: 30 mm..... 115

Figure 5.4 Folding of cones with different angular defect. Top: before heating; middle: after heating; bottom: angular defect value of the folded structures. Scale bars: 30 mm. 116

Figure 5.5 Folding results with central PS sheet surrounded by a ring of unfold flat origami structure. (a) Flat motif. (b) Perspective view of the folded structure (after taken the top image, sample was flipped over and rotated 90 degrees). (c) Top view illustrating two degenerate folding modes (images were taken from the same sample but different orientation as indicated in the main text). (d) Square lattice of the motif. (e) Top view of the folded 3D checkboard pattern. (f) Perspective view of the folded 3D checkboard pattern. 119

Figure 5.S1 Schematic of the folding of a truncated triangular pyramids 122

CHAPTER 1 Introduction

1.1 Shape transformation and its applications

Shape plays an important role in both natural and artificial systems. In nature, organisms optimized their shape and form through million years of evolution.^[1] In some situations, organisms need to change their shape as a response to environmental stimuli or to achieve some functions. On the other hand, some man-made tools also change their shape during the usage. Next, we will show some examples of shape transformation in different fields.

1.1.1 Shape transformation in soft systems

Soft systems are ubiquitous in nature. Examples from animals include tentacles of octopus, trunks of elephants and tongues of mammals.^[2] They are composed almost exclusively of muscles without any rigid components. Yet they are capable of complex shape changes to achieve desired functions. For example, elephants bend and curl their trunk to grab food. Humans bend and twist their tongues in delicate manners to articulate speeches.^[3] Due to lack of stiff components, deformation can occur everywhere across the structure, enabling a higher number of degrees of freedom and a wider range of movement.

Besides animals, some plants also change their shape in some circumstances.^[4] One example is the seed dispersal process. *Bauhinia variegata* opens its seed pods to disperse the seeds, during which a flat pod valve is turned into a helix.^[5] Conifers disperse their seeds by opening the pine cone.^[6] Wild wheat propels its seed into the ground by bending the awns attached to the seed.^[7] The filaree plant fling its seed by first storing elastic energy and then

releasing it via coiling of the awn; and the coiling and uncoiling of the awn can also bury the seed into the ground.^[8]

Some other processes also require shape changing of the plant tissues. Venus flytrap closes its leaf rapidly to capture the prey.^[9] Young sunflowers bend their stem to track the sun.^[10] Cucumber climbs up the support by winding the tendrils around it.^[11] Other examples include the deployment of leaves^[12] and blooming of flowers,^[13] both of which are critical for the survival of plants.

The shape transformation in nature inspired researchers to develop several artificial shape shifting structures based on soft materials,^[14-16] which is capable of complex and smooth movements in 3D space.^[17] A flat sheet can be shaped into various curved surfaces, including cylindrical, spherical and saddle surfaces.^[14, 15, 18] A rod can be bent or twisted, resulting in various 3D curves.^[19, 20] The shape morphing can be used to make grippers that can grab fragile objects with complex shapes.^[21] Moreover, it can be used to make soft robots,^[22] mimicking octopus in nature.

1.1.2 Shape transformation in rigid systems

For humans and some other animals, motion is enabled by the bending of limbs about the flexible joints. Most machines are also based on rigid components and flexible joints. In these rigid systems, deformation is localized at discrete locations. The degrees of freedom (DOF) are from the rotation/folding about the joints, thus number of DOF is limited.

People have developed some models to analyze the motion in rigid systems.^[23] One-dimensional structures can be modeled as mechanical linkages. Complex shape

transformations and motions can be achieved by designing the links and joints.^[24-27] This dissertation focuses on the transformation of two dimensional structures, which can be modeled as origami. Based on origami, a flat sheet can be transformed into a 3D object by folding along pre-defined creases. The results are piecewise planar structures. Algorithms have been developed to calculate the crease patterns that can give rise to desired 3D structures.^[28-30] In traditional origami, an intact piece of paper is used without cutting. During folding, some of the materials need to be tucked beneath the visible surface. In order to get rid of the tucking process, people cut and perforate the paper prior to folding, which is known as kirigami.^[31, 32] The algorithm of cutting and folding has also been solved.

Even though origami was initially invented by artists for aesthetic purpose. It became more and more involved in science and engineering applications.^[33] It can be potentially used as a new manufacturing technique, complementary to additive manufacturing (e.g. 3D printing) and subtractive manufacturing (e.g. machining or etching). The fabrication technique in planar structures is well-developed, but it's still a challenge to directly fabricate 3D structures. Origami provides a convenient approach to transform 2D sheets into desired 3D structures. This technique can be used to make robots^[34] and other 3D devices.^[35, 36]

Besides its application in fabricating 3D structures, origami can also be used to make metamaterials. As degrees of freedom are induced by the folding of creases, mechanical property of the folded structure can be tailored by modifying the crease patterns. This can give rise to abnormal mechanical behavior. For example, negative Poisson's ratio can be achieved in origami metamaterials.^[37] Moreover, the Poisson's ratio can be programmed by changing the crease patterns.^[38] Another interesting property arising from the origami folding is tunable

thermal expansion.^[39] Furthermore, stiffness of the metamaterial can be programmed by introducing defects and changing their arrangement.^[40]

Another capability of origami is bistable structures. For some crease patterns, folding is prohibited due to the internal constraints. However, the structure can be transformed to another stable state by bending those areas between the creases.^[41] The two stable states are separated by an energy barrier that is associated with the bending deformation. One example that takes advantage of the bistable mechanism is the paper shopping bag.^[42] The bag has a flat folded state and an opened state. The transformation from one state to the other requires bending of paper between the creases, which needs reasonably high energy. The energy barrier can stabilize the shopping bag in its opened state.

Origami principle can be used to design deployable structures.^[43] A famous example is the Miura-ori, which was proposed by Miura as a method of packing and deploying solar panels in space.^[44] By modifying the Miura-ori, a flat folded origami structure can be deployed into different shapes.^[28, 45] Another example is the self-deployable stent grafts, whose diameter can be changed by folding/unfolding the creases.^[46]

1.2 Different approaches to achieve shape transformation

There are several strategies to achieve the shape transformation.^[47, 48] They are divided into three categories: (1) bending induced by varying strain across the thickness; (2) buckling induced by compression; (3) Gaussian curvature change induced by non-uniform in-plane strain.

1.2.1 Shape transformation induced by bending

Varying strain across the thickness of a sheet or beam can cause it to bend.^[49] Most of the shape transformation in natural systems can be attributed to this reason. In soft animals, the varying strain is generated by unsymmetrical muscle shrinkage.^[2] In plants, it is caused by unsymmetrical cell growth or expansion.^[4] In artificial structures, the varying strain can be generated in many ways. It can be induced by unsymmetrical shrinkage in a heat shrinkable polymer sheet, which is induced by temperature gradient across the thickness of the sheet.^[50-52] A more common way is to use bilayer sheet. Two layers expands/shrinks differently when triggered by certain stimuli. The mismatch strain causes the bilayer sheet to bend. The stimuli can be heating,^[53-56] swelling,^[16, 57-59] or electric potential.^[60-63]

Depending on the strain state and in-plane geometry, the bilayer sheet can be bent into different shapes.^[62, 64-66] A bimorph strip can curl along the longitudinal direction.^[53, 62, 66] Helical structures can be obtained by changing the orientation of bending relative to the strip.^[67] A square/circular bilayer sheet can curl into a special surface^[68] or saddle surface.^[69] Besides curving on its own, the bilayer sheet can be embedded in a large passive sheet. In this case, it acts as an actuating hinge to fold the passive sheet.^[48, 58, 60] Origami structures can be folded by embedding actuating hinges along the creases. Folding is realized in the form of local bending.

1.2.2 Shape changing in the form of buckling

The abovementioned method utilizes strain variation across the thickness of the sheet. It requires the materials to be able to response to external stimuli, e.g. heat, solution or electric

potential, which makes the method applicable only to certain materials. Another method to achieve shape transformation is through compressive buckling.^[70-72] When a slender structure is compressed, it tends to buckle to release the compressive strain energy. The buckling deformation follows the path of lowest strain energy states.^[73] The resulting shape can be controlled by the layout and stiffness of the initial structure.

The buckling does not require the responsiveness of the materials, thus can be applied to a broader range of materials. Researchers have demonstrated the assembly of 3D structures from planar sheets through compressive buckling.^[36] The compression is induced by relaxation of a pre-stretched elastomer substrate. The buckling deformation can be localized at certain areas (i.e. creases) with reduced thickness (thus reduced bending stiffness). This can give rise to sharp folding. The technique is applicable to metals, semiconductors and polymers.^[74-78] In addition, the motion of limbs can also be regarded as compressive buckling of skeletons caused by the shrinking muscles attached to the skeletons.

The buckling deformation can be actuated by other forces as well. One powerful method is to use capillary interaction.^[79, 80] Liquid tends to reduce its surface area to minimize the surface energy. This can bring different ends of a thin sheet toward each other and cause the wrapping or folding.^[79, 81] Depending on the shape of the initial sheet, different 3D structures can be obtained. Again, the bending deformation can be concentrated at the creases. Another way to actuate the buckling is using cell traction force.^[82] The cell contracts and pulls the thin sheet, folding it along the creases.

1.2.3 Shape changing induced by change Gaussian curvature

Besides bending and buckling, there is another strategy to change the shape of thin sheet based on change of Gaussian curvature. Gaussian curvature characterizes how a surface is curved in 3D space. It is connected with the surface's metric (a tensor relates to the local distances between points in the surface).^[15] A flat surface has zero Gaussian curvature, a spherical surface has positive Gaussian curvature and a saddle surface has negative Gaussian curvature. The Gaussian curvature can be changed by in-plane deformation. No strain variation across the thickness is involved as the thickness of the surface can be regarded as zero. Also, no actuator outside the surface is required.

The Gaussian curvature of a surface can be changed by non-uniform in-plane strain. For a circular disk, expansion of the central area results in a spherical surface, while expansion of the peripheral area results in a saddle surface.^[15] There are several ways to cause the in-plane strain of a thin sheet. One way is swelling/deswelling of polymer. The swelling strain can be controlled by concentration,^[15] crosslinking density^[14] and temperature.^[83] Non-uniform strain can be generated by locally modifying these parameters. A flat polymer sheet can be shaped into a curved 3D surface. Another way to generate the in-plane strain is to use shrinkage in heat shrinkable polymers. The shrinkage can be tuned by local temperature.^[84] Non-uniform strain can be induced by non-uniform heating.

Besides uniformly curved surfaces, Gaussian curvature can also characterize polyhedral surface which is piecewise planar. However, the Gaussian curvature is concentrated at the vertex of the polyhedron. It is defined as the angular defect around the vertex, i.e. 2π

minus sum of the sector angles around the vertex. A flat surface has zero Gaussian curvature as angle around a point is 2π . When a sector is cut out, and the exposing edges are glued together, a cone is formed. The cone has a positive angular defect and a positive Gaussian curvature. Similarly, around the vertex of a polyhedron (e.g. cube), the sum of sector angle is less than 2π . There is also a positive angular defect and Gaussian curvature. In contrast, when a sector is inserted into a flat disk, the sum of angles is greater than 2π . The result is a saddle surface (e-cone),^[85] which has negative angular defect and Gaussian curvature.

References

- [1] D. W. Thompson, *On growth and form*. 1942.
- [2] W. M. Kier, K. K. Smith, *Zoological Journal of the Linnean Society* 1985, 83, 307.
- [3] K. M. Hiimae, J. B. Palmer, *Critical Reviews in Oral Biology & Medicine* 2003, 14, 413.
- [4] K. Oliver, A. Seddon, R. S. Trask, *Journal of Materials Science* 2016, 51, 10663.
- [5] S. Armon, E. Efrati, R. Kupferman, E. Sharon, *Science* 2011, 333, 1726.
- [6] E. Reyssat, L. Mahadevan, *Journal of the Royal Society Interface* 2009, 6, 951.
- [7] R. Elbaum, L. Zaltzman, I. Burgert, P. Fratzl, *Science* 2007, 316, 884.
- [8] D. Evangelista, S. Hotton, J. Dumais, *Journal of Experimental Biology* 2011, 214, 521.
- [9] Y. Forterre, J. M. Skotheim, J. Dumais, L. Mahadevan, *Nature* 2005, 433, 421.
- [10] H. S. Atamian, N. M. Creux, E. A. Brown, A. G. Garner, B. K. Blackman, S. L. Harmer, *Science* 2016, 353, 587.
- [11] S. J. Gerbode, J. R. Puzey, A. G. McCormick, L. Mahadevan, *Science* 2012, 337, 1087.
- [12] H. Kobayashi, B. Kresling, J. F. Vincent, *Proceedings of the Royal Society of London B: Biological Sciences* 1998, 265, 147.
- [13] H. Liang, L. Mahadevan, *Proceedings of the National Academy of Sciences* 2011, 108, 5516.
- [14] J. Kim, J. A. Hanna, M. Byun, C. D. Santangelo, R. C. Hayward, *Science* 2012, 335, 1201.
- [15] Y. Klein, E. Efrati, E. Sharon, *Science* 2007, 315, 1116.
- [16] A. S. Gladman, E. A. Matsumoto, R. G. Nuzzo, L. Mahadevan, J. A. Lewis, *Nature materials* 2016, 15, 413.
- [17] S. Bauer, S. Bauer-Gogonea, I. Graz, M. Kaltenbrunner, C. Keplinger, R. Schwödiauer, *Advanced Materials* 2014, 26, 149.
- [18] G. Kofod, W. Wirges, M. Paajanen, S. Bauer, *Applied Physics Letters* 2007, 90, 081916.

- [19] S. Kota, *Scientific American* 2014, 310, 58.
- [20] F. Connolly, C. J. Walsh, K. Bertoldi, *Proceedings of the National Academy of Sciences* 2017, 114, 51.
- [21] F. Ilievski, A. D. Mazzeo, R. F. Shepherd, X. Chen, G. M. Whitesides, *Angewandte Chemie* 2011, 123, 1930.
- [22] M. Wehner, R. L. Truby, D. J. Fitzgerald, B. Mosadegh, G. M. Whitesides, J. Lewis, R. J. Wood, *Nature* 2016.
- [23] E. D. Demaine, J. O'Rourke, *Geometric folding algorithms*, Cambridge university press Cambridge, 2007.
- [24] A. S. Hall, *Kinematics and Linkage Design*, Waveland Press Inc, 1986.
- [25] Y. Chen, Z. You, T. Tarnai, *International journal of solids and structures* 2005, 42, 2287.
- [26] I. Doroftei, I. A. Doroftei, "Deployable Structures for Architectural Applications-a Short Review", presented at *Applied Mechanics and Materials*, 2014.
- [27] C. Gantes, E. Konitopoulou, *International Journal of Solids and Structures* 2004, 41, 5517.
- [28] L. H. Dudte, E. Vouga, T. Tachi, L. Mahadevan, *Nature materials* 2016, 15, 583.
- [29] T. Tachi, "3D origami design based on tucking molecule", presented at *The Fourth International Conference on Origami in Science, Mathematics, and Education*, R. Lang, ed., Pasadena, 2009.
- [30] R. J. Lang, "A computational algorithm for origami design", presented at *Proceedings of the twelfth annual symposium on Computational geometry*, 1996.
- [31] D. M. Sussman, Y. Cho, T. Castle, X. Gong, E. Jung, S. Yang, R. D. Kamien, *Proceedings of the National Academy of Sciences* 2015, 112, 7449.
- [32] T. Castle, Y. Cho, X. Gong, E. Jung, D. M. Sussman, S. Yang, R. D. Kamien, *Physical review letters* 2014, 113, 245502.
- [33] P. Wang-Iverson, R. J. Lang, Y. Mark, *Origami 5: Fifth International Meeting of Origami Science, Mathematics, and Education*, CRC Press, 2016.
- [34] S. Felton, M. Tolley, E. Demaine, D. Rus, R. Wood, *Science* 2014, 345, 644.

- [35] J. P. Whitney, P. S. Sreetharan, K. Y. Ma, R. J. Wood, *Journal of Micromechanics and Microengineering* 2011, 21, 115021.
- [36] S. Xu, Z. Yan, K.-I. Jang, W. Huang, H. Fu, J. Kim, Z. Wei, M. Flavin, J. McCracken, R. Wang, *Science* 2015, 347, 154.
- [37] H. Yasuda, J. Yang, *Physical review letters* 2015, 114, 185502.
- [38] M. Schenk, S. D. Guest, *Proceedings of the National Academy of Sciences* 2013, 110, 3276.
- [39] E. Boatti, N. Vasios, K. Bertoldi, *Advanced Materials* 2017.
- [40] J. L. Silverberg, A. A. Evans, L. McLeod, R. C. Hayward, T. Hull, C. D. Santangelo, I. Cohen, *science* 2014, 345, 647.
- [41] J. L. Silverberg, J.-H. Na, A. A. Evans, B. Liu, T. C. Hull, C. D. Santangelo, R. J. Lang, R. C. Hayward, I. Cohen, *Nature materials* 2015, 14, 389.
- [42] D. J. Balkcom, E. D. Demaine, M. L. Demaine, "Folding paper shopping bags", presented at *Proceedings of the 14th Annual Fall Workshop on Computational Geometry*, 2004.
- [43] S. Pellegrino, *Deployable structures*, Vol. 412, Springer, 2014.
- [44] K. Miura, title *The Institute of Space and Astronautical Science report* 1985, 618, 1.
- [45] E. T. Filipov, T. Tachi, G. H. Paulino, *Proceedings of the National Academy of Sciences* 2015, 112, 12321.
- [46] K. Kuribayashi, K. Tsuchiya, Z. You, D. Tomus, M. Umemoto, T. Ito, M. Sasaki, *Materials Science and Engineering: A* 2006, 419, 131.
- [47] E. A. Peraza-Hernandez, D. J. Hartl, R. J. Malak Jr, D. C. Lagoudas, *Smart Materials and Structures* 2014, 23, 094001.
- [48] Y. Liu, J. Genzer, M. D. Dickey, *Progress in Polymer Science* 2016, 52, 79.
- [49] A. Cho, *Science* 2006, 313, 164.
- [50] Y. Liu, J. K. Boyles, J. Genzer, M. D. Dickey, *Soft Matter* 2012, 8, 1764.
- [51] Y. Liu, R. Mailen, Y. Zhu, M. D. Dickey, J. Genzer, *Physical Review E* 2014, 89, 042601.

- [52] D. Davis, B. Chen, M. D. Dickey, J. Genzer, *Journal of Mechanisms and Robotics* 2016, 8, 031014.
- [53] S. Timoshenko, *JOSA* 1925, 11, 233.
- [54] M. Ataka, A. Omodaka, N. Takeshima, H. Fujita, *Journal of Microelectromechanical Systems* 1993, 2, 146.
- [55] S. M. Felton, M. T. Tolley, B. Shin, C. D. Onal, E. D. Demaine, D. Rus, R. J. Wood, *Soft Matter* 2013, 9, 7688.
- [56] H. Wang, Y. Wang, B. C. K. Tee, K. Kim, J. Lopez, W. Cai, Z. Bao, *Advanced Science* 2015, 2.
- [57] G. Stoychev, S. Zakharchenko, S. b. Turcaud, J. W. Dunlop, L. Ionov, *ACS nano* 2012, 6, 3925.
- [58] J. H. Na, A. A. Evans, J. Bae, M. C. Chiappelli, C. D. Santangelo, R. J. Lang, T. C. Hull, R. C. Hayward, *Advanced Materials* 2015, 27, 79.
- [59] J. Jeong, Y. Cho, S. Y. Lee, X. Gong, R. D. Kamien, S. Yang, A. Yodh, *Soft matter* 2017, 13, 956.
- [60] E. Smela, O. Inganäs, I. Lundström, *Science* 1995, 268, 1735.
- [61] K. Takagi, J.-F. Li, S. Yokoyama, R. Watanabe, A. Almajid, M. Taya, *Science and Technology of Advanced Materials* 2002, 3, 217.
- [62] S. Alben, B. Balakrishnan, E. Smela, *Nano letters* 2011, 11, 2280.
- [63] T.-B. Xu, X. Jiang, J. Su, *Applied Physics Letters* 2011, 98, 243503.
- [64] M. Finot, S. Suresh, *Journal of the Mechanics and Physics of Solids* 1996, 44, 683.
- [65] N. Guyot, Y. Harmand, A. Mézin, *International journal of solids and structures* 2004, 41, 5143.
- [66] I. S. Chun, A. Challa, B. Derickson, K. J. Hsia, X. Li, *Nano letters* 2010, 10, 3927.
- [67] Z. Chen, *Nanoscale* 2014, 6, 9443.
- [68] G. G. Stoney, *Proceedings of the Royal Society of London. Series A, Containing Papers of a Mathematical and Physical Character* 1909, 82, 172.
- [69] Z. Chen, Q. Guo, C. Majidi, W. Chen, D. J. Srolovitz, M. P. Haataja, *Physical review letters* 2012, 109, 114302.

- [70] N. Hu, R. Burgueño, *Smart Materials and Structures* 2015, 24, 063001.
- [71] P. M. Reis, *Journal of Applied Mechanics* 2015, 82, 111001.
- [72] A. Rafsanjani, K. Bertoldi, *Physical Review Letters* 2017, 118, 084301.
- [73] A. E. H. Love, *A treatise on the mathematical theory of elasticity*, Cambridge university press, 2013.
- [74] Y. Zhang, Z. Yan, K. Nan, D. Xiao, Y. Liu, H. Luan, H. Fu, X. Wang, Q. Yang, J. Wang, *Proceedings of the National Academy of Sciences* 2015, 112, 11757.
- [75] Y. Liu, Z. Yan, Q. Lin, X. Guo, M. Han, K. Nan, K. C. Hwang, Y. Huang, Y. Zhang, J. A. Rogers, *Advanced Functional Materials* 2016, 26, 2909.
- [76] Y. Shi, F. Zhang, K. Nan, X. Wang, J. Wang, Y. Zhang, Y. Zhang, H. Luan, K.-C. Hwang, Y. Huang, J. A. Rogers, Y. Zhang, *Extreme Mechanics Letters* 2016, 11, 105.
- [77] Z. Yan, F. Zhang, F. Liu, M. Han, D. Ou, Y. Liu, Q. Lin, X. Guo, H. Fu, Z. Xie, M. Gao, Y. Huang, J. Kim, Y. Qiu, K. Nan, J. Kim, P. Gutruf, H. Luo, A. Zhao, K.-C. Hwang, Y. Huang, Y. Zhang, J. A. Rogers, *Sci. Adv.* 2016, 2, e1601014.
- [78] Z. Yan, F. Zhang, J. Wang, F. Liu, X. Guo, K. Nan, Q. Lin, M. Gao, D. Xiao, Y. Shi, Y. Qiu, H. Luan, J. Kim, Y. Wang, H. Luo, M. Han, Y. Huang, Y. Zhang, J. A. Rogers, *Advanced Functional Materials* 2016, 26, 2629.
- [79] C. Py, P. Reverdy, L. Doppler, J. Bico, B. Roman, C. N. Baroud, *Physical review letters* 2007, 98, 156103.
- [80] X. Guo, H. Li, B. Y. Ahn, E. B. Duoss, K. J. Hsia, J. A. Lewis, R. G. Nuzzo, *Proceedings of the National Academy of Sciences of the United States of America* 2009, 106, 20149.
- [81] M. Boncheva, D. A. Bruzewicz, G. M. Whitesides, *Pure and Applied Chemistry* 2003, 75, 621.
- [82] K. Kuribayashi-Shigetomi, H. Onoe, S. Takeuchi, *PloS one* 2012, 7, e51085.
- [83] C. Yu, Z. Duan, P. Yuan, Y. Li, Y. Su, X. Zhang, Y. Pan, L. L. Dai, R. G. Nuzzo, Y. Huang, *Advanced Materials* 2013, 25, 1541.
- [84] A. M. Hubbard, R. W. Mailen, M. A. Zikry, M. D. Dickey, J. Genzer, *Soft Matter* 2017, 13, 2299.
- [85] K. A. Seffen, *Physical Review E* 2016, 94, 013002.

CHAPTER 2 Controlling the self-folding of a polymer sheet using a local heater

2.1 Introduction

Fabrication of three-dimensional (3D) structures and devices is of increasing interest. An attractive strategy is to transform two-dimensional (2D) sheets into 3D architectures.^[1-6] One method is via controlled compressive buckling of planar structures.^[7-9] While ingenious, this method is challenging in fabricating structures with sharp angles and often requires sophisticated mechanics design. Another method is based on origami-inspired folding.^[10, 11] Various actuation mechanisms have been used to accomplish folding including capillary force,^[12] light-activated stress relaxation across the film thickness,^[13] and bimorph structure actuated by heat,^[14] swelling,^[15, 16] or electric field.^[5]

Shape memory materials,^[11, 17] especially shape memory polymers (SMPs)^{[18, 19], [20]} have attracted much recent attention for origami folding. SMPs can respond to many types of stimuli including light,^[21] heat,^[22-24] electricity,^[25] moisture,^[26] and pH change.^[27] SMPs can be pre-strained with a uniform tensile strain across the thickness and releasing of the tensile strain above a threshold temperature gives rise to in-plane shrinkage. To convert the in-plane shrinkage of a SMP sheet to out-of-plane deformation, several methods have been developed. One method was to use bilayer structure,^[28, 29] *i.e.* bonding a SMP layer to an un-shrinkable layer. When heated, shrinkage of the SMP layer caused (continuous) bending of the bilayer towards the SMP side. In another method, a heater strip was sandwiched between a SMP layer and a structural layer.^[1, 30, 31] Shrinkage of the SMP layer led to (localized) folding. In the third method, localized folding was achieved by generating a local gradient in shrinkage across the

thickness of the SMP sheet.^[32, 33] As demonstrated by Liu *et al.*,^[33] a temperature gradient across the thickness can be generated by local light absorption defined by a line pattern, leading to a gradient in shrinkage across the thickness. In the first two methods the heaters were fixed to the SMP sheets and the bending or folding was towards the SMP side, while in the third method there was no heater and the folding was towards the light (or against the SMP side). In all three cases the folding angles were limited (*e.g.* < 159 degrees for the second approach.^[30] and < 110 degrees for the third approach^[34]). It appears the SMP-heater interface plays an important role in controlling the folding behavior. It is thus of relevance to understand such an interfacial interaction and explore if the interaction can offer additional opportunities to control the folding.

Here we report self-folding of a SMP sheet triggered by local joule heating using a flexible heater, focusing on the effect of the SMP-heater interface. We identified three modes of operation depending on the interfacial interaction between the heater and the SMP sheet. In all modes, folding is caused by shrinkage variation across the thickness of SMP sheet. When the heater is placed on the SMP sheet with a weak interface (no constraint), the SMP sheet folds towards the heater. The shrinkage variation is caused by the temperature gradient across the thickness. By contrast, when the heater is fixed (glued) to the SMP sheet (total constraint), the SMP sheet can fold against the heater due to the constraining effect of the heater, *i.e.* the heater constrains the shrinkage of the SMP sheet on the interface side. In either mode, 180 degrees folding can be achieved. An intermediate mode with the heater delaminated from the SMP sheet along the interface but fixed at two edges (partial constraint) was also studied. As

demonstrations, several structures including numbers from zero to nine, a cube, a boat and a crane were fabricated by folding.

2.2 Materials and Methods

2.2.1 Materials

A commercially available SMP with the brand name of Shrinky Dinks was used in this study, which is made of pre-strained PS. PS sheet was cut into 12 mm stripes. The thickness was 10 mil (0.25 mm). Biaxial tensile strain is incorporated into the SMP sheet, which is uniform across the thickness. The PS sheet shrinks in plane by 50% in both directions upon relaxation above T_c (140 °C). The PI sheet was purchased from CAPLINQ with thickness of 1 mil (0.025 mm). The PI sheet can be cut into stripes with desired widths. Super glue was purchased from amazon under the name of Loctite Liquid Professional Super Glue 20-Gram Bottle.

2.2.2 Sample preparation

The heater was fabricated by coating silver nanowires (AgNWs) onto the PI sheet. AgNWs were synthesized following a standard approach.^[35] The PI sheet was taped onto a clean glass slide, while AgNWs dispersed in ethanol was dropped casted on top of PI. A Mayer Rod was used to make a uniform coating. Thermal treatment at 50 °C was conducted to evaporate the ethanol. Then the AgNW/PI heater was peeled off from glass slide and put onto PS stripe. For the case of partial constraint, a wide PI sheet was taped on PS stripe (in perpendicular direction). Heater was fabricated by coating AgNWs on the central region (two

edges were masked), leaving bare tape along each edge. For the case of total constraint, super glue was used to glue the heater onto the PS sheet.

2.2.3 Folding experiment

Agilent 6613C power supply was used to apply the current. Voltage was monitored using an Agilent 34401A digital multimeter. Thin copper wires were used to connect the heater to the power supply. Liquid metal or silver paste was used for the reliable contact between the copper wire and the heater. Two cameras were used to take images during the folding processes, one for top view, and the other for side view. For the top view, the distance between the camera and the sample was kept constant.

2.3 Results and Discussions

2.3.1 Folding mechanism

Figure 2.1a shows the experimental set up and **Figure 2.1b** shows the schematic of a heater on the SMP sheet. The heater was fabricated by coating AgNWs on a polyimide (PI) sheet. The SMP sheet used was pre-strained polystyrene (PS). It is important to isolate the AgNW film from the PS by another layer (*e.g.* PI used here), which can keep the AgNW film mechanically stable during folding. If the AgNWs were directly coated on top of the PS sheet, large deformation of the PS sheet during folding would severely deform the AgNWs, leading to significant resistance increase or even failure of the heater (**Figure 2.S1**, SI). The reason to choose PI for the heater was due to its high thermal stability; the glass transition temperature of PI is 410 °C, much higher than the temperature required to fold PS (~ 140 °C). PI is a widely used substrate material for flexible heaters.^[36] The AgNW/PI heater can reliably provide high

temperature up to 160 °C (**Figure 2.S2**, SI). The heat generated using the flexible heater is much more intense than that by the light absorption approach. For example, an infrared lamp typically provided 1 W/cm² power^[34] while the Joule heating can provide up to 5 W/cm² (e.g. in **Figure 2.5b**). Thus folding can be realized without the need of a hot plate under the PS substrate as in the light absorption approach.

Figure 2.1b shows the steady-state temperature distribution in the PS sheet calculated using finite element analysis (FEA), assuming a constant temperature in the heater as the boundary condition (the constraining effect of the heater was neglected here). In the red area the temperature is above the threshold temperature (T_c) for shrinkage of PS, which is taken as 140 °C here. It is known that the glass transition temperature (T_g) of PS is ~100 °C, but to achieve considerable shrinkage, temperature needs to be higher.^[28, 34] When the temperature reaches above T_c , the PS sheet shrinks (releasing its pre-strain of 50%). Since the top side heats more, a temperature gradient across the thickness of the PS sheet forms, as shown in **Figure 2.1b**. As a result, the top side shrinks more than the bottom side and hence the PS sheet tends to fold upwards (assuming the mechanical constraint of the heater is not significant). Folding angle is determined by the difference in shrinkage of the two sides. The heated region bends to an arc, as shown in **Figure 2.1c**. In an ideal case (best scenario), only the top surface shrinks by 50% while the bottom surface does not shrink. The folding angle (α) can be estimated by a simple geometric relationship,

$$\alpha = \frac{L}{R} = \frac{L/2}{R-h} \quad (2.1)$$

where L is length of the heated area on the top surface before folding (*i.e.* approximately the heater width), R is radius of curvature, and h is thickness of the PS sheet (0.25 mm used in this study). According to **Equation 2.1**, $R = 2h$ and 180 degrees folding can be obtained when the heater width reaches 1.57 mm.

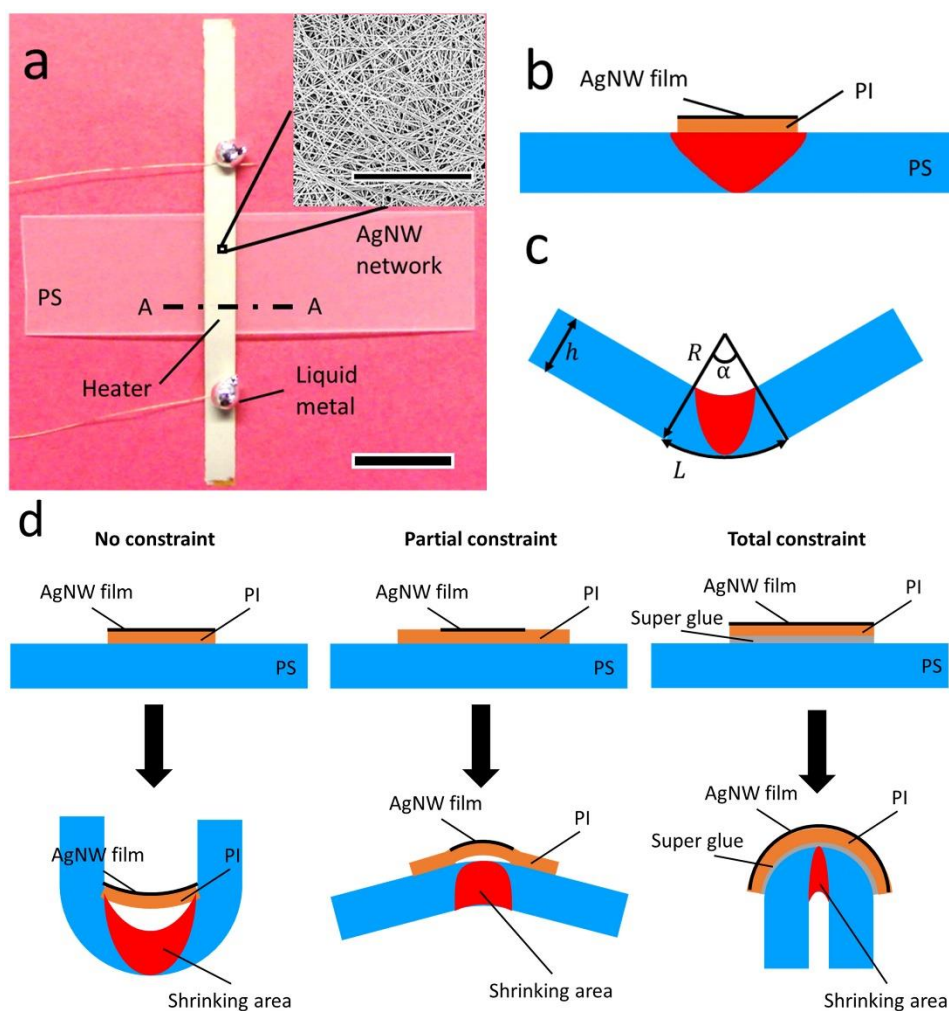


Figure 2.1 (a) Experimental setup showing the pre-strained PS sheet and the flexible AgNW/PI heater on top. Scale bar: 10 mm. The inset shows the AgNW network (scale bar: 10 μm); (b) Schematic of the cross section A-A in panel (a) and the temperature distribution in PS (according to FEA simulation). In the red area the temperature is above the threshold temperature for shrinkage of PS; (c) Schematic showing the folding geometry and related parameters; (d) Schematics showing the three modes of operation for folding a PS sheet: no constraint, partial constraint and total constraint.

When the mechanical constraint is considerable, upward folding will be intervened due to resistance from the heater. The mechanical interaction between the heater and the PS substrate can be considered in three cases – no constraint, partial constraint and total constraint. A schematic showing the three corresponding modes of operation is shown in **Figure 2.1d**. When the heater sits on top of the substrate with only weak adhesion like van der Waals interaction between them (*i.e.* no constraint), folding of the PS substrate can continue accompanied by sliding and delamination of the heater. When the adhesion is weak but both edges of the heater are fixed (*i.e.* partial constraint), shrinkage of the top surface of the substrate can cause buckle delamination of the heater. Without sliding of the heater, the resistance to folding becomes stronger, leading to reduced folding angle and even folding against the heater. When the heater is fixed to the substrate (*i.e.* total constraint), both sliding and buckle delamination are prohibited and so is shrinkage of the top surface of the substrate. Shrinkage of the bottom surface can cause folding against the heater. Here we define folding towards the heater as inward folding, while folding against the heater as outward folding. Note that the PI sheet used here is relatively stiff compared to the PS substrate. Otherwise the heater could wrinkle under compression and the AgNWs on top of the PI sheet might not survive such wrinkling.

2.3.2 Folding without constraint

In the case of no constraint (*e.g.* van der Waals interaction), the AgNW/PI heater was placed on top of the PS substrate. The heater can be peeled off after the folding, leaving a clean folded structure. **Figure 2.2** shows the folding results. PS folded toward the heater (inward folding). The folding angle as a function of the heater width is plotted in **Figure 2.2a**. With

heater width was less than 1 mm, the maximum folding angle was less than 180 degrees and varied from sample to sample. **Figure 2.S4** (SI) shows the inward folding for the heater width of 0.5 mm where the maximum folding angle was 140 degrees. Increasing heater width to 1 mm or wider can lead to complete folding. Folding stopped when two ends of the PS sheet touched each other, in which case the folding angle was 180 degrees as shown in **Figure 2.2a**. **Figure 2.3** shows the deformation of heater during folding. Folding can be stopped by turning off the power supply and resumed by turning it on. Black parallel lines drawn on the PS sheet were used to show the relative position between the heater and the substrate. As shrinkage of the substrate began, edges of the heater slid on the substrate in order to accommodate the shrinkage, which can be seen by comparing the images at different folding angles in **Figure 2.3**. For example, there were initially five black lines to the left of heater. There became four when the substrate folded to 90 degrees, which indicated that heater slid over one black line. As the substrate started to fold, the center of the heater started to delaminate from the substrate. This is shown schematically in the bottom of **Figure 2.3**. During folding, the heater initially bent with the substrate, and then transitioned to sliding and delamination (“climbing” up along the folded substrate) to reduce the bending energy. Bending of the heater decreased its chord length, which can be measured from the top view of the heater. From the chord length and folding angle (measured from the side view), the shape and position of the heater can be determined (**Figure 2.S5-2.S7**, SI).

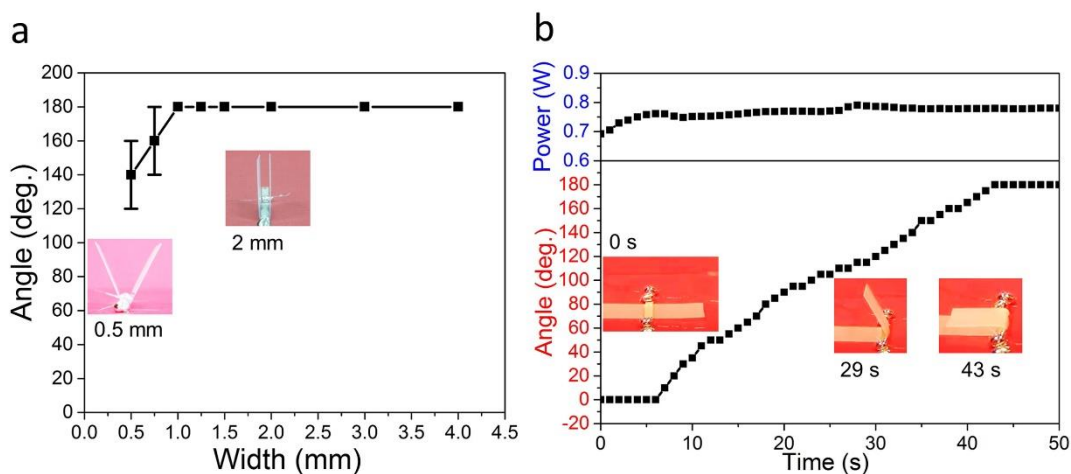


Figure 2.2 Folding results in the case of no constraint. (a) Relationship between inward folding angle and heater width. Insets are side views of the folded structures with 0.5 mm and 2 mm wide heaters; (b) Time response and power input during inward folding with a 2 mm wide heater. Insets show several snapshots during the folding.

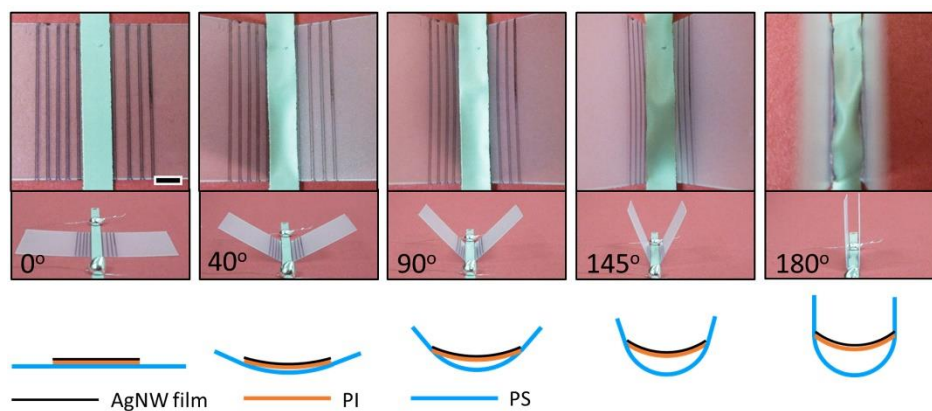


Figure 2.3 Deformation of heater in the case of no constraint. Top: top view; middle: side view; bottom: schematic of the cross section from side view. Scale bar: 2 mm. Folding was stopped by turning off the power supply. After taking images, folding was resumed by turning on the power supply.

As the heater climbed up and formed a gap with the folded region, one question would be how the folding process continued. Note that the two edges of the heater remained in contact with the substrate. With the heater sliding, more areas were heated (by edges of heater) and shrank, leading to progression of the folding. As a result of the sliding, a narrower heater width (*e.g.* 1 mm instead of 1.57 mm according to Equation 2.1) was able to give 180 degrees folding, as shown in **Figure 2.2a**. Moreover, the gap between the heater and the substrate can offer one additional advantage. Overheating of the folded region can cause unfolding as the bottom surface was also heated and shrank – see the case of total constraint to be discussed later. Forming such a gap can prevent the overheating and unfolding of the folded region.

2.3.3 Folding with partial constraint

In the case of partial constraint (*i.e.* no sliding), inward folding was resisted by the heater. **Figure 2.4** shows the folding with a bare tape on each edge of the heater to prevent sliding of the heater. Shrinkage of the top side of the PS compressed the heater and caused buckle delamination. The resistance force from the heater opposed shrinkage of the top side of the PS. Only two anchoring edges of the heater can heat up the PS sheet, which however cannot slide as in the case of no constraint. As a result shrinkage of the top side of the PS was limited. When the PS sheet was heated through, heating of the backside of the PS sheet can cause shrinkage of the backside, which soon surpassed that of the top side, leading to outward folding. The outward folding angle was quite small in this case, as shown in **Figure 2.4** and **Figure 2.S8** (SI). Note that if only one edge of the heater was constrained, the heater can still slide but with reduced delamination (climb) compared to the case of no constraint. As a result, 180 degrees folding was still achievable (**Figure 2.S9**, SI).

2.3.4 Folding with total constraint

The outward folding angle in the case of partial constraint was limited because the shrinkage of the top surface was not completely suppressed. It is thus of interest to explore the folding behavior in the case of total constraint, that is, delamination is also suppressed in addition to sliding (*e.g.* by gluing the heater to the substrate). The folding angle was found to depend on the heater width (**Figure 2.5a**). Note that positive angle corresponds to inward folding, while negative angle corresponds to outward folding. With a narrow heater, inward folding still occurred but the folding angle was smaller than that in the first case (no constraint). The inward folding angle decreased with the increasing heater width. At the heater width of ~ 0.75 mm, outward folding took over and the outward folding angle increased with the increasing heater width until ~ 1.5 mm where 180 degree outward folding was obtained.

The folding behavior in this case was dictated by the temperature distribution in the PS sheet. FEA shows that the heated area above T_c was slightly beyond the heater on the top surface (the extra heated area was nearly constant, regardless of the heater width) (**Figure 2.S10-2.S11**, SI). The heater was assumed stiff compared to the PS and not deformed under compression during the folding. For a narrow heater, the extra heated area on the top surface was larger than the heated area on the bottom surface, leading to inward folding. For a wide heater, the extra heated area on the top surface was smaller than the heated area on the bottom surface, leading to outward folding. **Figure 2.S12a** (SI) shows the inward folding for a heater width of 0.5 mm. The inset shows the mass accumulation adjacent to the heater, which indicates shrinkage of the extra heated area mentioned above. **Figure 2.S12b** (SI) shows the outward folding for a heater width of 2 mm. The inset shows that the heater was in close contact

with the PS. No wrinkles or buckle delamination can be observed, confirming that the heater was not deformed. This scenario can be viewed as the opposite of that described by **Equation 2.1** – the bottom surface shrank by 50% (under the heater) while the top surface did not shrink. As predicted by **Equation 2.1**, 180 degrees outward folding can be achieved with a heater width ~ 1.57 mm, in good agreement with the experimental results (**Figure 2.5a**). Also the bending of this bilayer structure (PS substrate and AgNW/PI heater) can be analyzed using a bimorph model (see details in Bimorph model analysis section in SI), which calculates a heater width of ~ 1.58 mm to achieve 180 degrees outward folding.

2.3.5 Time response of folding

Figure 2.2b and **2.5b** show the time responses of two representative samples corresponding to the first and third cases discussed above – no constraint and total constraint, respectively. A heater width of 2 mm was used in both cases. A constant current was applied to the heater while the voltage was monitored during the folding process. In the case of no constraint (**Figure 2.2b**), inward folding occurred. The folding started at 7 s after turning on the heater and stopped at 43 s with the folding angle of 180 degrees. The input power increased from 0.75 W to 0.8 W. The heating area was ~ 0.25 cm² and the power density was about 3 W/cm². In the case of total constraint (**Figure 2.5b**), outward folding occurred. The folding started at ~ 2 s after turning on the heater and stopped at ~ 6 s with the folding angle of 180 degrees, much faster than the previous case. The input power decreased from 1.6 W to 1.3 W. The heating area was ~ 0.25 cm² and the power density was close to 5 W/cm². In both cases, resistances of the AgNW films slightly changed before folding started and remained nearly constant during folding. The resistance change occurred as the temperature ramped up until

reaching T_c for folding to start, which can be attributed to several factors. For the inward folding, increase of resistance might be due to thermal expansion of the PI sheet,^[37] and/or reduced conductivity of Ag at elevated temperatures. In the case of outward folding where higher input power was used, the decrease of resistance might be caused by the annealing effect, which become dominate at high temperature.^[38] In the case of total constraint, the PS sheet was heated through before folding started to occur. That is why a higher input power was needed. The nearly constant resistances during folding indicated the reliable heater performances in both cases.

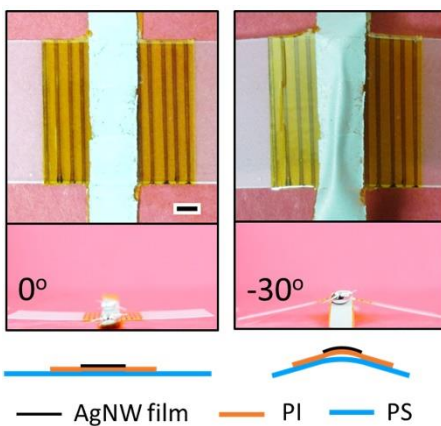


Figure 2.4 Deformation of heater in the case of partial constraint. Top: top view; middle: side view; bottom: schematic of cross section from side view. Scale bar: 2 mm.

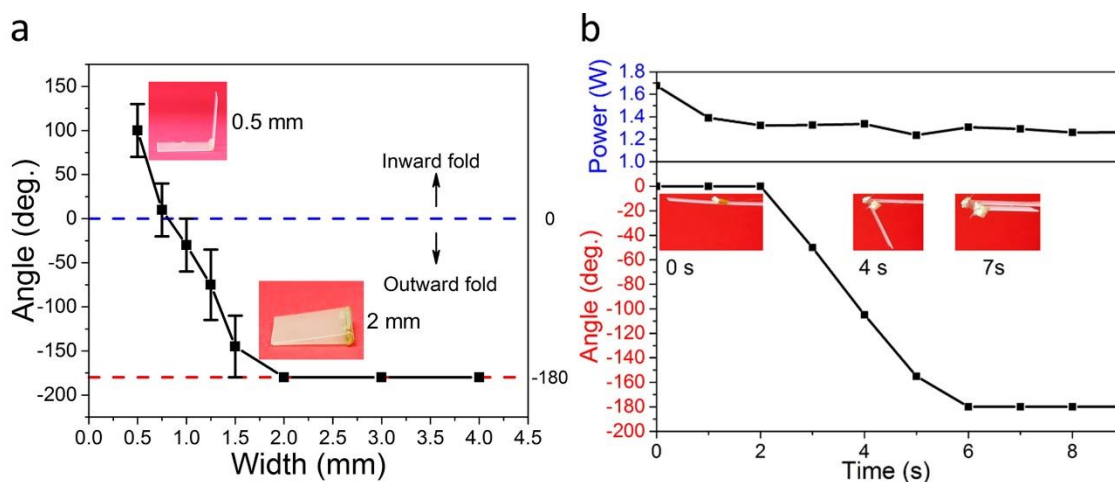


Figure 2.5 Folding results in the case of total constraint. (a) Relationship between folding angle and heater width. Insets are side views of the folded structures with 0.5 mm and 2 mm wide heaters; (b) Time response and power input during outward folding with a 2 mm wide heater. Insets show several snapshots during the folding.

2.3.6 Comparison with other folding methods for SMP

Now we can compare our method with the three methods for folding SMPs as mentioned in the Introduction. Wang et al. combined SMP sheet with a rigid heater to make a bimorph structure.^[28] But they covered the whole area of the SMP with another layer, thus the bimorph structure tended to wrap together instead of forming a sharp angle. In our case, sharp folding can be achieved due to the trigger of a local heater that serves as the hinge for the folding. Wood and co-workers folded various structures using a local heater.^[1, 30, 31] Their method is similar to our total-constraint case but with several differences: 1) They used three layers (SMP, heater and an additional rigid layer), while we used only the SMP and heater layers; 2) Their heater (Cu trace) was fabricated by lithography involving printing a mask and etching, while our AgNW heater was drop casted with a stencil; 3) Their maximum folding angle reported was 159 degrees while we can routinely achieve 180 degrees. On the other hand, the light-triggered local folding of SMP by Liu et al. is similar to our no-constraint case. Their method is simple, but the delivered power was relatively low (*e.g.* the SMP sheet has to be placed on a heated substrate to facilitate the folding^[33, 34]). Also it is quite challenging for their method to achieve sequential folding.^[39, 40]

2.3.7 Folded structures

To demonstrate the application of joule heating induced folding of SMPs, several structures were obtained by folding different hinges sequentially. Folding can be stopped at the desired angle by turning off the current. **Figure 2.6** shows several structures folded by inward and/or outward folding. **Figure 2.6a** shows digital numbers. 90 degrees were achieved

by inward folding (heaters was peeled off). 180 degrees (highlighted by black circles) were achieved by outward folding. **Figure 2.6b** shows a cube by inward folding (tiny notches are cut at the corner to make room for heater). **Figure 2.6c** shows a simple sailing boat by 180 degrees inward folding (heater was peeled off). **Figure 2.6d** shows a crane folded by inward folding (heater was peeled off).

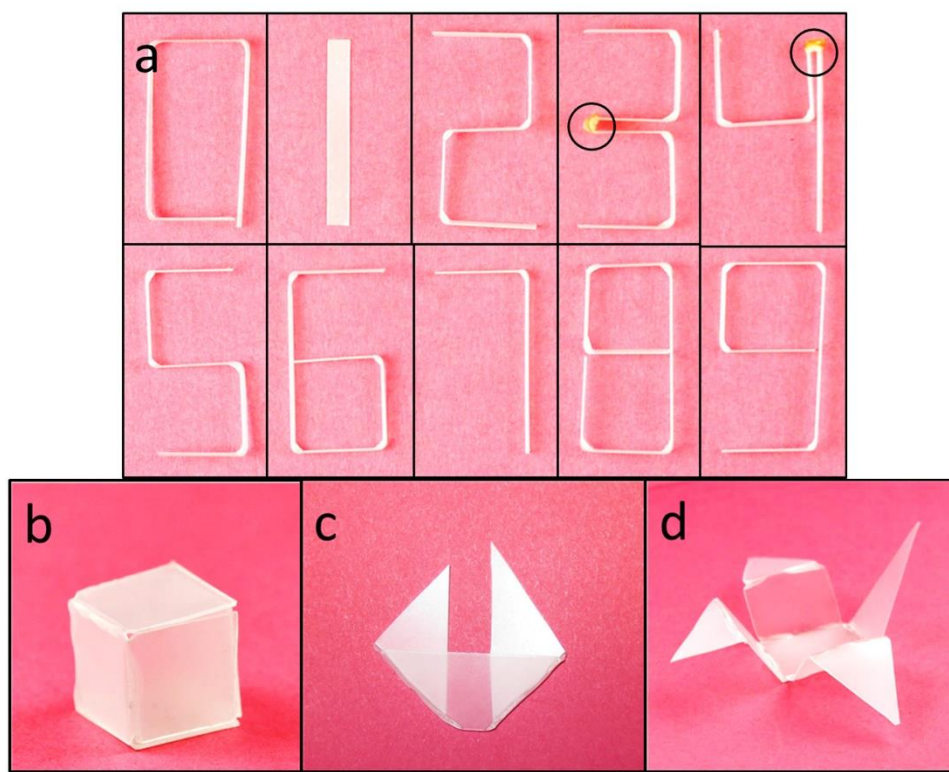


Figure 2.6 Structures folded with the AgNW/PI heaters. (a) Digital numbers (black circles indicate complete outward folding); (b) A cube folded by inward folding (heater was peeled off); (c) A simple sailing boat folded by 180 degrees inward folding (heater was peeled off); (d) A crane folded by inward folding (heater was peeled off).

2.4 Conclusion

In summary, we reported self-folding of pre-strained PS sheets triggered by local joule heating using flexible AgNW/PI heaters (with AgNW networks on top of PI sheets). Folding was caused by the temperature gradient across the thickness of a PS sheet. The folding behavior was found to depend on the mechanical interaction between the heater and the PS sheet. In the case of no constraint (weak interface between the heater and the PS sheet), the PS sheet folded towards the heater with the heater sliding and climbing up along the PS sheet. 180 degrees inward folding was achieved with the heater width over 1 mm. In the case of partial constraint (*i.e.* the heater delaminated from the PS sheet along the interface but fixed at two edges), the inward folding was resisted and outward folding became possible. In the case of total constraint (*i.e.* the heater fixed to the PS), the inward folding transitioned to the outward folding with the increasing heater width. 180 degrees outward folding was achieved with the heater width over 1.5 mm. Several structures including numbers from zero to nine, a cube, a boat and a crane were folded using the inward and/or the outward folding. The method is simple and can be used to fold structures with sharp angles in a sequential manner. The effect of interfacial interaction studied in this work can be extended to other folding mechanisms triggered by stimuli that are in contact with the structures to be folded.

Supplementary Information (SI)

2.S1 Failure of AgNW thin film directly coated on PS substrate

If the heater was fabricated by coating AgNW directly on top of PS, it tended to fail before folding occurs. This might be due to non-uniform heating of the PS. Hot spots can be generated where temperature was higher than the surrounding area. These hot spots shrank faster, thus generated local tensile strain on the surrounding area of PS substrate and the AgNW film on top, which lead to cracking of the AgNW film. **Figure 2.S1** shows cracks in the AgNW film.

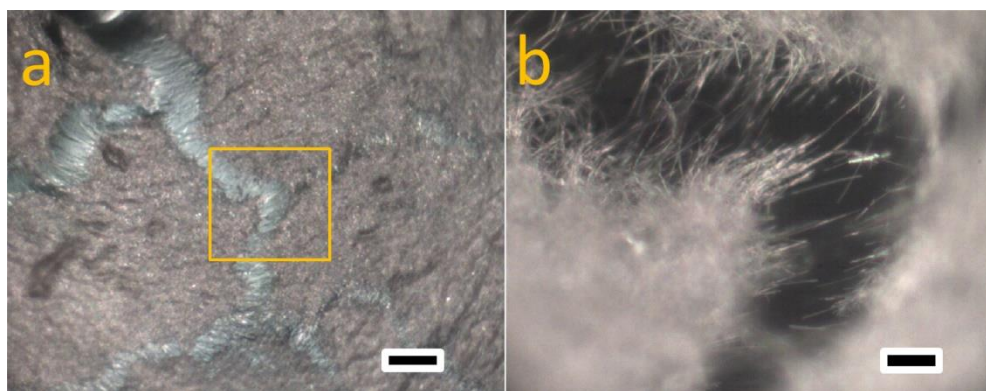


Figure 2.S1 Failure of an AgNW film heater on PS. (b) High magnification image of the highlighted region in (a). Scale bars: (a) 100 μm ; (b) 20 μm .

2.S2 Temperature characterization by IR camera

Heater temperature was characterized by a IR camera. **Figure 2.S2a** shows the temperature evolution of a heater when different input powers were applied. Constant current was applied for each power. With higher input power, higher equilibrium temperature was obtained. When current was turned off, the temperature decreased rapidly (decreased 20 degrees in less than 5 seconds). This explained why the folding can be stopped by turning off the current. The heater did not need to reach steady state to start the folding. With a high input power, it can reach the threshold temperature for shrinkage before reaching steady state.

Figure 2.S2b shows the IR images of PI heater at the corresponding input power of **Figure 2.S2a**. Heater appeared darker than the surrounding area (PS), which can be explained by working principle of the IR camera. IR camera measures radiance from the surface, which is determined by temperature and emissivity of the object. The color bar is based on the radiance. Brighter color corresponds to higher radiance. The emissivity is needed to get the correct temperature.^[41] AgNW heater appeared colder in IR image. This is due to the ultralow emissivity of AgNW.^[42] The emissivity value of AgNW was calibrated (~0.12). **Figure 2.S3** shows the IR images of a heater during folding. The heater was bonded to PS with superglue. Outward folding (folding against heater) occurred when temperature was about 140 degrees.

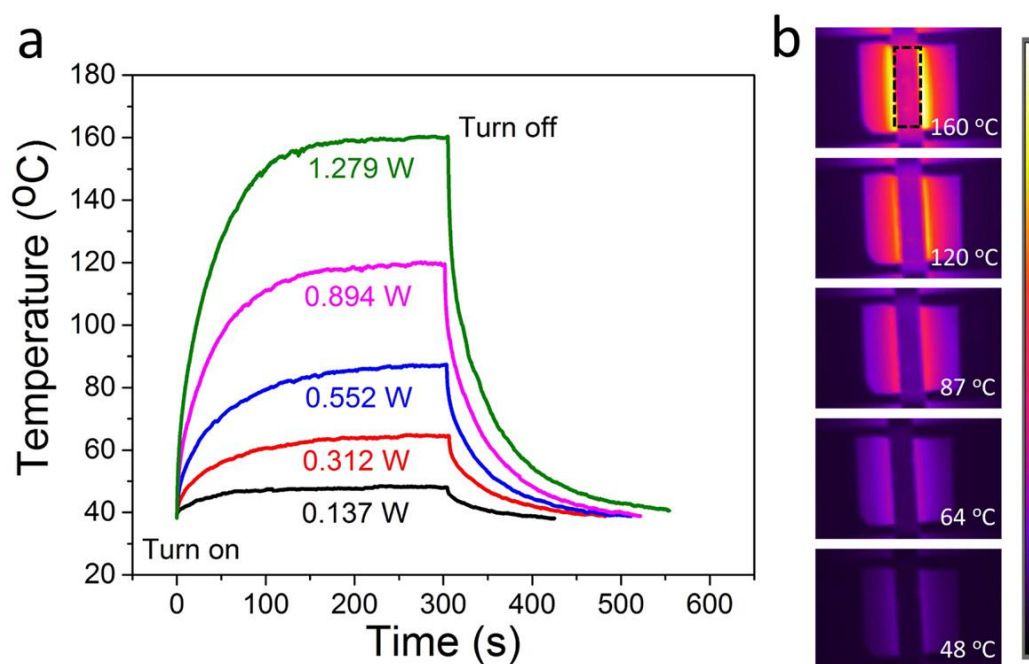


Figure 2.S2 Characterization of the heater using IR camera. (a) Temperature evolution of the heater at different input powers. (b) IR image of the heater at the corresponding input power of (a). The temperatures shown in (a) were the average temperatures in the area highlighted by the black dash line. A piece of PS without pre-strain was attached below the heater in order to replicate the condition for folding.

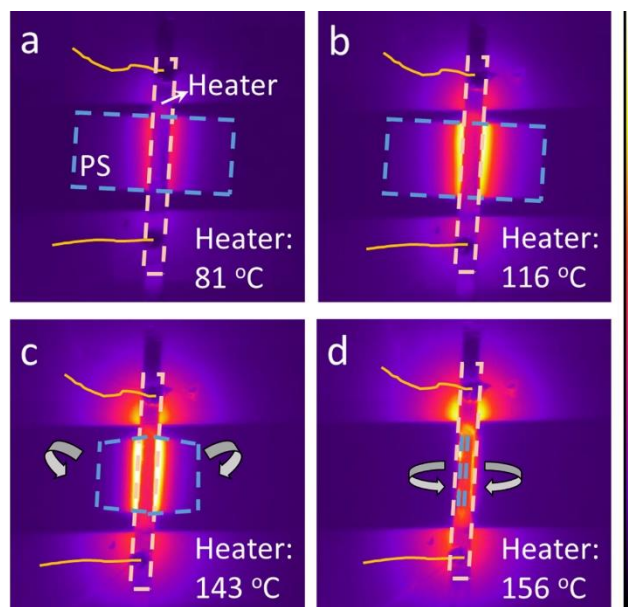


Figure 2.S3 IR image of a heater during outward folding. The heater is illustrated by yellow dash line and the PS sheet illustrated by blue dash line. PS sheet folded downwards.

2.S3 Folding results without constraint

The result is shown in **Figure 2.S4**.

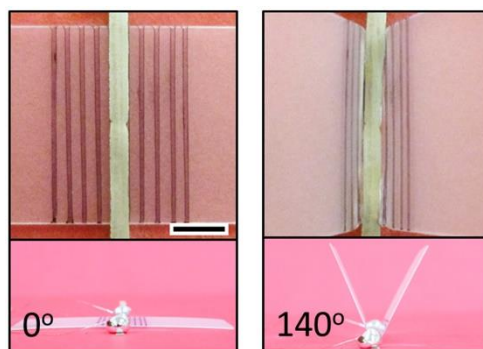


Figure 2.S4 Inward folding with a 0.5 mm wide heater. Scale bar: 2 mm.

2.S4 Geometric calculation of the heater climbing up process

Without constraint, heater tended to slide on PS to accommodate the folding. It cannot remain in conformal contact with PS during folding. Instead, the central part delaminated from PS while the edges slid along PS. This is shown schematically in **Figure 2.S5a**. The chord length was measured from the top view image (as the projected width of heater). From this chord length and the folding angle, the arc shape of PS beneath the heater can be determined (shown below). Note that central angle of the arc was equal to the folding angle. The shape of heater was also approximated by an arc, whose length was constant during folding. Once the arcs of PS and heater were determined, the displacement of the center relative to the edge can be determined. The gap between heater and PS (at the center of heater) was calculated and shown in **Figure 2.S5b**. The heater buckled considerably as a result of compression during the folding. The initial chord length was 2.3 mm, equal to the heater width. It was reduced to 2.13 mm when the heater was folded to 180 degrees. Initially, the heater and PS were in intimate contact. As folding continued, the gap between heater and PS increased. The gap at the center was 0.69 mm when PS was folded to 180 degrees.

Calculation of the arc shape from chord length and central angle is shown in **Figure 2.S6**. Central angle (α) is equal to folding angle. Chord length (l) was measured from the projected width of heater. Radius of curvature (R) can be calculated from **Equation 2.S1**. It needs to be noted that the radius of curvature might be bigger than the ideal case, since shrinkage of top surface might be incomplete and bottom surface might also shrink.

$$\sin\left(\frac{\alpha}{2}\right) = \frac{l/2}{R} \quad (2.S1)$$

The heater was also approximated by an arc. As shown in **Figure 2.S7**, the arc length (d) was equal to heater width measured from the initial configuration. Chord length (l) was measured from the top view image. Radius (R') and central angle (α') can be calculated from **Equations 2.S2** and **2.S3**.

$$\sin\left(\frac{\alpha'}{2}\right) = \frac{l/2}{R'} \quad (2.S2)$$

$$\alpha' = \frac{d}{R'} \quad (2.S3)$$

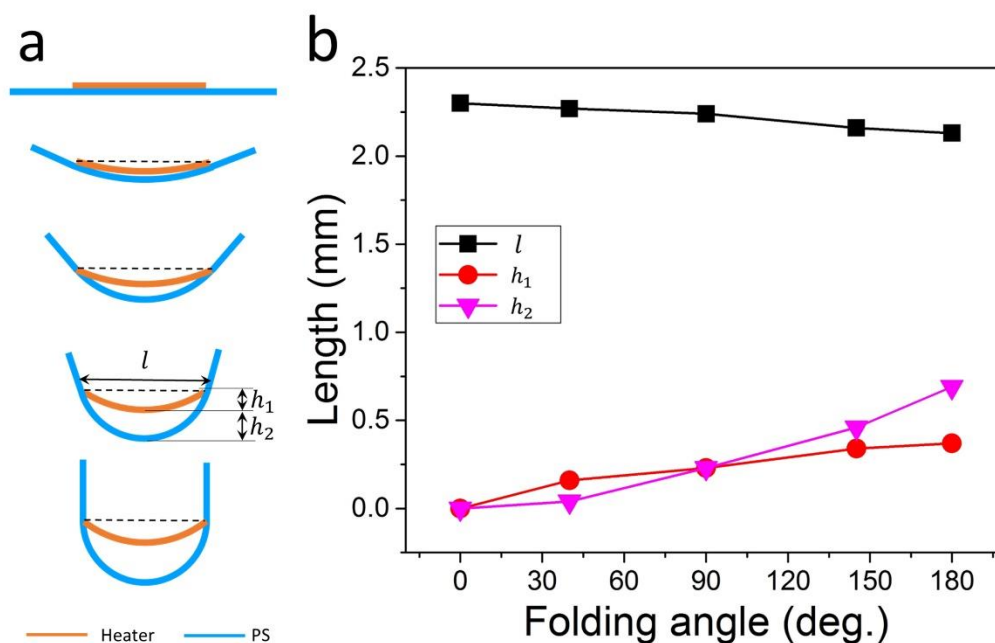


Figure 2.S5 Heater morphology during inward folding. (a) Schematics of cross sections of the heater on PS during folding. (b) The chord length and gaps between the heater and PS as a function of folding angle.

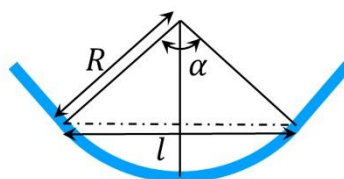


Figure 2.S6 Calculation of the arc from the chord length and central angle of the PS sheet.

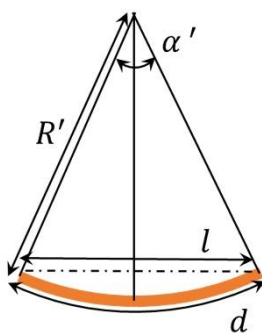


Figure 2.S7 Calculation of the arc from chord length and arc length of the heater.

2.S5 Folding with partial constraint

Heater can be anchored at two edges by bare tapes. In this case, sliding of the heater was not allowed. However, delamination of heater can still occur due to the weak adhesion. Inward folding was suppressed. **Figure 2.S8** shows folding results with a 0.5 mm wide heater with both edges of the heater constrained.

The sliding of heater can be partly suppressed by using bare tape on one side of the heater. **Figure 2.S9** shows the heater morphology during folding with the left edge of the heater constrained. Complete inward folding can be obtained in this case.

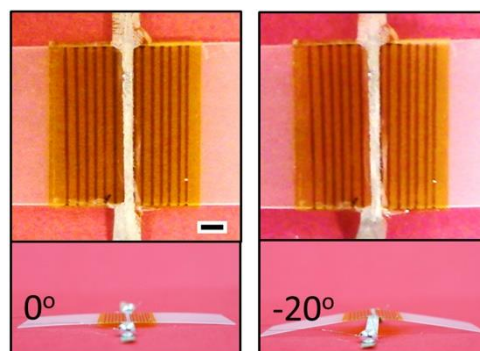


Figure 2.S8 Folding results with a 0.5 mm wide heater under partial constraint. Bare tape was applied on both edges to prevent sliding of the heater. Scale bar: 2 mm.

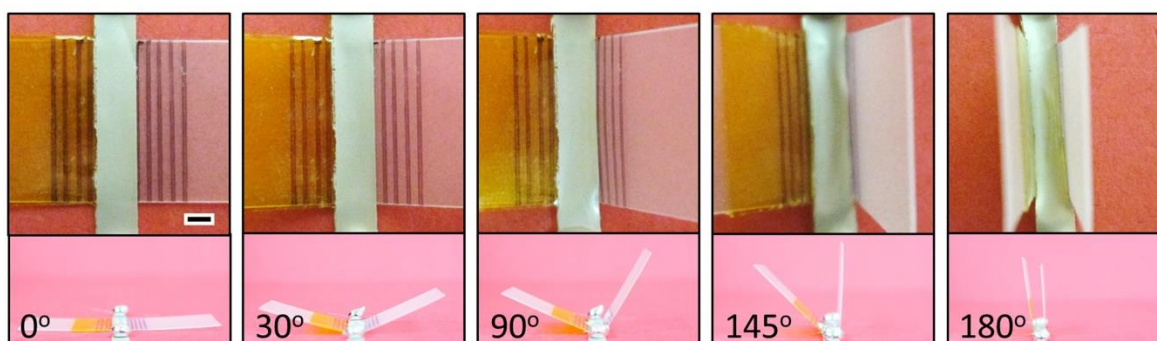


Figure 2.S9 Heater morphology during folding with bare tape on the left side to prevent sliding of the heater from left side. Scale bar: 2 mm.

2.S6 Finite element modeling

To achieve outward folding, bottom side needs to be heated up. As heat transferred to the bottom side through the thickness, it also spread in plane laterally. Thus an area beyond the heater on top surface can be heated up. We call this extra heated area. We used finite element analysis (FEA) to model the steady state temperature distribution. ANSYS version 16.1 was used for the modeling. A constant temperature (155 °C) at heater position was applied. Convective boundary condition was applied to the rest area. Ambient temperature was set to 25 °C, and convective heat transfer coefficient was set to $30 \text{ Wm}^{-1}\text{K}^{-1}$. Table S1 lists the material constants used in the finite element model. **Figure 2.S10** shows the temperature distributions across the PS for heaters with different widths. Extra heated area was found to be independent of the heater width, for a given PS thickness. But a wider heater can cause a wider area on bottom side to be heated up. This explained why narrow heater caused inward folding, while wide heater lead to outward folding (in the case of total constraint).

Transient FEA analysis was also performed to show the temperature evolution in the thickness direction as well as the lateral direction. **Figure 2.S11** shows the temperature distribution across the PS sheet as a function of time for a 2 mm heater. Constant heat flux boundary condition was assumed at the heater-PS interface. Heat flux was 6900 Wm^{-2} . This corresponded to 0.17 W (heat flux times heating area of 24 mm^2) of Joule heating power. Steady-state temperature at the heater position was about 155 °C. From the transient analysis, the temperature across the PS layer approached steady state in about 25 seconds

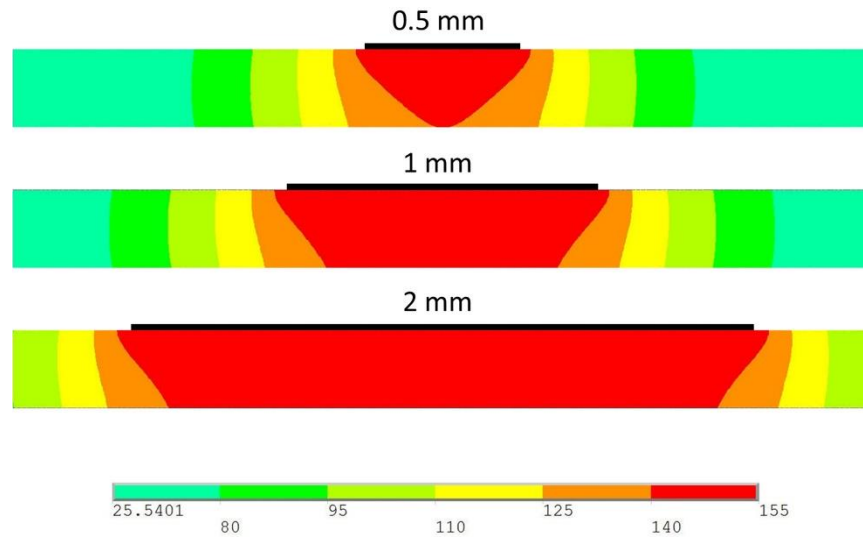


Figure 2.S10 Temperature distribution across the PS layer under the heater with different widths (FEA steady state analysis). The heater width is indicated by black line.

Table 1.S1 Material properties of PS used in finite element model.

Thermal conductivity	$0.14 \text{ W m}^{-1} \text{ K}^{-1}$
Density	1050 kg m^{-3}
Specific heat	$1300 \text{ J kg}^{-1} \text{ K}^{-1}$

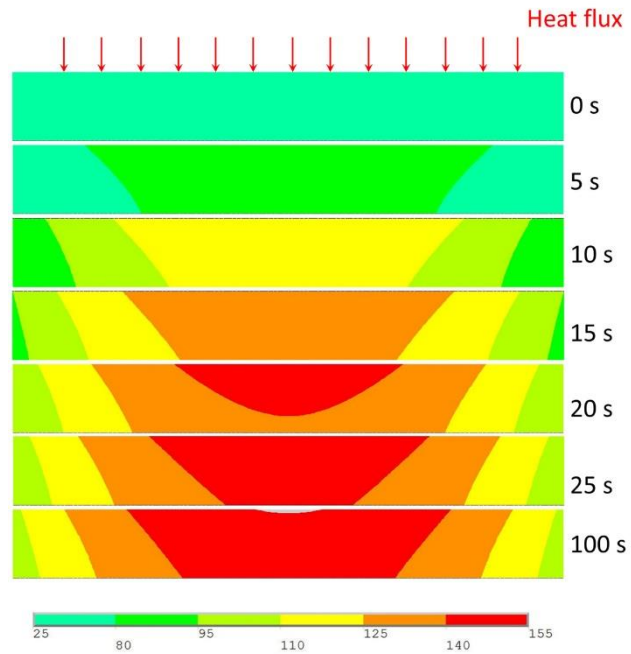


Figure 2.S11 Temperature evolution across the PS layer (FEA transient state analysis).

2.S7 Folding results in the case of total constraint

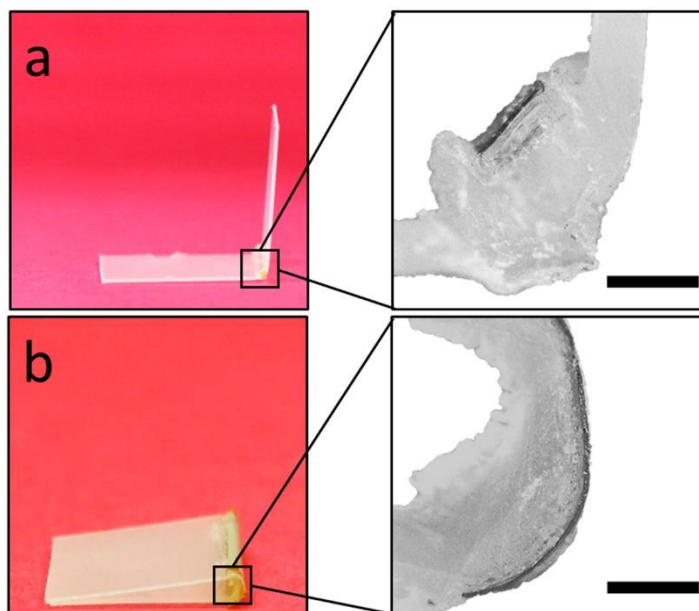


Figure 2.S12 Folding results in the case of total constraint. (a) Inward folding with a 0.5 mm wide heater. (b) Complete outward folding with a 2 mm wide heater. The inset in (a) and (b) shows optical microscopic images of the hinge region. Scale bars: 500 μm .

2.S8 Bimorph model analysis

The outward folding when PI heater was bonded to PS using super glue was analyzed using bimorph model.^[43] As shown in **Figure 2.S13**, the blue layer is PS and yellow layer is PI. The thicknesses of the two layers are $h_1 = 0.025mm$ and $h_2 = 0.25mm$. The Young's modulus are $E_1 = 2000 MPa$ and $E_2 = 1 MPa$. Width (perpendicular to the page) W can be unit width.

The forces acting on the PI layer can be represented by an axial compressive force P_1 and a bending moment M_1 . The forces acting on the PS layer can be represented by an axial tensile force P_2 and a bending moment M_2 . The condition of equilibrium requires that:

$$P_1 = P_2 = P \quad (2.S4)$$

$$M_1 + M_2 = \frac{P_1 h_1}{2} + \frac{P_2 h_2}{2} \quad (2.S5)$$

Bending moment can be related to the in radius of curvature R :

$$M_1 = \frac{E_1 I_1}{R} \quad (2.S6)$$

$$M_2 = \frac{E_2 I_2}{R} \quad (2.S7)$$

The area moment of inertia can be calculated using the following formula:

$$I_1 = \frac{w h_1^3}{12} \quad (2.S8)$$

$$I_2 = \frac{wh_2^3}{12} \quad (2.S9)$$

Combine **Equations (2.S4-2.S9)** one can get the relationship between axial force and radius of curvature:

$$\frac{E_1wh_1^3}{12R} + \frac{E_2wh_2^3}{12R} = P\frac{h_1}{2} + P\frac{h_2}{2} \quad (2.S10)$$

Another equation can be obtained by considering that there is no sliding at the interface. Strain on both surface must be equal at the interface. Assume PS layer shrinks to 50% and there is no shrinkage or expansion in PI layer.

$$-50\% + \frac{P}{E_2wh_2} + \frac{h_2}{2R} = -\frac{P}{E_1wh_1} - \frac{h_1}{2R} \quad (2.S11)$$

Substitutes in the materials properties and geometric parameters. The radius of curvature is calculated to be:

$$R = 0.504 \text{ mm} \quad (2.S12)$$

This is similar to the results by assuming one surface cannot shrink while the other shrink freely to 50% (which corresponds to 0.5 mm radius of curvature). Based on the **Equation 2.1** in the main text, the width required to be heated to achieve complete folding is

$$L = R\pi = 1.58 \text{ mm} \quad (2.S13)$$

It needs to be noted that this is an oversimplified model, since it neglects the thickness of the bilayer when calculating the radius of curvature. However, it does show that the radius of

curvature is quite small, which is comparable with the thickness of the bilayer structure. This analysis is similar to what has been reported in Bao's work.^[28]

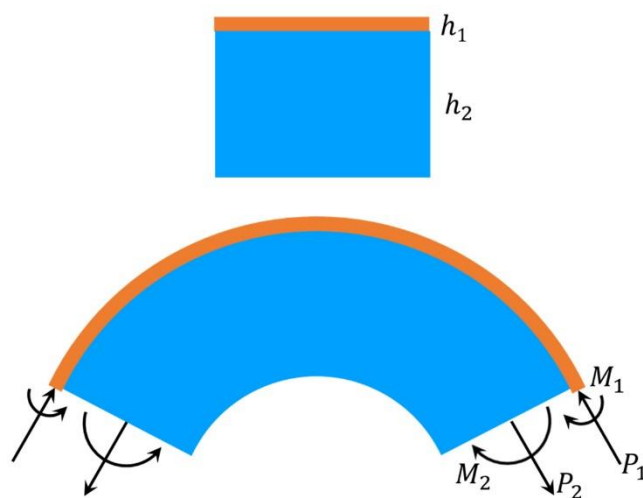


Figure 2.S13 Structure and force diagrams of the bilayer structure. Yellow layer: PI; blue layer: PS.

References

- [1] S. Felton, M. Tolley, E. Demaine, D. Rus, R. Wood, *Science* 2014, 345, 644.
- [2] R. Fernandes, D. H. Gracias, *Adv. Drug Deliv. Rev.* 2012, 64, 1579.
- [3] X. Guo, H. Li, B. Y. Ahn, E. B. Duoss, K. J. Hsia, J. A. Lewis, R. G. Nuzzo, *Proc. Natl. Acad. Sci. USA* 2009, 106, 20149.
- [4] T. G. Leong, B. R. Benson, E. K. Call, D. H. Gracias, *Small* 2008, 4, 1605.
- [5] J. Shintake, S. Rosset, B. Schubert, D. Floreano, H. Shea, *Adv. Mater.* 2016, 28, 231.
- [6] Z. M. Song, T. Ma, R. Tang, Q. Cheng, X. Wang, D. Krishnaraju, R. Panat, C. K. Chan, H. Y. Yu, H. Q. Jiang, *Nat. Commun.* 2014, 5, 3140.
- [7] S. Xu, Z. Yan, K. I. Jang, W. Huang, H. R. Fu, J. Kim, Z. Wei, M. Flavin, J. McCracken, R. Wang, A. Badea, Y. Liu, D. Q. Xiao, G. Y. Zhou, J. Lee, H. U. Chung, H. Y. Cheng, W. Ren, A. Banks, X. L. Li, U. Paik, R. G. Nuzzo, Y. G. Huang, Y. H. Zhang, J. A. Rogers, *Science* 2015, 347, 154.
- [8] Y. H. Zhang, Z. Yan, K. W. Nan, D. Q. Xiao, Y. H. Liu, H. W. Luan, H. R. Fu, X. Z. Wang, Q. L. Yang, J. C. Wang, W. Ren, H. Z. Si, F. Liu, L. H. Yang, H. J. Li, J. T. Wang, X. L. Guo, H. Y. Luo, L. Wang, Y. G. Huang, J. A. Rogers, *Proc. Natl. Acad. Sci. USA* 2015, 112, 11757.
- [9] Z. Yan, F. Zhang, J. C. Wang, F. Liu, X. L. Guo, K. W. Nan, Q. Lin, M. Y. Gao, D. Q. Xiao, Y. Shi, Y. T. Qiu, H. W. Luan, J. H. Kim, Y. Q. Wang, H. Y. Luo, M. D. Han, Y. G. Huang, Y. H. Zhang, J. A. Rogers, *Adv. Funct. Mater.* 2016, 26, 2629.
- [10] P. Wang-Iverson, R. J. Lang, M. Yim, *Origami 5 Fifth International Meeting of Origami Science, Mathematics, and Education*, CRC Press, Boca Raton 2011.
- [11] E. Hawkes, B. An, N. Benbernou, H. Tanaka, S. Kim, E. Demaine, D. Rus, R. Wood, *Proc. Natl. Acad. Sci. USA* 2010, 107, 12441.
- [12] C. Py, P. Reverdy, L. Doppler, J. Bico, B. Roman, C. N. Baroud, *Phys. Rev. Lett.* 2007, 98, 156103.
- [13] J. Ryu, M. D'Amato, X. Cui, K. N. Long, H. J. Qi, M. L. Dunn, *Appl. Phys. Lett.* 2012, 100, 161908.
- [14] E. Smela, O. Inghanas, I. Lundstrom, *Science* 1995, 268, 1735.

- [15] J. H. Na, A. A. Evans, J. Bae, M. C. Chiappelli, C. D. Santangelo, R. J. Lang, T. C. Hull, R. C. Hayward, *Adv. Mater.* 2015, 27, 79.
- [16] G. Stoychev, S. Zakharchenko, S. b. Turcaud, J. W. Dunlop, L. Ionov, *ACS Nano* 2012, 6, 3925.
- [17] K. Otsuka, C. M. Wayman, *Shape memory materials*, Cambridge University Press, New York 1998.
- [18] Q. Zhao, W. Zou, Y. Luo, T. Xie, *Sci. Adv.* 2016, 2, e1501297.
- [19] Y. Liu, J. Genzer, M. D. Dickey, *Prog. Polym. Sci.* 2016, 52, 79.
- [20] Q. Zhao, H. J. Qi, T. Xie, *Progress in Polymer Science* 2015, 49, 79.
- [21] A. Lendlein, H. Y. Jiang, O. Junger, R. Langer, *Nature* 2005, 434, 879.
- [22] A. Lendlein, S. Kelch, *Angew. Chem. Int. Ed. Engl.* 2002, 41, 2035.
- [23] Y. Liu, K. Gall, M. L. Dunn, P. McCluskey, *Mech. Mater.* 2004, 36, 929.
- [24] Q. Zhang, J. Wommer, C. O'Rourke, J. Teitelman, Y. Tang, J. Robison, G. Lin, J. Yin, *Extreme Mech. Lett.* 2016, 11, 111.
- [25] J. W. Cho, J. W. Kim, Y. C. Jung, N. S. Goo, *Macromol. Rapid Commun.* 2005, 26, 412.
- [26] W. Huang, B. Yang, L. An, C. Li, Y. Chan, *Appl. Phys. Lett.* 2005, 86, 114105.
- [27] X. J. Han, Z. Q. Dong, M. M. Fan, Y. Liu, Y. F. Wang, Q. J. Yuan, B. J. Li, S. Zhang, *Macromol. Rapid Commun.* 2012, 33, 1055.
- [28] H. Wang, Y. Wang, B. C. K. Tee, K. Kim, J. Lopez, W. Cai, Z. Bao, *Adv. Sci.* 2015, 2, 1500103.
- [29] M. T. Tolley, S. M. Felton, S. Miyashita, D. Aukes, D. Rus, R. J. Wood, *Smart Mater. Struct.* 2014, 23, 094006.
- [30] S. Felton, K. Becker, D. Aukes, R. Wood, J. Micromech. Microeng. 2015, 25, 085004.
- [31] S. M. Felton, M. T. Tolley, B. Shin, C. D. Onal, E. D. Demaine, D. Rus, R. J. Wood, *Soft Matter* 2013, 9, 7688.
- [32] D. Davis, B. Chen, M. D. Dickey, J. Genzer, *J. Mech. Robot.* 2016, 8, 031014.
- [33] Y. Liu, J. K. Boyles, J. Genzer, M. D. Dickey, *Soft Matter* 2012, 8, 1764.

- [34] Y. Liu, R. Mailen, Y. Zhu, M. D. Dickey, J. Genzer, *Phys. Rev. E* 2014, 89, 042601.
- [35] Y. Sun, Y. Yin, B. T. Mayers, T. Herricks, Y. Xia, *Chem. Mater.* 2002, 14, 4736.
- [36] Q. Huang, W. Shen, X. Fang, G. Chen, J. Guo, W. Xu, R. Tan, W. Song, *RSC Adv.* 2015, 5, 45836.
- [37] X. Y. Zeng, Q. K. Zhang, R. M. Yu, C. Z. Lu, *Adv. Mater.* 2010, 22, 4484.
- [38] T.-B. Song, Y. Chen, C.-H. Chung, Y. Yang, B. Bob, H.-S. Duan, G. Li, K.-N. Tu, Y. Huang, Y. Yang, *ACS Nano* 2014, 8, 2804.
- [39] Y. Lee, H. Lee, T. Hwang, J.-G. Lee, M. Cho, *Sci. Rep.* 2015, 5, 16544.
- [40] Y. Mao, K. Yu, M. S. Isakov, J. Wu, M. L. Dunn, H. J. Qi, *Scientific reports* 2015, 5, 13616.
- [41] R. P. Madding, "Emissivity measurement and temperature correction accuracy considerations", presented at *AeroSense'99*, 1999.
- [42] P.-C. Hsu, X. Liu, C. Liu, X. Xie, H. R. Lee, A. J. Welch, T. Zhao, Y. Cui, *Nano Lett.* 2014, 15, 365.
- [43] S. Timoshenko, *JOSA* 1925, 11, 233.

CHAPTER 3 Self-folding of Al foil with local bimorph actuator

3.1 Introduction

A flat bilayer sheet can be bent by mismatch strain across the layers.^[1] Both mechanical property (e.g. stiffness)^[2] and geometric shape (e.g. thickness, aspect ratio, orientation)^[3-6] can affect the bending behavior. Complex three-dimensional (3D) structures can be fabricated by bending two-dimensional (2D) precursors, which can take advantage of the well-developed fabrication technique in 2D structures.^[7-10] This approach is accessible to multiple materials systems, including metals,^[11, 12] semiconductors^[7-9] and polymers.^[10, 13] Potential applications of the technique include microelectromechanical systems (MEMS),^[14] optoelectronic devices,^[15, 16] biomedical applications,^[17, 18] sensors and actuators.^[19, 20]

For most cases, the strain is equi-biaxial. The bending behavior of a bilayer sheet under equi-biaxial mismatch strain has been studied for a long time.^[2-6] At small strain, the bilayer sheet curls equi-biaxially into a spherical surface. However, at large strain, spherical surface is not stable, because it is non-developable and involves stretching of the sheet, which is energetically much more expensive than bending. To reduce the strain energy, the sheet tends to curl along one direction, forming a cylindrical surface, which is developable and contains no stretching deformation.^[2, 4] The curling direction is affected by the in-plane aspect ratio of the sheet. A freestanding bilayer strip prefers to curl in the longitudinal direction, which has lower strain energy than transverse curling.^[4, 5]

The curling behavior of a bilayer sheet can be harnessed to make an actuating hinge and fold a passive sheet along a specific line.^[21] This provides an approach to fold origami

structures, i.e. fabricate 3D structures by folding 2D sheets along pre-defined creases. The folded origami structures can be applied in various areas, including packaging,^[22] metamaterials,^[23-25] drug containers^[26] and energy absorbers.^[27, 28] Typically, the actuating hinge is a strip of bilayer sheet aligned along the crease. Due to constraint from the passive sheet, the bilayer strip cannot curl in longitudinal direction. Instead, it curls in the transverse direction and folds the passive sheet along the crease.

In this chapter, the bilayer actuator was used to fold Al foil. Several origami structures were folded. Furthermore, anisotropic bending stiffness was used to tune the curling behavior of the passive sheet. Anisotropic bending stiffness was achieved via a topographical feature in the Al foil. The resulting passive sheet tends to curl in the softest direction, regardless of the orientation of the actuating hinge. By changing orientation of the softest bending direction in the passive sheet, various 3D curved surfaces can be obtained, including cylindrical, left-handed/right handed helical surfaces.

3.2 Materials and Methods

The passive sheet used in this work was made of Al foil (1100 Al sheet, McMaster-Carr, Atlanta, GA, USA). The bilayer sheet was made of pre-strained polystyrene (PS) sheet (Grafix Shrink Film) and Al foil, which were glued together using superglue (Loctite Liquid Professional Super Glue 20-Gram Bottle). The PS sheet shrinks equi-biaxially upon heating (150 °C), while the Al foil does not shrink. Actuating hinge was embedded by gluing a strip of PS sheet (aligned along the crease) on a large sheet of Al foil.

3.3 Results and Discussions

Figure 3.1 shows the curling behaviors of a freestanding bilayer actuator and one embedded in a passive sheet (Al foil). Stretching is energetically much more expansive than bending in Al foil. The foil tends to curl into a developable surface (cylindrical surface) to avoid stretching, i.e. it curls in one direction and remains straight in the perpendicular direction. The freestanding bilayer actuator curled in the longitudinal direction, as shown in **Figure 3.1a**. This state has lower strain energy than the transverse curling state.^[4-6] In contrast, when the actuator was embedded in an Al foil, it curled in the transverse direction, as shown in **Figure 3.1b**. The bilayer region curled, while the single layer Al foil (on two sides of the bilayer actuator) remained flat. The whole Al foil still took the form of a developable surface. From the experimental results, we can draw the conclusion that strain energy of transverse curling becomes lower than longitudinal curling when bilayer actuator is embedded in a passive Al foil.

Since the single layer of Al foil was not deformed in **Figure 3.1b**, the entire strain energy was due to the bending deformation of bilayer actuator. Thus, the strain energy for transverse curling is the same with and without the passive sheet. However, the strain energy for longitudinal curling will become higher with the passive sheet for the following reason. If the embedded bilayer actuator curls in the longitudinal direction, the single layer Al foil on two sides of the actuator cannot remain flat. They need to curl together with the bilayer region. This is shown in **Figure 3.5a**. In this way, the whole Al foil still curls into a cylindrical surface. The curling of passive sheet on two sides of the bilayer actuator generates extra strain energy, which scales linearly with the dimension (in the transverse direction) and elastic modulus,

cubically with the thickness of the passive sheet. At some point, for the embedded bilayer actuator, strain energy of transverse curling could become lower than longitudinal curling. As shown in **Figure 3.1b**, 2 mm of Al foil (thickness: 0.025 mm) in the transverse direction is enough to change the curling direction. As a comparison, when Al foil is replaced with a softer material (e.g. polyimide sheet), the extra strain energy may not be able to counter balance the energy difference between transverse and longitudinal curling. The whole passive sheet still curls in the longitudinal direction (See SI).

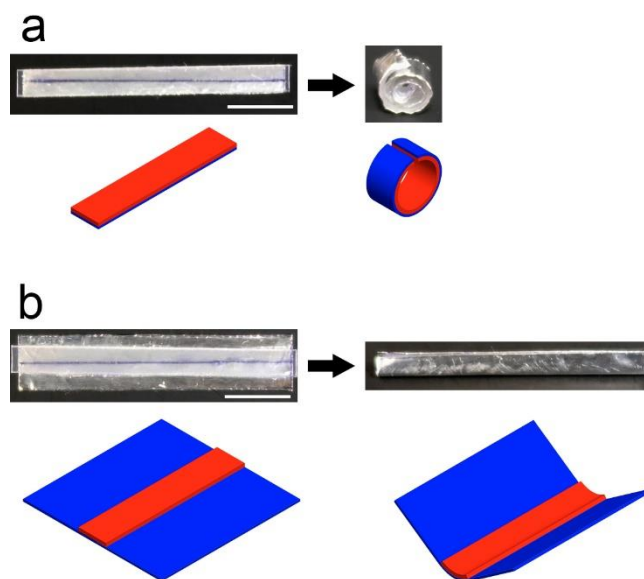


Figure 3.1 The curling behaviors of PS & Al bilayer sheet. (a) Isolated bilayer structure. (b) Bilayer structure embedded in a large passive sheet. Schematics of the curling process are shown below the optical images. Scale bars: 10 mm.

We have shown that Al foil can be folded by bilayer actuating hinge. Next, we study the parameters that affect the folding angle. As shown in **Figure 3.2a**, the bilayer region curls into an arc, while the single layer region remains straight and tangent to the arc. The folding angle, which is equal to the central angle of the arc (α), can be calculated from

$$\alpha = \frac{L}{R} * \frac{180 \text{ deg}}{\pi} \quad (3.1)$$

where L is the width of the bilayer region, R is the radius of curvature (measured to the interface between PS and Al). Here we neglect the thickness of Al foil (thickness of PS: 0.25 mm, thickness of Al: 0.025~0.05 mm) and assuming its dimension does not change during curling. The folding angle (α) as a function of the hinge width (L) is plotted in **Figure 3.2b**. Al foil with different thicknesses were folded. The experimental results were fitted with lines through the origin (**Equation 3.1**). The radius of curvature (R) can be obtained from the fitting, which is 0.67 mm for 0.025 mm thick foil, 1.08 mm for 0.038 mm thick foil and 2.49 mm for 0.05 mm thick foil. Smaller radius of curvature means sharper folding. To achieve complete folding (180 degrees), the hinge width L needs to be wider than πR . As shown in the plot, 2.1 mm wide PS strip can completely fold 0.025 mm thick foil, 3.4 mm wide PS strip can completely fold 0.038 mm thick foil, while 7.8 mm wide PS strip is required to completely fold 0.05 mm thick foil.

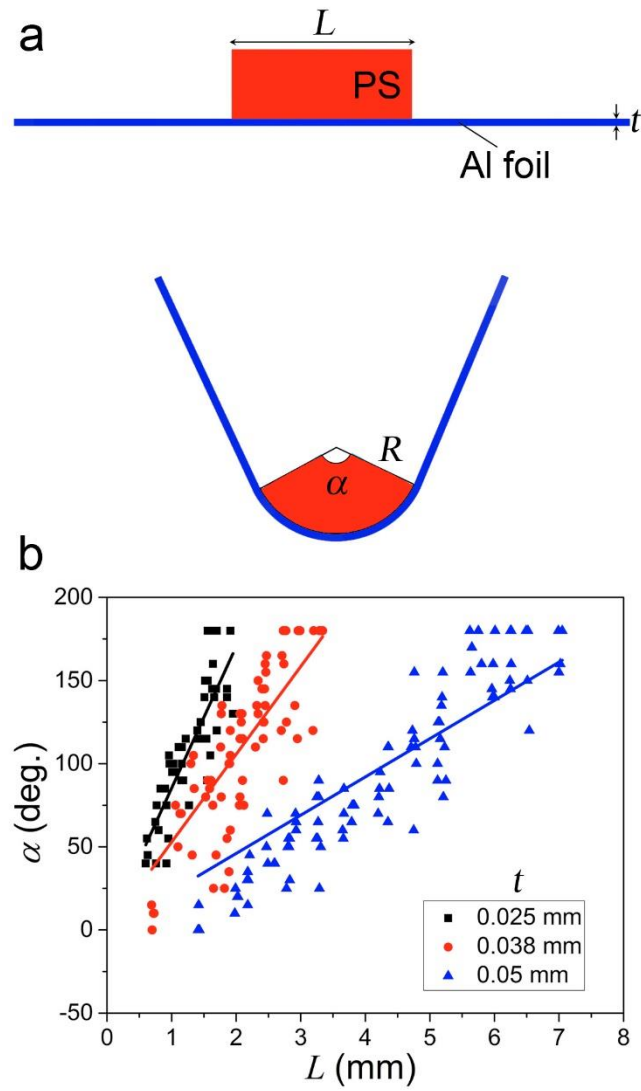


Figure 3.2 Folding angle caused by the actuating hinge. (a) Schematic of the folding. (b) Folding angle (α) as a function of hinge width (L). Fitting lines are included.

Next, we utilized the actuating hinge to fold origami structures of Al foil. **Figure 3.3** shows some flat origami structures. Only complete folding (which is also called flat folding in origami) is used. The folding is stopped mechanically at 180 degrees. It has been proved that a strip can be folded into a flat origami that takes the shape of any polygonal region (silhouette origami).^[29] **Figure 3.3a** shows the method of turning an Al strip by a desired angle. The turning angle can be controlled by the orientation of the actuating hinge. By turning the Al strip to specific angles at specific locations, various 2D shapes can be created. **Figure 3.3b** shows that Al strips were folded into letters “N”, “C”, “S” and “U”. The actuating hinge can also be used to open a pre-folded structure, as shown in **Figure 3.3c**. The initial state was a plastically folded structure (peripheral panels lie within the central panel). Upon heating, the actuating hinges folded the peripheral panels in the outward direction, and deployed the structure. Star-shape polygons were obtained. The deployment doubled the areas of the structures.

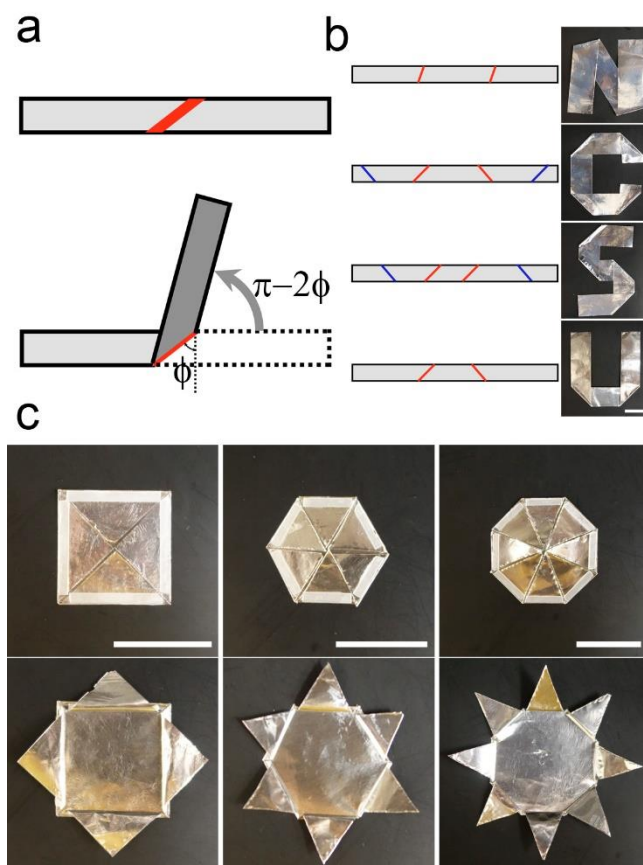


Figure 3.3 Flat origami structures. (a) Schematic showing turning a strip by desired angle. (b) Some letters folded from a strip of Al foil. Left is the crease pattern (blue: mountain fold; red: valley fold). (c) Deployment of pre-folded structures. Scale bars: 30 mm.

In the folding of an individual crease using the actuating hinge, angle variation was quite large (except at 180 degrees), as shown in **Figure 3.2b**. However, when multiple creases were folded in a parallel manner, the angle variation became reduced.^[30] This is due to the coupling effect between adjacent creases. **Figure 3.4** shows the folding of Miura-ori structure.^[31, 32] **Figure 3.4a** shows the crease patterns. The creases are coupled in such a way that all the creases are folded synchronously, resulting in a structure with only one degree of freedom. Folding result is shown in **Figure 3.4b**. A flat Al foil was folded into a corrugated sheet. The folding reduced the dimension in lateral directions and increased the dimension in the vertical direction. This increased the effective thickness of the structure. Bending stiffness of the sheet, which scales cubically with the thickness, was also increased. This is illustrated in **Figure 3.4c**, where two bridges made of Al foil were used to support glass slides. The left bridge was made of flat Al foil, while the right one was made of corrugated Al foil. As the folding reduced the projected area of the Al foil, the areal density was increased. To compensate for this effect, we used double layers flat Al foil in the left bridge and single layer corrugated foil in the right bridge, resulting in equal amounts of Al foil in the two bridges. The corrugated foil bridge greatly outperformed the flat one. The flat bridge collapsed under 3 glass slides, while the corrugated one can support 16 glass slides without collapsing. The supported weight (74.9 g) was much heavier than the weight of the bridge itself (1.7 g).

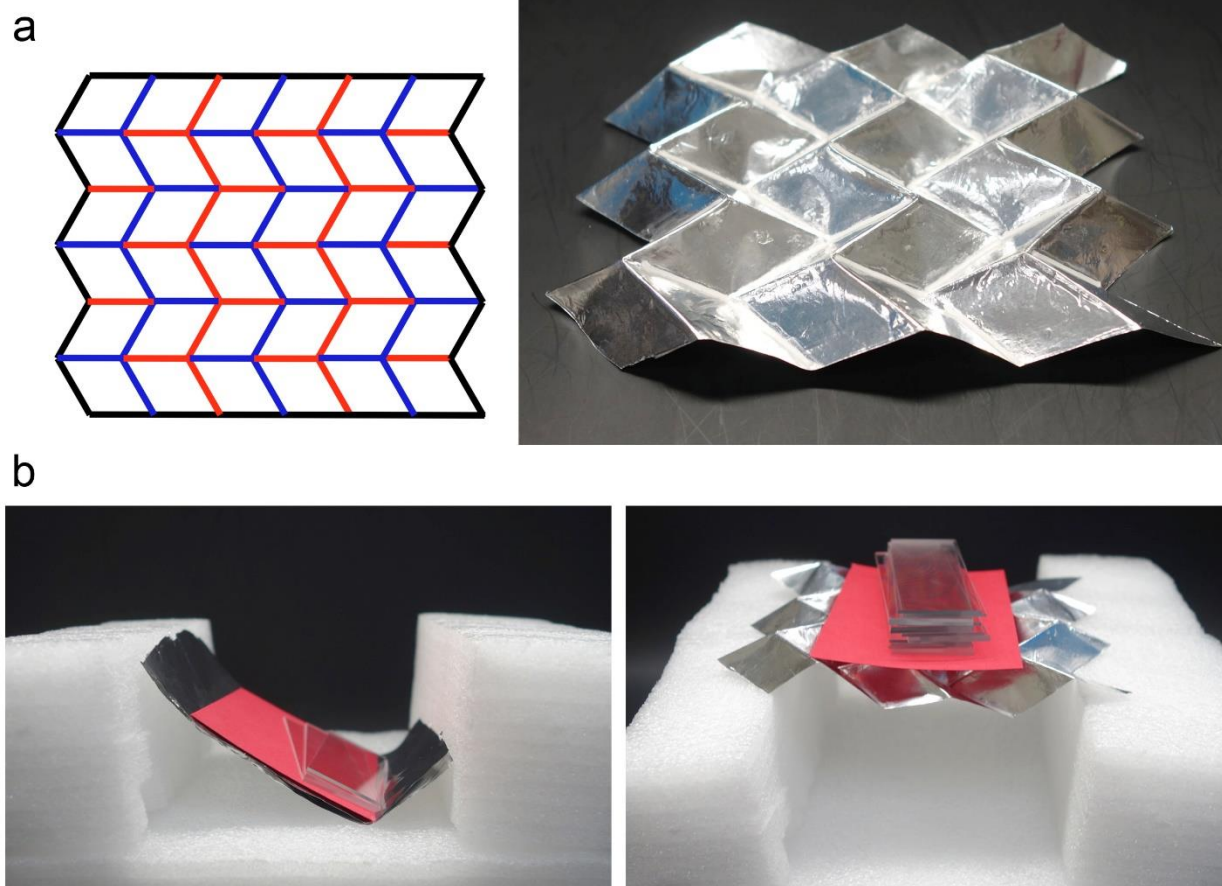


Figure 3.4 Miura-ori structure. (a) Crease patten (blue: mountain fold; red: valley fold). (b) Optical images of Miura-folded Al foil. (c) Using Miura-folded foil as a bridge. Left: two layers of flat Al foil; right: one layer of Miura-folded Al foil.

In the above experiments, the passive sheet had isotropic stiffness, and the curling direction was determined by the orientation of the actuating hinge. If the passive sheet has anisotropic stiffness, the curling direction will be influenced by orientation of the passive sheet. Here, we used a topographical feature to bestow anisotropic stiffness to the Al foil. The idea of making anisotropic passive sheet was inspired by the flexible dermal armors of animals.^[33, 34] The dermal armors exhibit different flexibility under different loading modes, e.g. allows the body movement but resists the punctation. Here, a pleat folded Al foil was used as the passive sheet. The schematic of the structure is shown in **Figure 3.5a**. Note that there are three layers of Al foil in the vertical direction. When the pleated Al foil is bent perpendicular to the pleat lines (**Figure 3.5a**, right panel), only the inner layer of Al foil (in purple) is bent. The outer two layers of Al foil remains flat and rotates about the pleat lines, similar to the rotation of scales on fish skin. As only one layer of Al foil contributes to the bending resistance, the bending stiffness is relatively low in this direction, making it the softest bending direction. When the sheet is bent along other directions, the bending stiffness becomes much higher since rotation of the pleats is not allowed, and all three layers of Al foil are deformed.

To demonstrate the effect of anisotropic bending stiffness on curling behavior, we changed the angle between pleat lines and actuating hinge. As shown in **Figure 3.5b**, **3.5c** and **3.5d**, a strip of actuating hinge was embedded in a rectangular sheet of pleated foil. The actuating hinge was oriented in the longitudinal direction of the rectangular sheet. In **Figure 3.5b**, pleat lines were perpendicular to the actuating hinge. In **Figure 3.5c** and **3.5d**, they were at an oblique angle (± 45 degrees) to the actuating hinge. The pleated foil tends to curl in the softest bending direction (the direction perpendicular to the pleat lines) to minimize the strain

energy. In **Figure 3.5b**, the pleated foil curled into a cylindrical surface, whose axis is parallel to the pleat lines. Note that bilayer actuator curled in the longitudinal direction in this case. Also, the radius of curvature was larger than previous case, because the curling of pure passive sheet on two sides of the actuator increased the bending resistance. In **Figure 3.5c** and **3.5d**, the pleated foils curled into left-handed/right-handed helical structures. The helical structures can be regarded as part of a cylindrical surface, whose axis is parallel to the pleat lines. The pleat lines remained straight during the curling process.

Anisotropic stiffness has been used by others to control the curling behavior of 2D sheets. One approach is to use anisotropic property of a single crystal.^[8] Along certain crystal orientation, the stiffness is lower and bending is more favorable. For materials with isotropic property (e.g. polycrystals or polymers), anisotropy can be induced by topographical features. Besides the abovementioned pleat folding, trench array was used by others to guide the curling direction of thin sheet.^[35, 36] In the trench region, bending stiffness is greatly reduced (to the third power of thickness). This makes bending perpendicular to the trench lines much easier than along them.

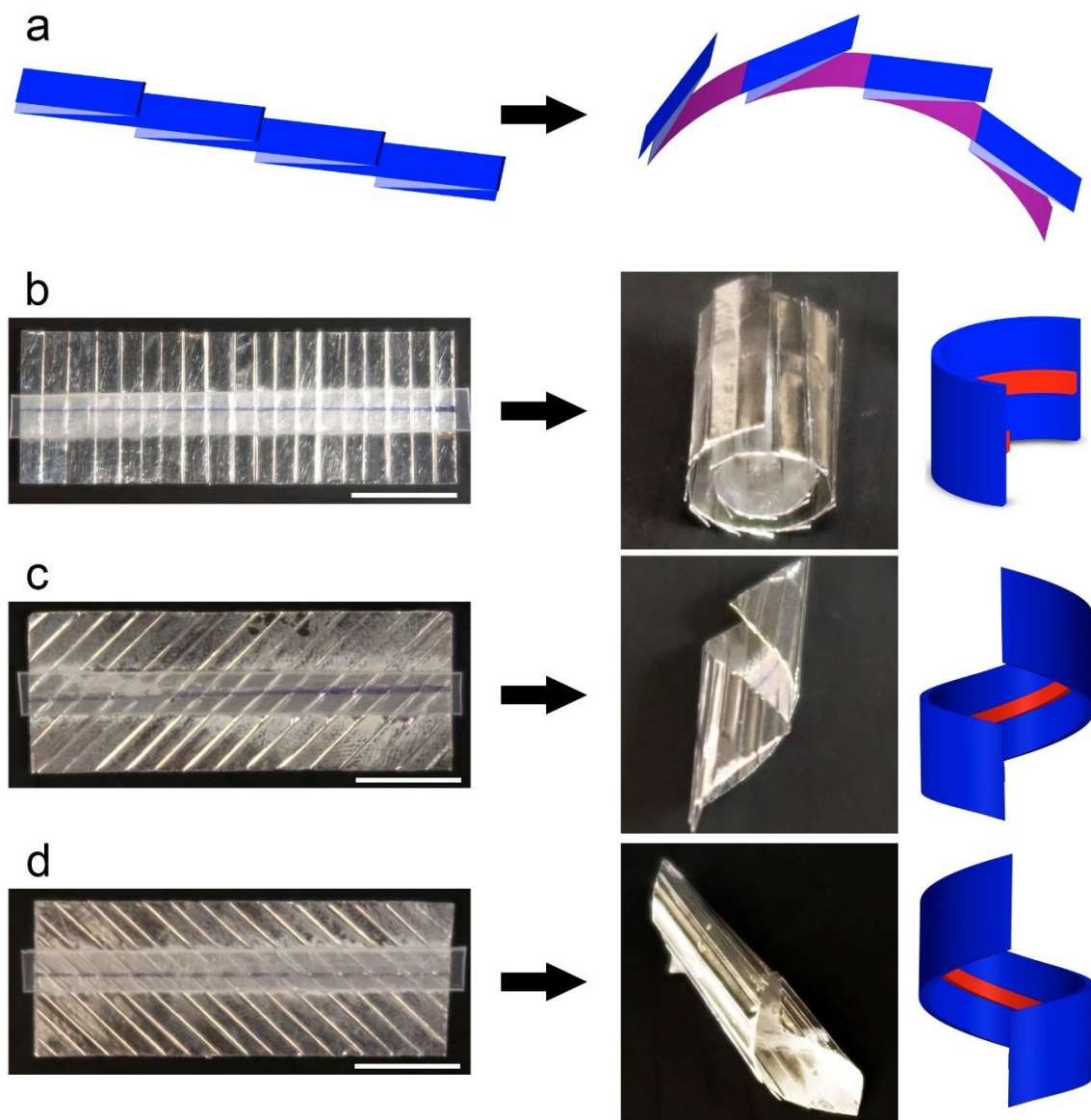


Figure 3.5 Curling behavior of pleated Al foil. (a) Schematic of the pleating and Curling process. (b) Pleat lines along the transverse direction. (c) Pleat lines at an angle (45 degrees) to the transverse direction. (d) Pleat lines at an angle (-45 degrees) to the transverse direction. Scale bars: 10 mm.

3.4 Conclusion

We have demonstrated the self-folding of Al foil actuated by a bilayer actuating hinge, which is made by laminating a PS strip onto Al foil. Upon heating, the PS sheet shrinks and cause the bilayer structure to curl. Curling is induced by strain mismatch between PS layer and Al layer. The PS shrinks equi-biaxially upon heating. However, biaxial curling is difficult due to the large stretching deformation involved. Instead the bilayer sheet curls along one direction to form a cylindrical surface. When the bilayer sheet is embedded in a passive sheet, it curls along the transverse direction, acting as an actuating hinge that folds the passive sheet. Several flat origami structures were folded from an Al strip. Miura-ori structure was folded from an Al foil.

We also demonstrated a method to make passive sheet with anisotropic bending stiffness. Inspired by the flexible dermal armors of animals, we pleat folded the Al foil. The bending stiffness in the direction perpendicular to the pleat lines is much lower than that along the pleat lines. The pleats can be used to guide the curling direction of the Al foil. Helical (left-handed/right-handed) structures can be obtained by changing the orientation of the pleats.

Supplementary Information (SI)

3.S1 Fold polyimide sheet with a bilayer actuator

Figure 3.S1 shows curving behavior when bilayer actuator is embedded in a soft polyimide (PI) sheet. Here the passive sheet was isotropic. Bilayer actuator still curves in the longitudinal direction. Even though the curving deformation of PI generated extra strain energy, it cannot compensate for the energy difference between longitudinal curving and transverse curving.

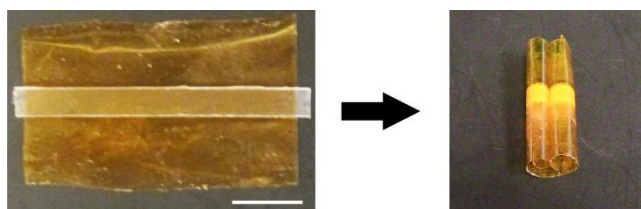


Figure 3.S1 Fold polyimide sheet with a bilayer actuator. Scale bar: 10 mm.

References

- [1] A. Cho, *Science* 2006, 313, 164.
- [2] L. Freund, *Journal of the Mechanics and Physics of Solids* 2000, 48, 1159.
- [3] N. Guyot, Y. Harmand, A. Mézin, *International journal of solids and structures* 2004, 41, 5143.
- [4] M. Finot, S. Suresh, *Journal of the Mechanics and Physics of Solids* 1996, 44, 683.
- [5] S. Alben, B. Balakrishnan, E. Smela, *Nano letters* 2011, 11, 2280.
- [6] I. S. Chun, A. Challa, B. Derickson, K. J. Hsia, X. Li, *Nano letters* 2010, 10, 3927.
- [7] P. Froeter, X. Yu, W. Huang, F. Du, M. Li, I. Chun, S. H. Kim, K. J. Hsia, J. A. Rogers, X. Li, *Nanotechnology* 2013, 24, 475301.
- [8] L. Zhang, E. Deckhardt, A. Weber, C. Schönenberger, D. Grützmacher, *Nanotechnology* 2005, 16, 655.
- [9] S. Golod, V. Y. Prinz, V. Mashanov, A. Gutakovsky, *Semiconductor science and technology* 2001, 16, 181.
- [10] A. S. Gladman, E. A. Matsumoto, R. G. Nuzzo, L. Mahadevan, J. A. Lewis, *Nature materials* 2016, 15, 413.
- [11] N. Bassik, G. M. Stern, D. H. Gracias, *Applied physics letters* 2009, 95, 091901.
- [12] S. Timoshenko, *JOSA* 1925, 11, 233.
- [13] G. Stoychev, S. Zakharchenko, S. b. Turcaud, J. W. Dunlop, L. Ionov, *ACS nano* 2012, 6, 3925.
- [14] V. Y. Prinz, V. A. Seleznev, A. V. Prinz, A. V. Kopylov, *Science and technology of advanced materials* 2009, 10, 034502.
- [15] F. Li, Z. Mi, S. Vicknesh, *Optics letters* 2009, 34, 2915.
- [16] C. Strelow, H. Rehberg, C. Schultz, H. Welsch, C. Heyn, D. Heitmann, T. Kipp, *Physical review letters* 2008, 101, 127403.
- [17] C. L. Randall, E. Gultepe, D. H. Gracias, *Trends in biotechnology* 2012, 30, 138.
- [18] G. Huang, Y. Mei, D. J. Thurmer, E. Coric, O. G. Schmidt, *Lab on a Chip* 2009, 9, 263.

- [19] M. Weng, P. Zhou, L. Chen, L. Zhang, W. Zhang, Z. Huang, C. Liu, S. Fan, *Advanced Functional Materials* 2016, 26, 7244.
- [20] Y. Hu, G. Wu, T. Lan, J. Zhao, Y. Liu, W. Chen, *Advanced Materials* 2015, 27, 7867.
- [21] E. Smela, O. Inganäs, I. Lundström, *Science* 1995, 268, 1735.
- [22] C. Py, P. Reverdy, L. Doppler, J. Bico, B. Roman, C. N. Baroud, *Physical review letters* 2007, 98, 156103.
- [23] E. T. Filipov, T. Tachi, G. H. Paulino, *Proceedings of the National Academy of Sciences* 2015, 112, 12321.
- [24] H. Yasuda, J. Yang, *Physical review letters* 2015, 114, 185502.
- [25] J. L. Silverberg, A. A. Evans, L. McLeod, R. C. Hayward, T. Hull, C. D. Santangelo, I. Cohen, *science* 2014, 345, 647.
- [26] R. Fernandes, D. H. Gracias, *Advanced drug delivery reviews* 2012, 64, 1579.
- [27] S. Heimbs, in *Dynamic failure of composite and sandwich structures*, Springer, 2013, 491.
- [28] S. S. Tolman, I. L. Delimont, L. L. Howell, D. T. Fullwood, *Smart Materials and Structures* 2014, 23, 094010.
- [29] E. D. Demaine, M. L. Demaine, J. S. Mitchell, *Computational Geometry* 2000, 16, 3.
- [30] M. T. Tolley, S. M. Felton, S. Miyashita, D. Aukes, D. Rus, R. J. Wood, *Smart Materials and Structures* 2014, 23, 094006.
- [31] M. Schenk, S. D. Guest, *Proceedings of the National Academy of Sciences* 2013, 110, 3276.
- [32] K. Miura, title *The Institute of Space and Astronautical Science report* 1985, 618, 1.
- [33] M. M. Porter, N. Ravikumar, F. Barthelat, R. Martini, *Journal of the Mechanical Behavior of Biomedical Materials* 2017, 73, 114.
- [34] W. Yang, I. H. Chen, B. Gludovatz, E. A. Zimmermann, R. O. Ritchie, M. A. Meyers, *Advanced Materials* 2013, 25, 31.
- [35] J. Jeong, Y. Cho, S. Y. Lee, X. Gong, R. D. Kamien, S. Yang, A. Yodh, *Soft matter* 2017, 13, 956.
- [36] C. Danielson, A. Mehrnezhad, A. YekrangSafakar, K. Park, *Soft Matter* 2017.

CHAPTER 4 Pop up assembly of 3D structures via compressive buckling

4.1 Introduction

There is a growing interest in transforming two dimensional (2D) sheets into three dimensional (3D) structures, which can find a wide range of applications including self-folding robots, ^[1-3] deformable batteries, ^[4, 5] containers for drug delivery, ^[6, 7] reconfigurable metamaterials, ^[8-10] and 3D electronic devices. ^[11, 12] The transformation can be achieved via origami-inspired approaches, ^[11, 13] i.e. folding a 2D sheet along pre-defined creases. Slits or perforations can also be introduced in the 2D sheet prior to folding (known as kirigami), which increases the diversity of accessible 3D shapes. ^[14-18]

In general the 2D-to-3D transformation requires pre-defined crease patterns in the 2D sheet where localized folding occurs and an actuating component. ^[19, 20] According to the relative location of the actuating component and the creases, two general strategies can be used to realize the transformation. In the first strategy, transformation is actuated by responsive hinges (at the same locations as the creases), ^[2] which fold when triggered. The responsive hinge can be created by a local bimorph actuator, where folding occurs due to mismatch in thermal expansion ^[21-24] or swelling. ^[25] The hinge can also be made directly on the 2D sheet. In this case the 2D sheet is locally modified at the creases, e.g. by light-induced stress relaxation ^[26] or light-induced heating, ^[27-30] to create a stress gradient across the thickness of the 2D sheet. In the second strategy, the actuating component is away from the creases. For example, an external compressive force can be used to trigger buckling of the 2D sheet, where the buckling is localized at the creases that are more compliant than the rest of the sheet. This

strategy does not require responsiveness of the 2D sheet. A number of complex 3D structures have been assembled by controlled compressive buckling.^[31-34] However, a pre-stretching step was needed in order to apply the compressive force, which is not trivial especially for biaxial stretching and cannot be remotely operated.

In this chapter we report a new method to achieve controlled mechanical buckling following the second strategy. Here a heat shrinkable polymer sheet is used to trigger the buckling upon noncontact heating (e.g. in an oven) instead of the pre-stretching. Two approaches are demonstrated. In the first approach, the 2D precursor is inscribed in a perforated pattern (of a specific shape) in the polymer sheet, thus pushed from outside upon heating. After transformation, a 3D structure inscribed in the shrunk perforation is assembled. Several assembled 3D structures are demonstrated including prismatic/pyramidal structures with different base shapes, house roof, partial soccer ball, Miura-ori structure and insect wing. In the second approach, a small piece of polymer sheet with a specific shape is placed on top of the 2D precursor, and pulls it from inside upon heating. After transformation, a 3D structure enclosing the shrunk polymer sheet is formed. Prismatic/pyramidal structures with a variety of base shapes are assembled, which can be tessellated horizontally to create cellular structures and stacked vertically as complex multilayer structures.

4.2 Materials and Methods

4.2.1 Materials

The heat shrinkable polymer sheet, with the brand name of Shrinky-Dinks, was made of pre-strained polystyrene (PS), which shrinks to 46% equi-biaxially (i.e. isotropically) when

heated above its glass transition (~ 100 °C). The Kapton tape (CAPLINQ, Ottawa Canada) had a thickness of 1 mil (0.025 mm). The Super Glue was purchased under the name of Loctite Liquid Professional Super Glue 20-Gram Bottle. Paperboard was cut from Staples colored file folder (red color in this experiment). The samples were placed in an oven (150 °C) for heating. Assembly typically finished in 2 minutes.

4.2.2 Pop-up by pushing from outside

The 2D precursor was fabricated by gluing red paperboard on a PS sheet (on both sides to make it symmetric). After the glue was fully cured, the paperboard/PS/paperboard sandwich became rigid and cannot shrink. A small gap (about 2 mm) was left between adjacent sandwich structures, i.e. bare PS strip without the paperboard. Since PS softens when heated, the gap acted as the soft crease during the buckling. The length of crease can be reduced to facilitate the folding. The PS sheets were perforated using a laser cutter.

4.2.3 Pop-up by pulling from inside

The 2D precursor was fabricated by connecting two panels of paperboard with a kapton tape. A small gap (about 2 mm) was left between the paperboard panels to make the soft crease. PS strips or sheets (of specific shape) were bonded onto the 2D precursor using Super Glue (with small gluing area, around 3 mm in size).

4.3 Results and Discussions

4.3.1. Buckling induced by pushing from outside

First, we present buckling of 2D precursor that is pushed from outside. The 2D precursor was fabricated by modifying the polymer sheet locally (i.e. gluing rigid materials such as paperboard on both sides of the sheet). Folding along a single crease (i.e. uniaxial compression) is shown in **Figure 4.1**. Within the polymer sheet (blue area) is the 2D precursor, which consists of two rigid panels (polymer sheet with paperboard bonded on both sides, in red) and a soft crease (polymer sheet only, in blue). In this case the 2D precursor can be viewed as a 1D structure (short in the transverse direction) inscribed in a narrow perforation in the polymer sheet, with the two ends anchored to and the two edges separated from the sheet by slits, respectively. As the polymer sheet shrinks, the perforation shrinks too with the same shrinkage ratio, causing buckling of the 1D structure. The buckling is concentrated at the crease due to its low stiffness while the rigid panels remain flat, forming a sharp angle. Note that the rigid panels rotate about the anchoring lines during the buckling. Based on the geometric relationship shown in **Figure 4.1a**, the folding angle can be calculated by

$$\cos(\alpha) = \frac{1 + \lambda^2 - [\zeta(1 + \lambda)]^2}{2\lambda} \quad (4.1)$$

where λ is the ratio between lengths of the two segments, ζ is the shrinkage ratio of the polymer sheet. The calculated and measured folding angles are plotted in **Figure 4.1b** as functions of λ , where an equi-biaxially pre-strained polystyrene (PS) sheet was used as the actuation material, which shrinks to 46% of its initial length upon heating ($\zeta = 46\%$). The

largest angle (55 degree) was obtained under the symmetric condition, i.e. $\lambda = 1$. The folding angle decreased with the increasing λ , until 0 degree at $\lambda = 2.7$. Note that **Equation 4.1** was not applicable when $\lambda > 2.7$, in which case the perforation shrank to $\lambda - 1$ in length (the minimum distance allowed by the two rigid panels), instead of $\zeta(1 + \lambda)$ (the distance obtained when PS fully shrinks to ζ). In other words, the shrinkage of the PS sheet/perforation was constrained by the rigid panels. The folding angle remained at 0 degree when λ was larger than 2.7.

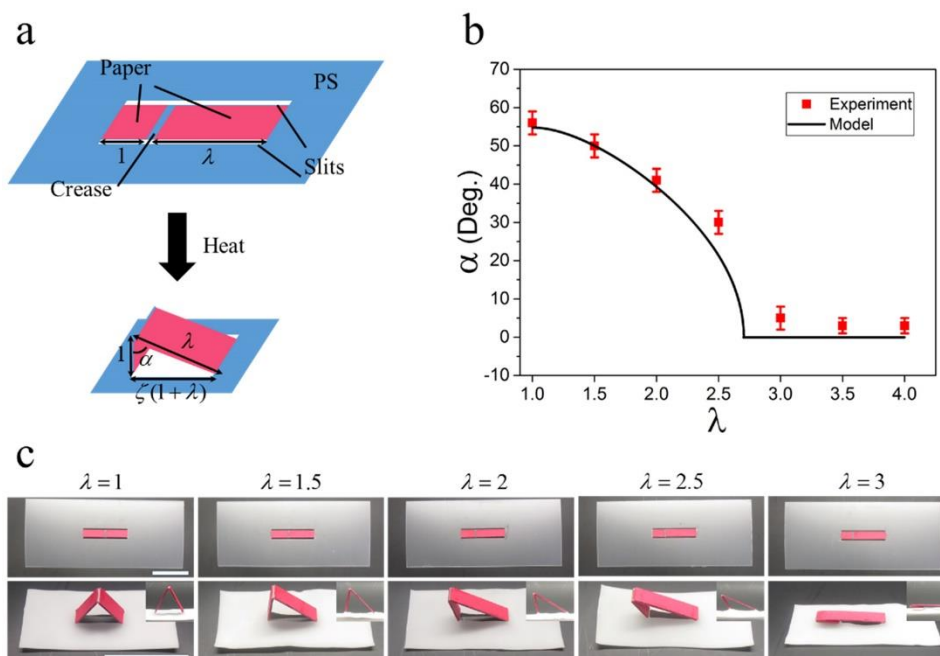


Figure 4.1 Folding along a single crease via the first approach. (a) Schematic of the folding process and geometric parameters; (b) Relationship between folding angle (α) and length ratio (λ); (c) Images of folding results at different length ratios (λ). Scale bars: 50 mm.

The above is a special case with a 1D precursor. In general the 2D precursor is inscribed in a 2D perforation of a specific shape in the polymer sheet with its boundaries anchored to the sheet. The shrinkage of the polymer sheet causes the 2D precursor to buckle into a 3D structure. An example of this 2D-to-3D transformation is shown in **Figure 4.2**. Here the 2D precursor includes a square panel surrounded by four rectangular panels (all rigid, red areas) and four soft creases (blue lines). The length of the creases (δ in **Figure 4.2a**) can be reduced to facilitate the folding. As shown in **Figure 4.2a**, four sides shrink in a symmetric manner, thus the square shape is retained. Slits (κ) are introduced in the anchoring lines to tailor the size of the perforation after shrinking, which determines the size of the final 3D structure. Initially (in the flat state), the square perforation has side length of $1+2\lambda$. As shown in **Figure 4.2a**, it shrinks to $(1-2\kappa)+2\zeta(\lambda+\kappa)$ upon heating; the side length after shrinking decreases with increasing κ . Note that the portion anchored to the polymer sheet cannot shrink. The folding angle at the creases can be calculated by

$$1-2\lambda\cos(\alpha)=(1-2\kappa)+2\zeta(\lambda+\kappa) \quad (4.2)$$

In order to get a right square prism ($\alpha=90^\circ$), the side of the perforation needs to shrink to 1, which means

$$(1-2\kappa)+2\zeta(\lambda+\kappa)=1 \quad (4.3)$$

Figure 4.2b shows the experimental realization of a square prism using a PS sheet. In order to monitor the deformation during the shrinking and buckling, black gridlines were drawn on the PS sheet and PS/paperboard panels before heating. The PS/paperboard panels were constrained from shrinking, as the black lines remained straight. The shrinkage was

locally disturbed by the rigid PS/paperboard panels, which can be seen in the side view in **Figure 4.2b** and more clearly when the slit length is reduced to zero. As shown in **Figure 4.S1**, SI, without the slit, the size of the perforation after shrinking was larger than 1, which resulted in an open structure, instead of a closed prism.

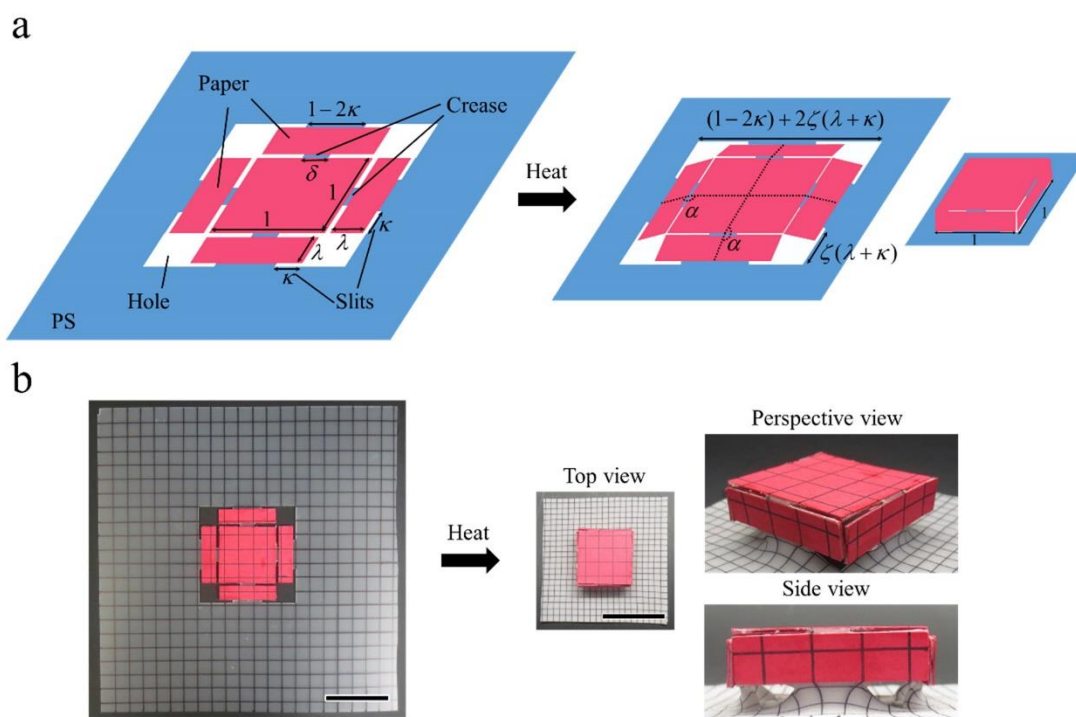


Figure 4.2 Assembling a square prism from its 2D precursor (first approach). (a) Schematic of the buckling process and geometric parameters. (b) Experimental realization of a square prism. Black gridlines were drawn to track the deformation. Scale bars: 30 mm.

This approach can be used to assemble prismatic and (truncated) pyramidal structures with different base shapes. Note that the in-plane shrinkage of the polymer sheet is isotropic and homogeneous, regardless of the perforation patterns. During shrinking, the perforation reduces its size while retaining its shape, which is different from the case when the equi-biaxial prestrain is applied mechanically (**Figure 4.S2**, SI). A number of 3D structures are presented in **Figure 4.3**, including triangular prism/pyramid, square prism/pyramid, pentagonal prism and hexagonal prism. To assemble a 2D precursor into a closed prismatic/pyramidal structure, the perforation needs to shrink to the size of the base of the prism/pyramid. A partial soccer ball consisting of one pentagon and five hexagons was assembled with a pentagonal base. This approach can go beyond folding axisymmetric structures, i.e. regular polygon (equal angles/side lengths) based structures shown above. A house roof with a rectangular base was assembled as an example, where the 2D precursor is composed of two rectangles and two triangles surrounding a narrow strip. The 2D precursor is positioned in a rectangular perforation in the PS sheet. After shrinking, the size of the perforation is identical with the base of the house roof. Detailed calculations for each structure are given in **Figures 4.S3** and **4.S4**, SI.

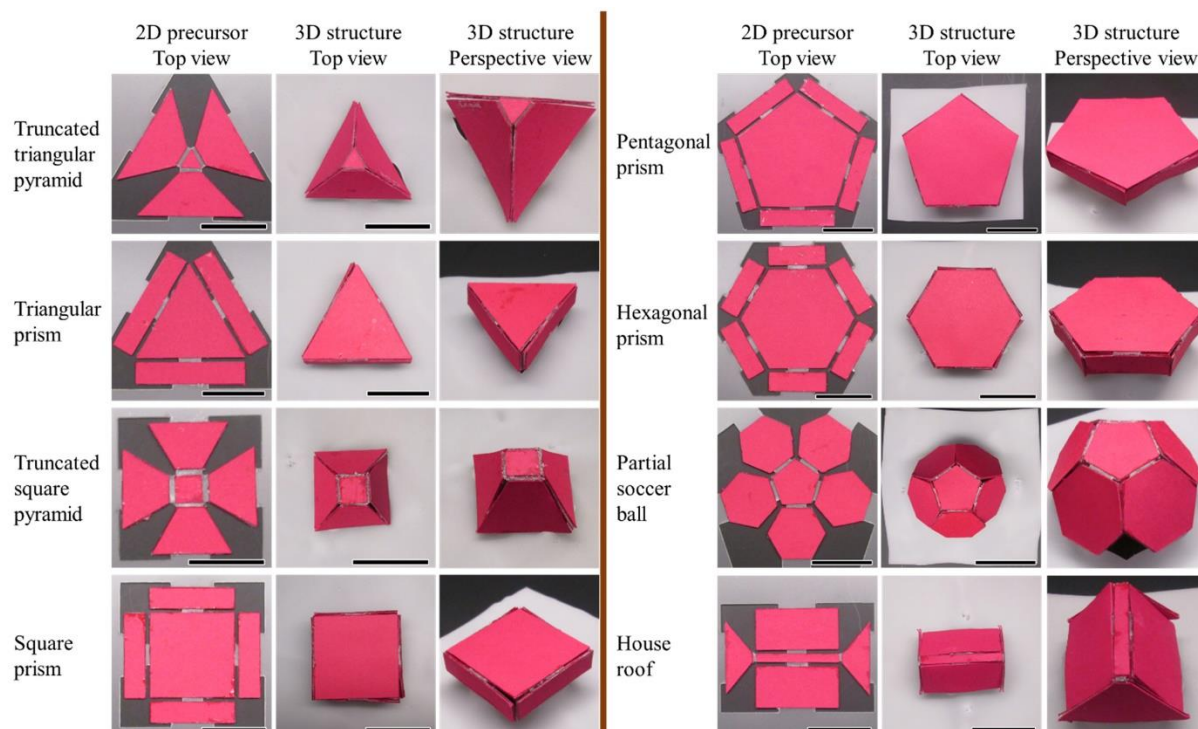


Figure 4.3 A number of 3D structures assembled via the first approach. Scale bars: 30 mm.

Figure 4.4 shows two special types of origami structures that can be folded using the above approach, each consisting of four rigid panels connected by four soft creases. These structures have only one degree of freedom, thus can be activated by uniaxial actuation. **Figure 4.4a** shows the Miura-ori structure, originally proposed by Miura as a method of packaging large membranes ^[10, 35]. Even though folding involves size reduction in both horizontal and vertical directions and pop-up out of plane, it can be activated solely by shrinking in the horizontal direction. This structure provides an excellent example of converting one-dimensional deformation into all three dimensions. **Figure 4.4b** shows another type of structure mimicking an insect wing.^[36] When at rest, some insects (e.g. beetles) need to fold their delicate hindwings and tuck them under the protective forewings. The folding needs to be actuated by the basal muscles, since there are no muscles inside the wing. In other words, the actuation mechanism can be only connected to the structure (wing) on one side. This example illustrates that our approach can achieve 3D folding of a structure by contraction of a base on one side of the structure.

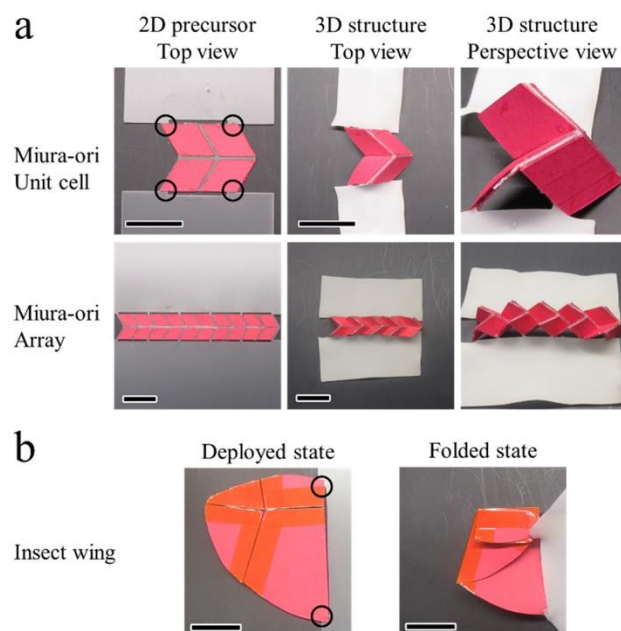


Figure 4.4 Origami with one degree of freedom. (a) Miura-ori and (b) Insect wing. Scale bars: 30 mm. The 2D precursor is bonded to the polymer sheet at discrete points (highlighted by black circles) with a slit between two points.

The approach shown above shares some characteristics with the compressive buckling reported previously ^[31]. While both are relatively simple and can be applied to fold many complicated structures, they have some limitations. For example, a large piece of polymer sheet (much larger than 2D precursor) is required. In addition, the assembled structure is always bounded by a polymer sheet, which may not be desirable for some applications.

4.3.2. Buckling induced by pulling from inside

In order to circumvent such limitations, we developed another approach, where the polymer sheet pulls the 2D precursor from inside instead of pushing from outside. **Figure 4.5** shows folding of a single crease using this approach as a starting case. Here the 2D precursor consists of two pieces of rigid paperboard connected with a soft crease (e.g. a strip of kapton tape). Note that here the rigid structure is the paperboard only, instead of the paperboard/polymer/paperboard sandwich in the first approach. A heat shrinkable polymer strip is placed on top of the 2D precursor, with two ends glued to two paperboard panels. The polymer strip shrinks upon heating, pulling the two paperboard panels toward each other and causing buckling. Again the buckling deformation is concentrated at the crease due to its low stiffness. Note that here λ is defined as the ratio of the two distances between the two bonding positions and the crease (**Figure 4.5a**). In this approach, shrinkage of the polymer strip can be further controlled by constraining a certain fraction of it (e.g. by gluing rigid paperboard on both sides of the polymer sheet). The constrained fraction cannot shrink, while the rest of the polymer strip can shrink freely to ζ . As shown in **Figure 4.5a**, the folding angle is governed by

$$\cos(\alpha) = \frac{1 + \lambda^2 - \{(1 + \lambda)[\rho + \zeta(1 - \rho)]\}^2}{2\lambda} \quad (4.4)$$

where ρ is the fraction of the polymer strip that is constrained from shrinking. Here we show two special cases to tailor the folding angle. The first case is to fix ρ at 0 and vary λ . The relationship between folding angle and λ is shown in the bottom panel of **Figure 4.5b**. Angles from 0 to 55 degrees can be obtained in theory. But practically angles smaller than 30 degree are difficult to achieve due to accumulation of the shrunk polymer strip inside the crease (as can be seen from the deviation of experimental results from the model at large λ). The second way is to fix λ at 1 and vary ρ . The relationship between folding angle and ρ is shown in the top panel of **Figure 4.5b**. Angles from 55 to 180 degrees can be obtained. PS was used again as the actuating polymer with $\zeta = 46\%$. **Figure 4.5c** shows several folded structures with different angles. **Figure 4.5d** shows a wavy structure by folding a chain of paperboard in alternated directions. According to **Equation 4.4**, the folding angle is determined by the length ratio λ and the constraining fraction ρ , while the total length of the PS strip does not come into play here. This makes possible reducing the length of the PS strip without changing the folding angle. In the extreme condition that the PS strip is very short, it basically works as a hinge to cause folding of the 2D precursor, which is similar to the first strategy with responsive hinges as discussed in the Introduction ^[1, 21, 22].

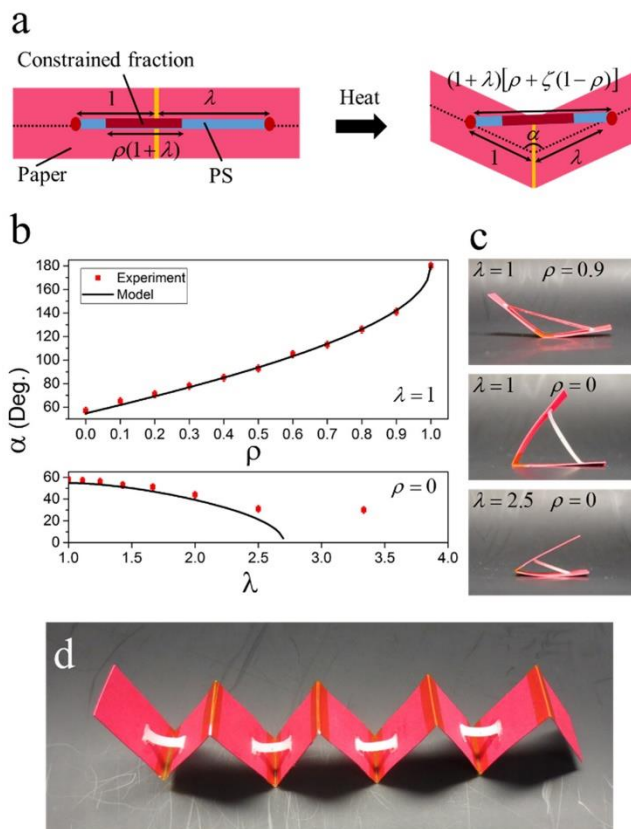


Figure 4.5 Folding a single crease via the second approach. (a) Schematic of the buckling process and geometric parameters; (b) Relationship between folding angle and length ratio (λ) /constrained fraction (ρ) for two special conditions; (c) Several folded samples; (d) A wavy structure.

Next, this approach is generalized to folding 2D precursor into 3D structures. **Figure 4.6** shows the schematic of assembling a square prism from its 2D precursor as an example. The geometric rules are similar to those shown in **Figure 4.2a**. The bonding areas between the paperboard and the polymer sheet are very small (marked as the red dots in **Figure 4.6**) and can be regarded as points. This corresponds to $(1 - 2\kappa) = 0$ as shown in **Figure 4.2a**, where $1 - 2\kappa$ is the length of the anchoring line. In other words, there is no constraint on edges of the polymer sheet, thus the entire polymer sheet can shrink to ζ . The shape of 3D structure is determined by the size of the shrunk polymer sheet. The folding angle at the creases can be calculated by substituting $\kappa = 0.5$ in **Equation 4.2**, which becomes

$$1 - 2\lambda \cos(\alpha) = \zeta(1 + 2\lambda) \quad (4.5)$$

Polymer sheets of different sizes $(1 + 2\lambda)$ can lead to different folding angles. In order to get a right square prism ($\alpha = 90^\circ$), the shrunk polymer sheet needs to be identical in size with the base of the prism (1×1), which means

$$\zeta(1 + 2\lambda) = 1 \quad (4.6)$$

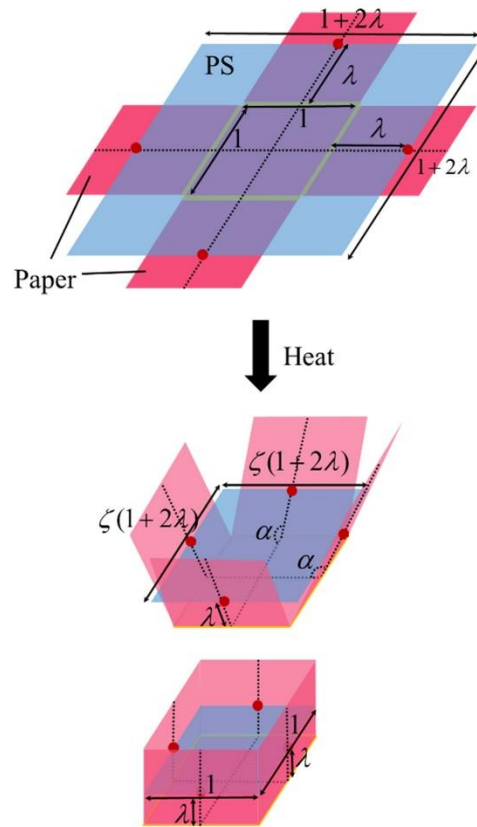


Figure 4.6 Assembling a square prism from its 2D precursor (second approach). Schematic of the buckling process and geometric parameters.

Figure 4.7 shows a set of 3D structures assembled using this approach, including uniform triangular prism/pyramid, square prism/pyramid, pentagonal prism, hexagonal prism, general triangular prism and rhombic prism. All structures were folded by PS sheets upon heating. The geometric calculations are the same as those for the truncated pyramids using the first approach as given in **Figure 4.S3** and **4.S4**, SI. Three features distinguish this approach from the first approach discussed above and the one reported in literature ^[31]. First, the shrunk polymer sheet is within the 3D structure, instead of supporting it from underneath and/or surrounding it, which often times could be conducive to better appearances. Second, the panels of the 2D precursor can go beyond the bonding points, which allow increasing the height of the 3D structure and even form an enclosed structure while keeping the same base. For example, enclosed pyramids can be assembled using this approach (with a shrunk PS sheet inside). Third, the isolated 3D structures folded in this approach are easier to be tessellated or stacked to make more complex structures, as discussed in the following.

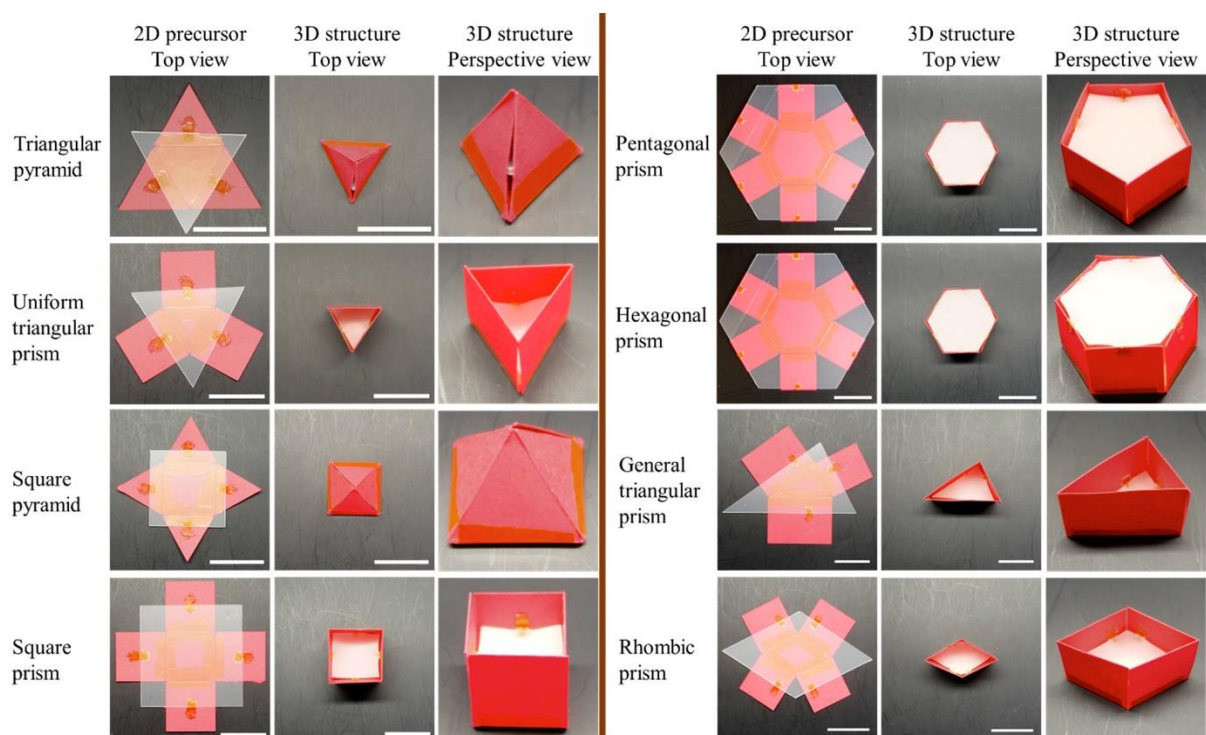


Figure 4.7 A number of 3D structures assembled via the second approach. Scale bars: 30 mm.

The prisms/pyramids shown in **Figure 4.7** can be tessellated side by side to make cellular structures. **Figure 4.8a** shows some examples of the cellular structures. Depending on the position of the PS sheet (i.e. above or below the 2D precursor), the 2D precursor can buckle upward or downward, which results in an array of prisms facing in alternated directions, resembling the checkboard pattern.

Another way to combine the prismatic/pyramidal structures is to stack them vertically, as shown in **Figure 4.8b**.^[32] Two square pyramids were combined (base to base) to make an octahedron, which consisted of 8 equal lateral triangles. Another example is a paperboard animal model. Multiple (truncated) hexagonal pyramids were stacked in the vertical direction, resulting in a paperboard animal. Both head and body were made of two (truncated) hexagonal pyramids facing each other. Both structures shown in **Figure 4.8b** were popped up from multilayer 2D precursors, i.e. multiple 2D precursors stacked in the vertical direction.

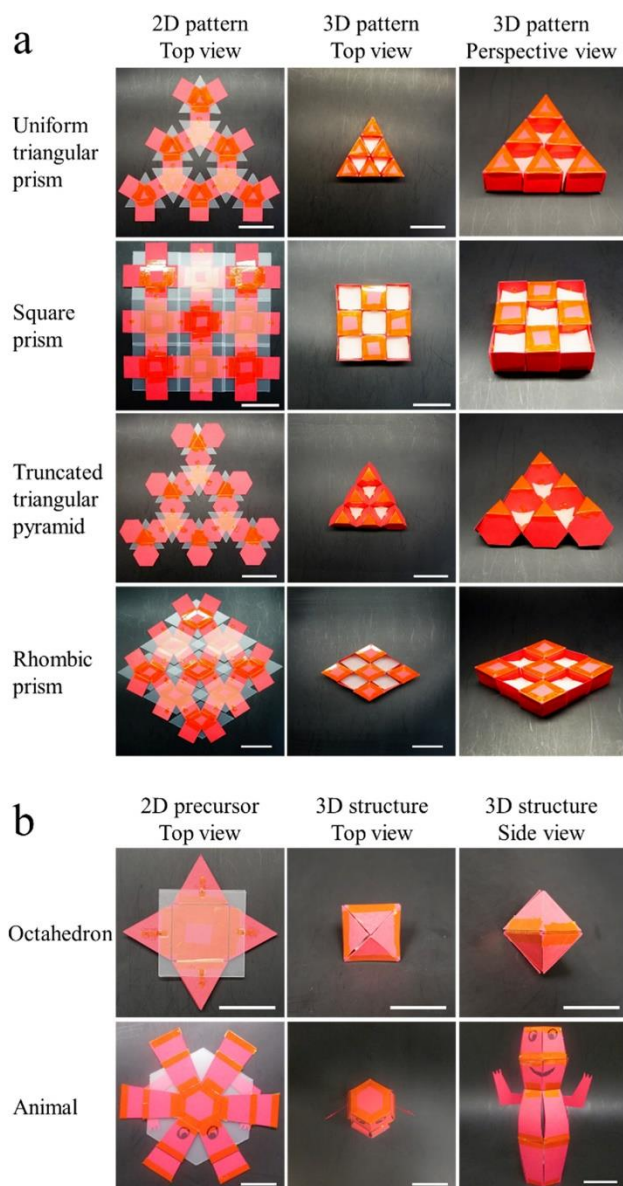


Figure 4.8 Combination of prismatic/pyramidal structures. (a) Horizontal tessellation (scale bars: 50 mm); (b) Vertical stack (scale bars: 30 mm).

4.3.3. Application of the cellular structures

Cellular structures can find applications in many fields, including packaging, energy absorbing and thermal insulating^[37]. We used tessellation of the square prisms to demonstrate the thermal insulating property (**Figure 4.9**). The assembled structure was sandwiched between two pieces of paperboard and placed on a hot plate. IR camera (model FLIR A655sc, FLIR Systems) was used to measure the temperature distribution. Another structure with three layers of paperboard was also placed on the hot plate for comparison. Black tapes (with emissivity ~0.95) were put on the hot plate and tested structures for the IR temperature measurement. Temperature of the hot plate was set to 150 °C. At thermal equilibrium, temperatures of the sandwich structure and the comparison structure were 51 and 118 °C, with the corresponding heat transfer coefficient calculated to be 2.6 and 29.1 Wm⁻²K⁻¹, respectively (Assuming heat transfer coefficient of air to be 10 Wm⁻²K⁻¹ and ambient temperature as 25 °C). By assembling paperboard into cellular structures with enclosed air, the heat transfer coefficient was reduced by more than an order of magnitude.

The energy absorbing ability of the same structure was tested under compression. The cellular structure was about 25 g in weight, 90 mm × 90 mm in the horizontal plane and 30 mm in height. It was able to sustain 260 N compressive force before being crushed, corresponding to a nominal compressive stress of 32.1 KPa. The load-displacement curve shown in **Figure 4.9b** consists of three stages. The displacement increases with the load initially (elastic stage) and then increases at a constant load (plateau stage) before the load increases rapidly (densification stage). The large deformation at the plateau stage contributes largely to the energy absorption. The energy absorbed in this case was 9.5 J (integrated area

under load displacement curve) with the energy absorption per unit volume as 39 KJ/m^3 . This is smaller than the reported value for paper honeycomb structures (50 KJ/m^3).^[38] The difference might be caused by the fact that in our structure, the vertical panels are separated from each other, thus deforms independently. While in the honeycomb structure, vertical panels are bonded together, thus the deformation are coupled together and requires more energy.

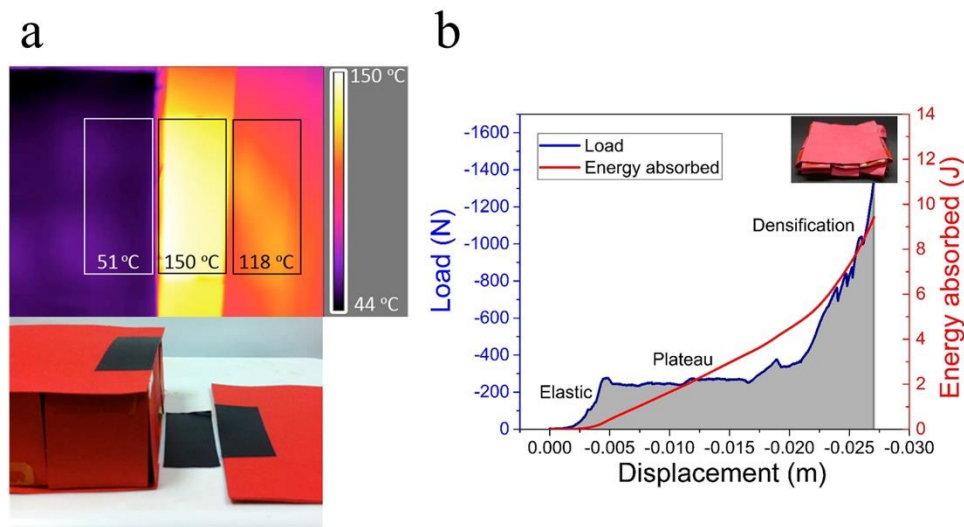


Figure 4.9 Application of cellular structure. (a) Thermal insulator; (b) Crash energy absorber.

4.4 Conclusion

We have demonstrated self-assembly of complex 3D structures from their 2D precursors, actuated by a heat shrinkable polymer sheet. When heated, the polymer sheet shrinks in plane and causes the 2D precursor to buckle. The buckling is guided by the pre-defined creases in the 2D precursor due to their low stiffness. An equi-biaxially pre-strained PS sheet was used in this work as the actuation material. Two approaches were employed to achieve the assembly. In the first approach, the 2D precursor was inscribed in a perforation in the polymer sheet and pushed from outside upon heating. After transformation, a 3D structure inscribed in the shrunk perforation can be obtained. Assembled 3D structures included prisms/pyramids with different base shapes, partial soccer ball, house roof, Miura-ori structure and insect wing. In the second approach, the polymer sheet was placed on top of the 2D precursor, thus pulled it from inside. After transformation, the shrunk polymer sheet was enclosed within the 3D structure. Prisms/pyramids with bases of different shapes were assembled. The prisms can be tessellated to create cellular structures, which exhibited good thermal insulating and energy absorbing ability. They can also be stacked vertically to make multilayer complex structures. The geometric rules developed in this work are independent of length scale.

Supplementary Information (SI)

4.S1 Use slits to tailor the size of perforation after shrinking

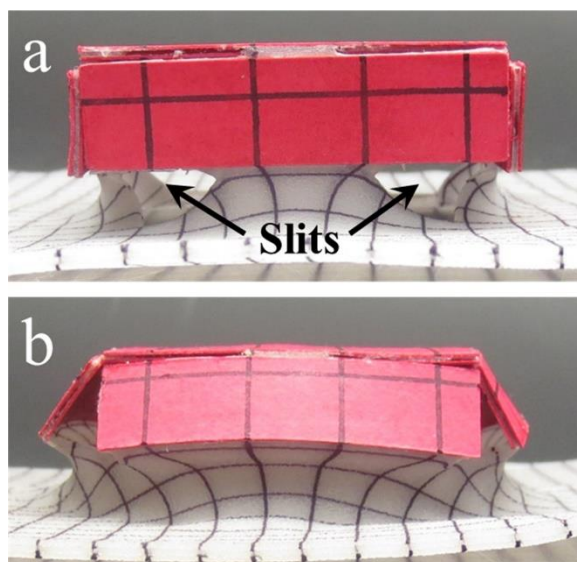


Figure 4.S1. Assembly of a square prism with and without slit. (a) With slits ($\kappa > 0$); (b) Without slits ($\kappa = 0$).

4.S2 The effect of perforation on strain distribution

Figure 4.S2 shows the effect of perforation on strain distribution. A comparison is made between thermally induced strain and mechanical strain. **Figure 4.S2a** shows the thermal shrinking of PS sheet. Before shrinking, gridlines were drawn on the PS sheet and a square perforation was cut out. It can be seen that the perforation did not affect the thermally induced strain. The square perforation shrank to the same size as the square PS sheet cut out from it.

Mechanical strain was studied by FEA simulation (ANSYS 16.1), where a membrane with a square a hole in the center was equi-biaxially stretched. Young's modulus was taken as 10 MPa. Poisson's ratio was 0.4. An equi-biaxial stress of 5 MPa was applied. **Figure 4.S2b** shows deformation of the membrane under equi-biaxial tension. It can be seen that the square perforation caused severe stress concentration and the sharp corners were significantly blunted such that the square became nearly a circle. In other words, an equi-biaxially pre-stretched membrane with a circle perforation would turn into a membrane with a square perforation upon releasing the prestrain. **Figure 4.S2c** shows the strain distribution. ε_x was suppressed on the left and right sides of the perforation, but increased on the top and bottom sides, while ε_y was suppressed on the top and bottom sides but increased on the left and right sides. Similar conclusions were drawn about the mechanical strain in a previous study.^[39]

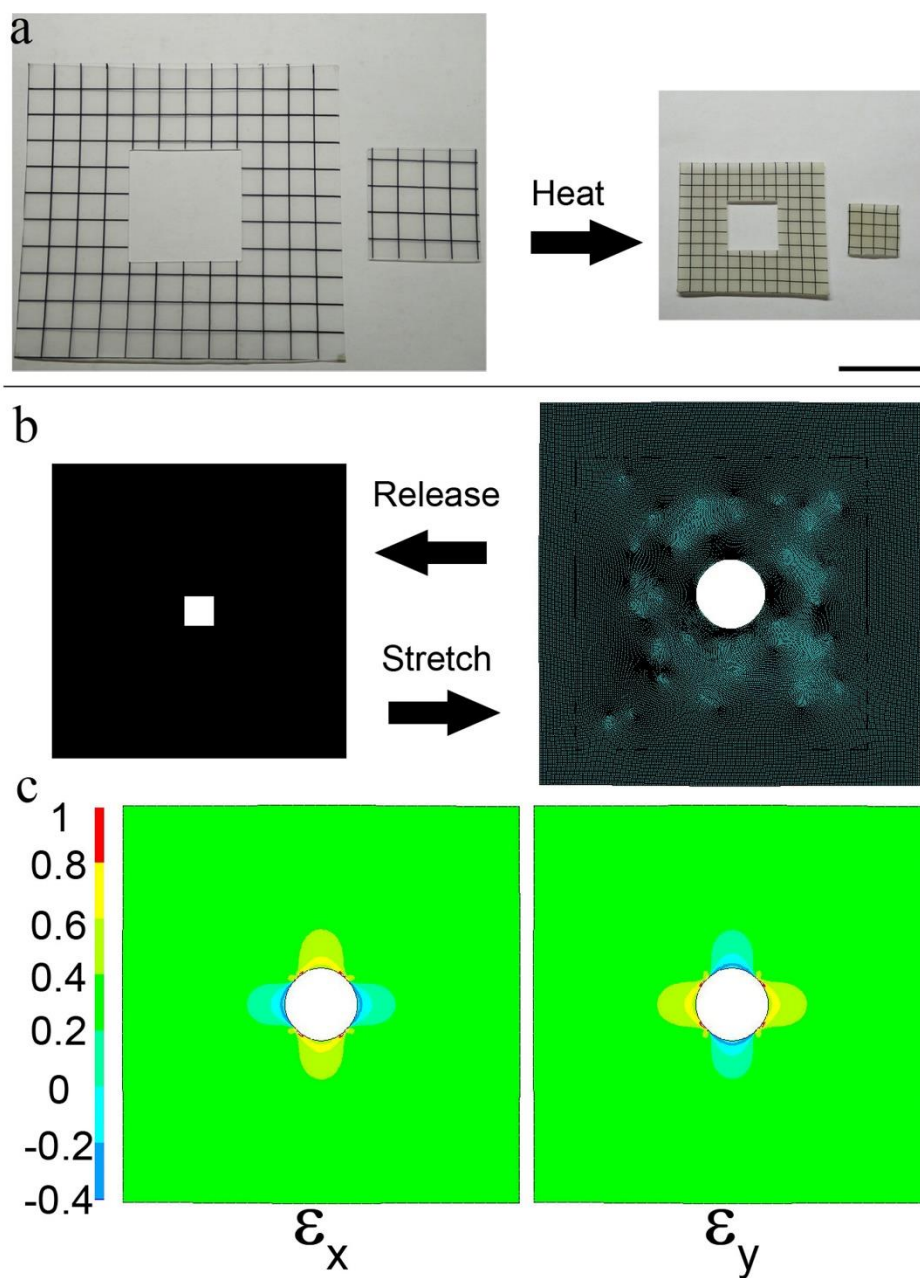


Figure 4.S2 Effect of a perforation on thermally induced strain and mechanical strain. (a) Equi-biaxial shrinkage of a PS sheet upon heating (scale bar: 30 mm); (b) FEA simulation of the deformation of a membrane under equi-biaxial tension; (c) Strain distribution (FEA simulation).

4.S3 Geometric models

Figure 4.S3 shows schematically the assembling truncated pyramids with different base shapes, of which prisms can be regarded as a special case ($\theta = 90^\circ$, where θ is the base angle of the side surface, as shown in **Figure 4.S3**). The geometric models for both approaches are given.

The left column shows the first approach. To fully fold the truncated pyramids, the perforation needs to shrink to the size of the base of the truncated pyramid, which means

$$1 + 2\lambda \cot(\theta) - 2\kappa + 2\zeta(\lambda(\cot(\varphi) - \cot(\theta)) + \kappa) = 1 + 2\lambda \cot(\theta) \quad (4.S1)$$

where φ is half of the inner angle of the base in the truncated pyramid, e.g. 30° , 45° , 72° , 60° for triangle, square, pentagon, hexagon respectively. Note that in this case $\theta < 90^\circ$, the shrunk perforation becomes the bottom of the truncated pyramid, which tapers from the bottom to the top. Note that partial soccer ball is similar to truncated pentagonal pyramid (replacing trapezoid side surfaces with hexagonal ones).

The right column shows the second approach. The anchoring length is small and can be regarded as zero (corresponds to $1 + 2\lambda \cot(\theta) = 2\kappa$ in the first approach). The entire polymer sheet shrinks to ζ . To fully fold the truncated pyramids, the size of shrunk polymer sheet needs to be equal to the cross-section of the truncated pyramid (here the base of the truncated pyramid is the central paperboard panel), which means

$$2\zeta(\lambda(\cot(\varphi) - \cot(\theta)) + 1/2 + \lambda \cot(\theta)) = 1 + 2\lambda \cot(\theta) \quad (4.S2)$$

Note that in the case $\theta > 90^\circ$, the shrunk polymer sheet becomes the top of the truncated pyramid, which still tapers from the bottom to the top. A full pyramid can be obtained by extending the lateral panels beyond the bonding points.

Figure 4.S4 shows assembly of two special structures – house roof via the first approach and rhombic prism via the second approach. For the rhombic prism, the side length of the PS sheet is l/ζ , where l is the side length of the base of the prism. While for the house roof, the perforation needs to shrink to the base of the house roof, which means the following two equations must be both satisfied.

$$b - 2\kappa_1 + \zeta(2\lambda_1 - (b - 2\kappa_1)) = b \quad (4.S3)$$

$$a - 2\kappa_2 + 2\zeta(\lambda_2 + \kappa_2) = a \quad (4.S4)$$

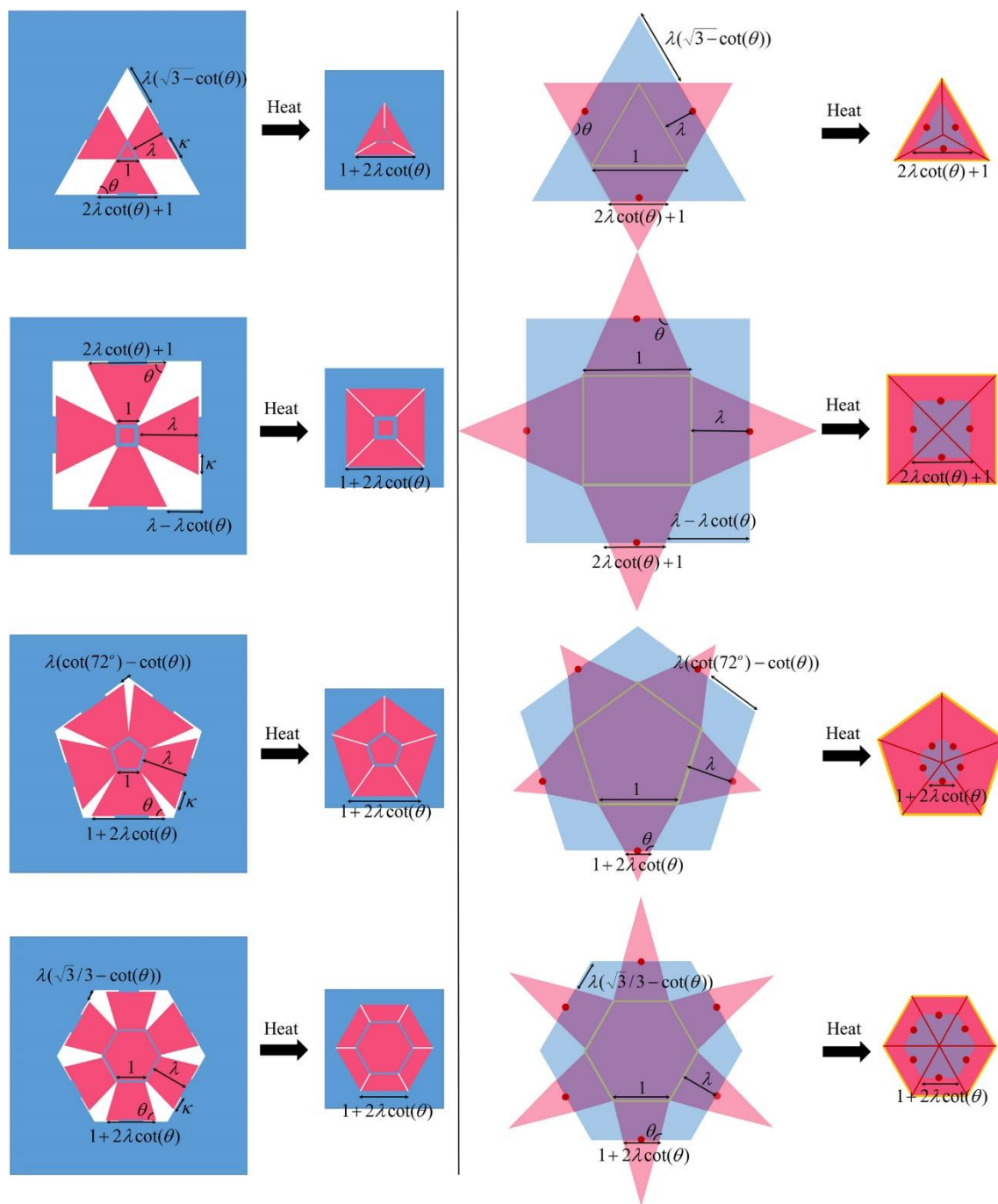


Figure 4.S3 Schematic showing the assembly of several (truncated) pyramids (top view). Left: the first approach; right: the second approach.

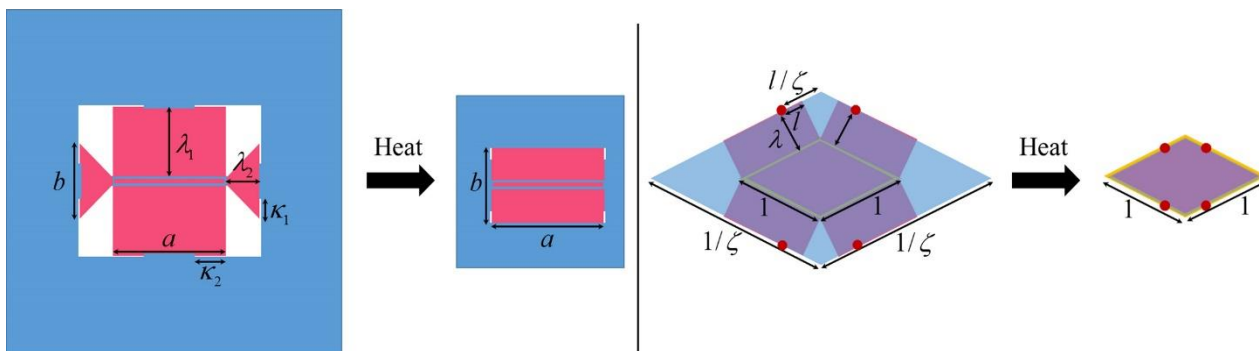


Figure 4.S4 Schematic showing the assembly of two special structures (top view). Left: house roof via the first approach; right: rhombic prism via the second approach.

4.S4 Distorted shrinkage of PS and defective structures

During the heating of PS sheet in the oven, it may be bent or distorted temporarily. However, the final state is always a flat fully-shrunk sheet. This is shown in **Figure 4.S5a**. The sample was taken out of the oven during the heating. After photographed, it was put in the oven to resume the transformation. Finally, the PS sheet was flat and the 3D structure was successfully assembled.

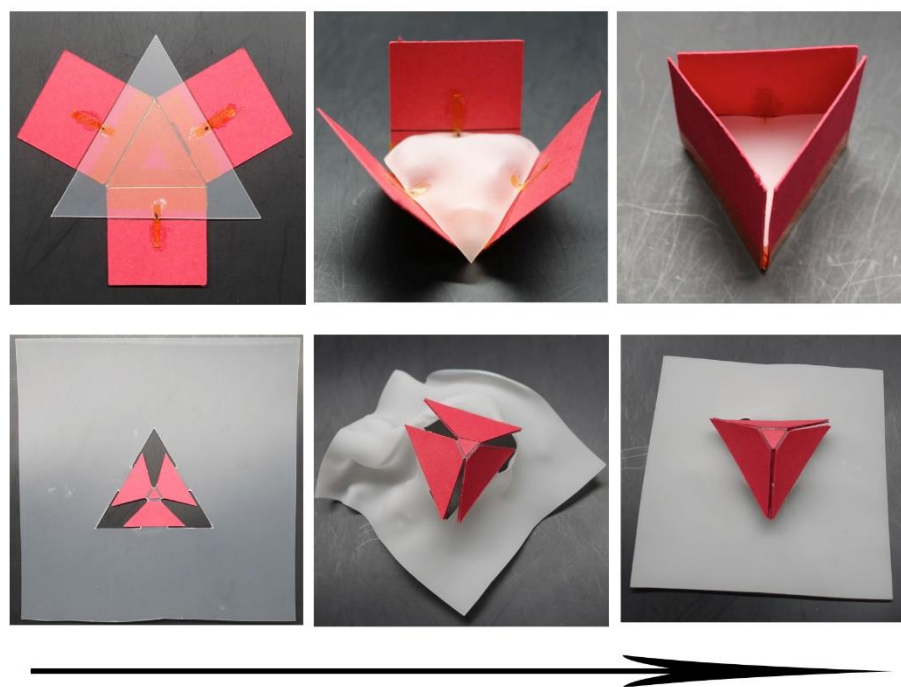


Figure 4.S5 Time evolution of the assembly process.

References:

- [1] S. Felton, M. Tolley, E. Demaine, D. Rus, R. Wood, *Science* 2014, 345, 644.
- [2] E. Hawkes, B. An, N. Benbernou, H. Tanaka, S. Kim, E. Demaine, D. Rus, R. Wood, *Proceedings of the National Academy of Sciences of the United States of America* 2010, 107, 12441.
- [3] T. G. Leong, C. L. Randall, B. R. Benson, N. Bassik, G. M. Stern, D. H. Gracias, *Proceedings of the National Academy of Sciences of the United States of America* 2009, 106, 703.
- [4] Z. Song, T. Ma, R. Tang, Q. Cheng, X. Wang, D. Krishnaraju, R. Panat, C. K. Chan, H. Yu, H. Jiang, *Nat. Commun.* 2014, 5, 3140.
- [5] Q. Cheng, Z. Song, T. Ma, B. B. Smith, R. Tang, H. Yu, H. Jiang, C. K. Chan, *Nano letters* 2013, 13, 4969.
- [6] R. Fernandes, D. H. Gracias, *Adv. Drug Deliv. Rev.* 2012, 64, 1579.
- [7] J. Guan, H. He, L. J. Lee, D. J. Hansford, *Small* 2007, 3, 412.
- [8] E. T. Filipov, T. Tachi, G. H. Paulino, *Proc. Natl. Acad. Sci. U. S. A.* 2015, 112, 12321.
- [9] J. L. Silverberg, A. A. Evans, L. McLeod, R. C. Hayward, T. Hull, C. D. Santangelo, I. Cohen, *science* 2014, 345, 647.
- [10] M. Schenk, S. D. Guest, *Proc. Natl. Acad. Sci. U. S. A.* 2013, 110, 3276.
- [11] J. A. Rogers, Y. Huang, O. G. Schmidt, D. H. Gracias, *Mrs Bulletin* 2016, 41, 123.
- [12] X. Guo, H. Li, B. Y. Ahn, E. B. Duoss, K. J. Hsia, J. A. Lewis, R. G. Nuzzo, *Proceedings of the National Academy of Sciences of the United States of America* 2009, 106, 20149.
- [13] E. A. Peraza-Hernandez, D. J. Hartl, R. J. Malak Jr, D. C. Lagoudas, *Smart Materials and Structures* 2014, 23, 094001.
- [14] A. Rafsanjani, K. Bertoldi, *Physical Review Letters* 2017, 118, 084301.
- [15] D. M. Sussman, Y. Cho, T. Castle, X. Gong, E. Jung, S. Yang, R. D. Kamien, *Proc. Natl. Acad. Sci. U. S. A.* 2015, 112, 7449.
- [16] T. Castle, Y. Cho, X. Gong, E. Jung, D. M. Sussman, S. Yang, R. D. Kamien, *Physical review letters* 2014, 113, 245502.

- [17] K. Saito, S. Pellegrino, T. Nojima, *J Mech Design* 2014, 136, 051011.
- [18] Y. Tang, G. Lin, S. Yang, Y. K. Yi, R. D. Kamien, J. Yin, *Advanced Materials* 2017, 29.
- [19] S. Tibbits, *Architectural Design* 2012, 82, 68.
- [20] Y. Liu, J. Genzer, M. D. Dickey, *Progress in Polymer Science* 2016, 52, 79.
- [21] M. T. Tolley, S. M. Felton, S. Miyashita, D. Aukes, D. Rus, R. J. Wood, *Smart Materials and Structures* 2014, 23, 094006.
- [22] S. M. Felton, M. T. Tolley, B. Shin, C. D. Onal, E. D. Demaine, D. Rus, R. J. Wood, *Soft Matter* 2013, 9, 7688.
- [23] N. Bassik, G. M. Stern, D. H. Gracias, *Applied physics letters* 2009, 95, 091901.
- [24] J. Cui, S. Yao, Q. Huang, J. G. Adams, Y. Zhu, *Soft Matter* 2017, 13, 3863.
- [25] J. H. Na, A. A. Evans, J. Bae, M. C. Chiappelli, C. D. Santangelo, R. J. Lang, T. C. Hull, R. C. Hayward, *Advanced Materials* 2015, 27, 79.
- [26] J. Ryu, M. D'Amato, X. Cui, K. N. Long, H. Jerry Qi, M. L. Dunn, *Applied Physics Letters* 2012, 100, 161908.
- [27] Y. Liu, B. Shaw, M. D. Dickey, J. Genzer, *Science Advances* 2017, 3, e1602417.
- [28] Y. Liu, J. K. Boyles, J. Genzer, M. D. Dickey, *Soft Matter* 2012, 8, 1764.
- [29] Q. Zhang, J. Wommer, C. O'Rourke, J. Teitelman, Y. Tang, J. Robison, G. Lin, J. Yin, *Ext Mech Lett* 2017, 11, 111.
- [30] Y. Liu, R. Mailen, Y. Zhu, M. D. Dickey, J. Genzer, *Physical Review E* 2014, 89, 042601.
- [31] Z. Yan, F. Zhang, J. Wang, F. Liu, X. Guo, K. Nan, Q. Lin, M. Gao, D. Xiao, Y. Shi, Y. Qiu, H. Luan, J. Kim, Y. Wang, H. Luo, M. Han, Y. Huang, Y. Zhang, J. A. Rogers, *Advanced Functional Materials* 2016, 26, 2629.
- [32] Z. Yan, F. Zhang, F. Liu, M. Han, D. Ou, Y. Liu, Q. Lin, X. Guo, H. Fu, Z. Xie, M. Gao, Y. Huang, J. Kim, Y. Qiu, K. Nan, J. Kim, P. Gutruf, H. Luo, A. Zhao, K.-C. Hwang, Y. Huang, Y. Zhang, J. A. Rogers, *Sci. Adv.* 2016, 2, e1601014.
- [33] S. Xu, Z. Yan, K.-I. Jang, W. Huang, H. Fu, J. Kim, Z. Wei, M. Flavin, J. McCracken, R. Wang, A. Badea, Y. Liu, D. Xiao, G. Zhou, J. Lee, H. U. Chung, H. Cheng, W. Ren, A.

Banks, X. Li, U. Paik, R. G. Nuzzo, Y. Huang, Y. Zhang, J. A. Rogers, *Science* 2015, 347, 154.

[34] Y. Zhang, Z. Yan, K. Nan, D. Xiao, Y. Liu, H. Luan, H. Fu, X. Wang, Q. Yang, J. Wang, W. Ren, H. Si, F. Liu, L. Yang, H. Li, J. Wang, X. Guo, H. Luo, L. Wang, Y. Huang, J. Rogers, *Proc. Natl. Acad. Sci. U. S. A.* 2015, 112, 11757.

[35] K. Miura, The Institute of Space and Astronautical Science report 1985, 618, 1.

[36] F. Haas, R. J. Wootton, *Proc R Soc Lond B Biol Sci* 1996, 263, 1651.

[37] L. J. Gibson, M. F. Ashby, *Cellular solids: structure and properties*, Cambridge university press, 1999.

[38] D. Wang, *Int J Impact Eng* 2009, 36, 110.

[39] K. Nan, H. Luan, Z. Yan, X. Ning, Y. Wang, A. Wang, J. Wang, M. Han, M. Chang, K. Li, Y. Zhang, W. Huang, Y. Xue, Y. Huang, Y. Zhang, J. A. Rogers, *Advanced Functional Materials* 2017, 27

CHAPTER 5 Folding 2D sheets by changing their Gaussian curvature

5.1 Introduction

Shape morphing of thin sheet structure is involved in many areas. Striking examples can be found in nature, including the deployment of leaves,^[1] blooming of flowers,^[2] opening of seed pods^[3] and closure of flytrap leaves.^[4] These phenomena have fascinated scientists and engineers for a long time.^[5] Several mechanical and geometric models have been proposed to explain the phenomena.^[1-4] Artificial structures that mimic natural morphing process have been developed, which can find applications in many fields, including reconfigurable devices,^[6, 7] deployable structures,^[8] soft robotics,^[9, 10] smart textiles^[11, 12] and containers for drug delivery.^[13]

A bilayer sheet can be shaped via out-of-plane bending, which is caused by varying strain across the thickness. The strain variation can be induced by mismatch in thermal expansion^[14] or swelling.^[15] Depending on the strain states of two layers, the bilayer sheet can be bent into different shapes (e.g. cylindrical, spherical, saddle).^[16] On the other hand, a single layer sheet can be shaped by changing its Gaussian curvature, which can be achieved by non-uniform in-plane strain.^[17, 18] A flat sheet (zero Gaussian curvature) can be shaped into spherical (positive Gaussian curvature) or saddle (negative Gaussian curvature) surface. The in-plane strain can be induced by swelling/deswelling in a hydrogel sheet, which can be tuned by modulating the concentration,^[18] crosslinking density^[9, 19] or temperature.^[20] Non-uniform strain can also be induced by non-uniform heating in a heat shrinkable polymer sheet.^[21]

The abovementioned shape morphing process typically occurs in soft materials and gives rise to smoothly curved structures. On the other hand, kirigami and origami, ancient art of paper cutting and folding, provide strategy for shape transformation in relatively rigid systems. Two dimensional (2D) sheets can be transformed into three dimensional (3D) structures by folding along specific crease lines.^[22, 23] The results are piecewise planar structures. The folded structures can be applied in different engineering fields, such as robotics,^[23] foldcore sandwich panel^[24] and metamaterials.^[22] Folding can be accomplished in various ways.^[25-28] The strategies can be divided into two categories: folding actuated by responsive hinges^[23, 25, 27] and folding induced by compressive buckling.^[7, 28] The Gaussian curvature change associated with the folding is seldom studied.^[29]

In this work, Gaussian curvature change, which is induced by non-uniform in-plane strain, is used to fold origami structures. The origami structure, in its flat unfold state, is embedded in a flat heat shrinkable polymer sheet (which shrinks equi-biaxially and uniformly upon heating). The shrinkage becomes non-uniform due to the constraining effect of the origami structure. This changes the Gaussian curvature of the composite sheet and causes shape transformation. The shape transformation is guided by the origami mechanism, as the degrees of freedom are from the folding of creases. The results are seamless 3D surface structures with embedded folded origami structures.

The paper is presented in the following order. First, an angular shrinkage gadget based on constrained shrinkage is demonstrated. It is then utilized to create angular defect (with positive Gaussian curvature) around a vertex, which is used to fold creases. A single gadget can fold a single crease. Multiple gadgets can fold multiple creases in a parallel manner,

resulting in complex 3D structures. After that, saddle surfaces (with negative Gaussian curvature) are created through constrained shrinkage. It is used to fold origami structures surrounding it. The origami structures are then tessellated into 2D array.

5.2 Materials and Methods

The heat shrinkable polymer sheet is made of pre-strained polystyrene (PS) (Grafix Shrink Film). The rigid bar in **Figure 5.1a** is made of metal wire. The origami structure is fabricated by gluing paperboard panels (cut from Staples file folder) on selective areas of PS sheet. The paperboard panels are glued on both sides of PS sheet using superglue (Loctite Liquid Professional Super Glue 20-Gram Bottle). A space is left between adjacent panels to make the crease. The PS sheet shrinks equi-biaxially upon heating (150 °C), while the paperboard panel does not deform.

5.3 Results and Discussions

Without constraint, the PS sheet shrinks equi-biaxially upon heating. The shrinkage is uniform across the entire sheet. The sheet undergoes a similarity transformation, i.e. the size is reduced while the shape is preserved. The sheet remains flat (zero Gaussian curvature) after shrinking. Constraint can distort the shrinkage. **Figure 5.1a** shows the case when two radii of a PS sector were constrained by rigid bars. The rigid bars constrained the two radii from shrinking and bending. However, the driving force to shrink the area of PS sheet still existed. Here, the only degree of freedom was the rotation of rigid bars about the center. Thus, two rigid bars rotated toward each other to reduce the bounding area. The angle of the sector shrank upon heating, resulting in an angular shrinkage gadget.

Sectors of different angles were studied. Images before and after shrinking are shown in **Figure 5.1a**. The shrunk angle as a function of initial angle is plotted in **Figure 5.1b**. Experimental data are fitted with a line through origin. The results show that the angle shrinks to about $1/3$ of its initial value. Note that without constraint, the in-plane distance in PS sheet shrinks to $1/2$ of its initial value, regardless of the direction. The different shrinkage ratios between distance and angle might be due to the non-uniform constraint. The flat PS sheet was shaped into a saddle surface, which is a minimal surface and commonly observed in systems trying to minimize the surface area.^[17]

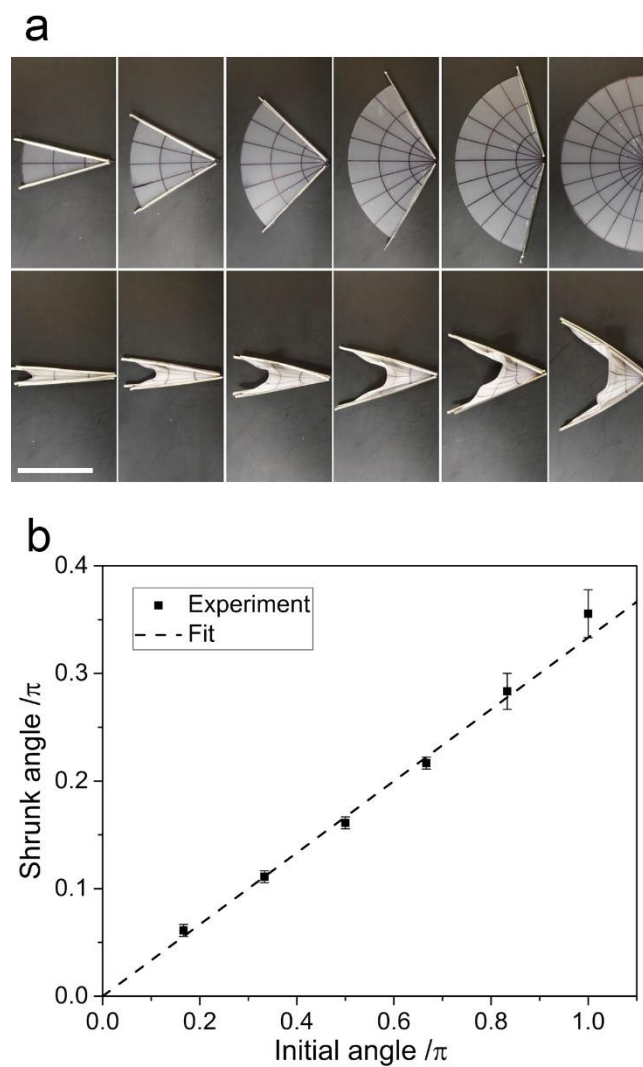


Figure 5.1 Angular shrinkage gadget. (a) Images showing the angular shrinkage. Top: before heating; bottom: after heating. Scale bar: 30 mm. (b) Plot of the shrunk angle as a function of the initial angle. Both experimental results (square dot) and linear fitting line ($y = x/3$) are shown.

Next, this angular shrinkage gadget was utilized to change the Gaussian curvature of a flat sheet. Note that on a flat surface, which has zero Gaussian curvature everywhere, the angle around a point is 2π . If a sector is cut out a circular disk and exposing edges are glued together, a cone can be obtained, which has an angular defect and a positive Gaussian curvature on the vertex. Here, the angular defect is generated by shrinking a sector instead of cutting out a sector. The result is also an angular defect and a cone. In a typical cone, the lateral surface is uniformly curved since the stiffness is uniform. In this work, the curving deformation is localized at the creases due to their lower stiffness.

Figure 5.2 shows the folding of a single crease induced by an angular defect. **Figure 5.2a** shows the schematic of folding. The initial state is a flat composite sheet, composed of three sectors: two paperboard sectors (in red) and one PS sector (in blue). Two paperboard sectors are hinged with a soft crease that is free to rotate. The Gaussian curvature is zero for this flat sheet. In the flat state, the structure can be fully characterized by two independent parameters: angle β of one paperboard sector and angle α of the PS sector. Angle of the other paperboard sector can be calculated by subtract α and β from 2π , since the total angle around a vertex on a flat surface is 2π . Upon heating, the PS sector shrinks in angle, generating an angular defect. A cone is formed, which is accompanied by the folding of the paperboard sectors along the crease. There exists a relationship between the angular defect and the folding angle, which is defined as the dihedral angle (θ) between two paperboard sectors. To shrink the PS sector angle to $\alpha/3$ (corresponding to an angular defect of $2\alpha/3$), the paperboard sectors need to fold to a certain dihedral angle (θ). This can be solved via

spherical trigonometry, as shown in **Figure 5.2a**. The structure is drawn in a sphere of unit radius. The sector angle is equal to the arc length of big circle on the surface of the sphere, while the dihedral angle is equal to the angle formed by arcs on the surface of the sphere. The dihedral angle (θ), sector angles ($\alpha/3, \alpha + \beta - \pi, \pi - \beta$) are related by spherical law of cosines

$$\cos(\alpha/3) = \cos(\alpha + \beta - \pi) \cos(\pi - \beta) + \sin(\alpha + \beta - \pi) \sin(\pi - \beta) \cos(\theta) \quad (5.1)$$

The dihedral angle (θ), after the PS sector angle (α) shrank to ($\alpha/3$), can be obtained by solving this equation. **Figure 5.2b** shows the contour plot of θ as a function of α and β . Note that only certain combinations of (α, β) can lead to folding. For example, when $\alpha + \beta = \pi$, folding/rotation of the crease does not change the PS sector angle. The PS sector angle is constrained by the origami structure. No angular defect is generated and no folding occurs.

From the contour plot, maximum dihedral angle ($\theta = \pi/3$) can be obtained at $\alpha = \pi, \beta = \pi/2$. Dihedral angle decreases rapidly with decreasing β at $\alpha = \pi$. The accessible dihedral angle can be fully captured by changing β on $(0, \pi/2)$, while keeping $\alpha = \pi$. θ as a function of β at $\alpha = \pi$ is plotted in **Figure 5.2d**. Images of experimental results are shown in **Figure 5.2c**. On one end of the crease, a PS sector of angle $\alpha = \pi$ was bounded by two paperboard panels. On the other end, the edges of paperboard panels were perpendicular to the crease. Thus the angle between two edges was equal to the dihedral angle (θ). Minimum

dihedral angle ($\theta = 0$) is obtained at $\beta = \pi/4$, and maximum angle ($\theta = \pi/3$) is obtained at $\beta = \pi/2$.

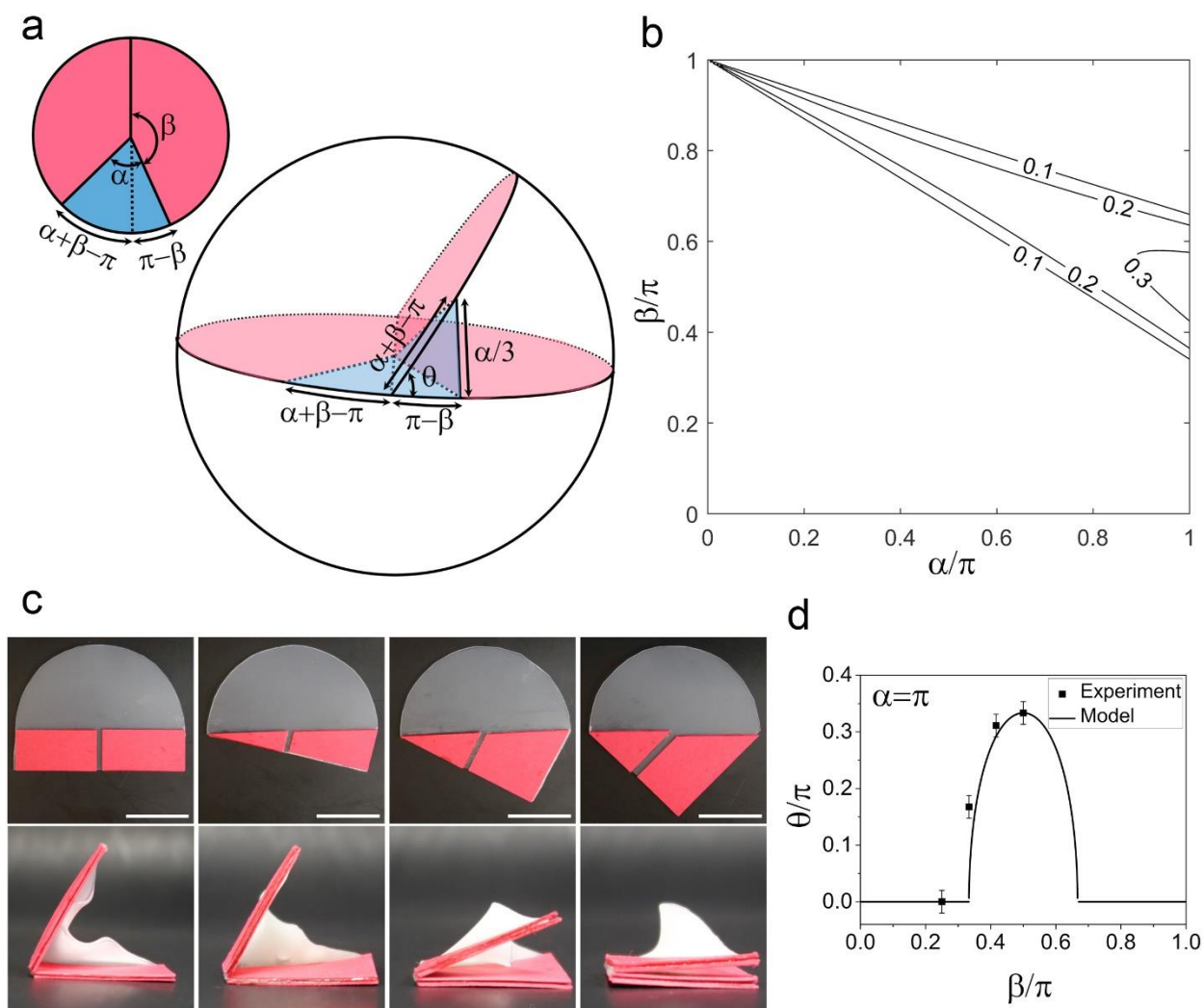


Figure 5.2 Folding of a single crease using angular shrinkage gadget. (a) Schematic of the folding and related parameters. Red: paperboard sector; blue: PS sector. (b) Contour plot of the dihedral angle (θ) as a function of the sector angles (α, β). (c) Images showing folding results with fixed sector angle ($\alpha = \pi$) and varying β , Top: before heating; bottom: after heating (side view). Scale bars: 30 mm. (d) Plot of θ as a function of β (with $\alpha = \pi$).

One crease corresponds to one degree of freedom. Each gadget can be regarded as a constraint. Thus, one crease can be deterministically folded by one gadget. Multiple creases can be deterministically folded when equal number of gadgets are used. Here truncated pyramids were folded in this manner. **Figure 5.3a** shows schematic of the folding. Truncated triangular pyramid is used as an example. Around each vertex there are three rigid paperboard sectors (in red) and one PS sector (in blue). The shrinkage of PS sector creates an angular defect $(2\alpha/3)$ at each vertex. A cone is formed, which is accompanied by the folding of paperboard sectors along the creases. Even though there are two creases and only one gadget around each vertex, the total number of gadgets is equal to that of creases, since some creases are shared by two vertices. The whole structure can be folded in a deterministic manner. Also, due to symmetricity of the structure, all creases are folded to the same angle.

The paperboard sector angle β_1 is equal to the interior angle of the base, which can only take discrete values

$$\beta_1 = \pi - 2\pi/n \quad (5.2)$$

Where n is the number of sides of the base ($n = 3,4,5,6$). The other two paperboard sectors are identical, whose angle can be calculated by subtracting β_1 and α from 2π , i.e.

$$\beta_2 = (2\pi - \alpha - \beta_1)/2 \quad (5.3)$$

Folding angle is defined as the dihedral angle (θ) between lateral surface and base of the pyramid. Again, around each vertex, the angular defect $(2\alpha/3)$ is related to the dihedral angles (θ). The calculation can be found in supporting information. θ as a function of α is plotted

in **Figure 5.3b**. The dihedral angle θ decreases with increasing α , indicating that bigger angular defect leads to higher degree of folding. With the same angular defect, dihedral angles are different for different pyramids. The dihedral angle increases in the order of hexagon, pentagon, square, and triangle. In other words, for the same angular defect, larger sector angle β_1 leads to smaller dihedral angle between. **Figure 5.3c** shows the optical images of truncated pyramids with different bases and different angular defects.

Another way to fold origami structures with angular shrinkage gadget is shown in **Figure 5.4**. Around the central vertex there were alternated PS sectors and paperboard sectors. Again, shrinkage of the PS sectors generated an angular defect around the vertex, transforming the flat disk into a cone. The paperboard sectors remained flat while the PS sectors were curved. The angular defect was determined by total angle of PS sectors. Larger angular defect made a sharper cone.

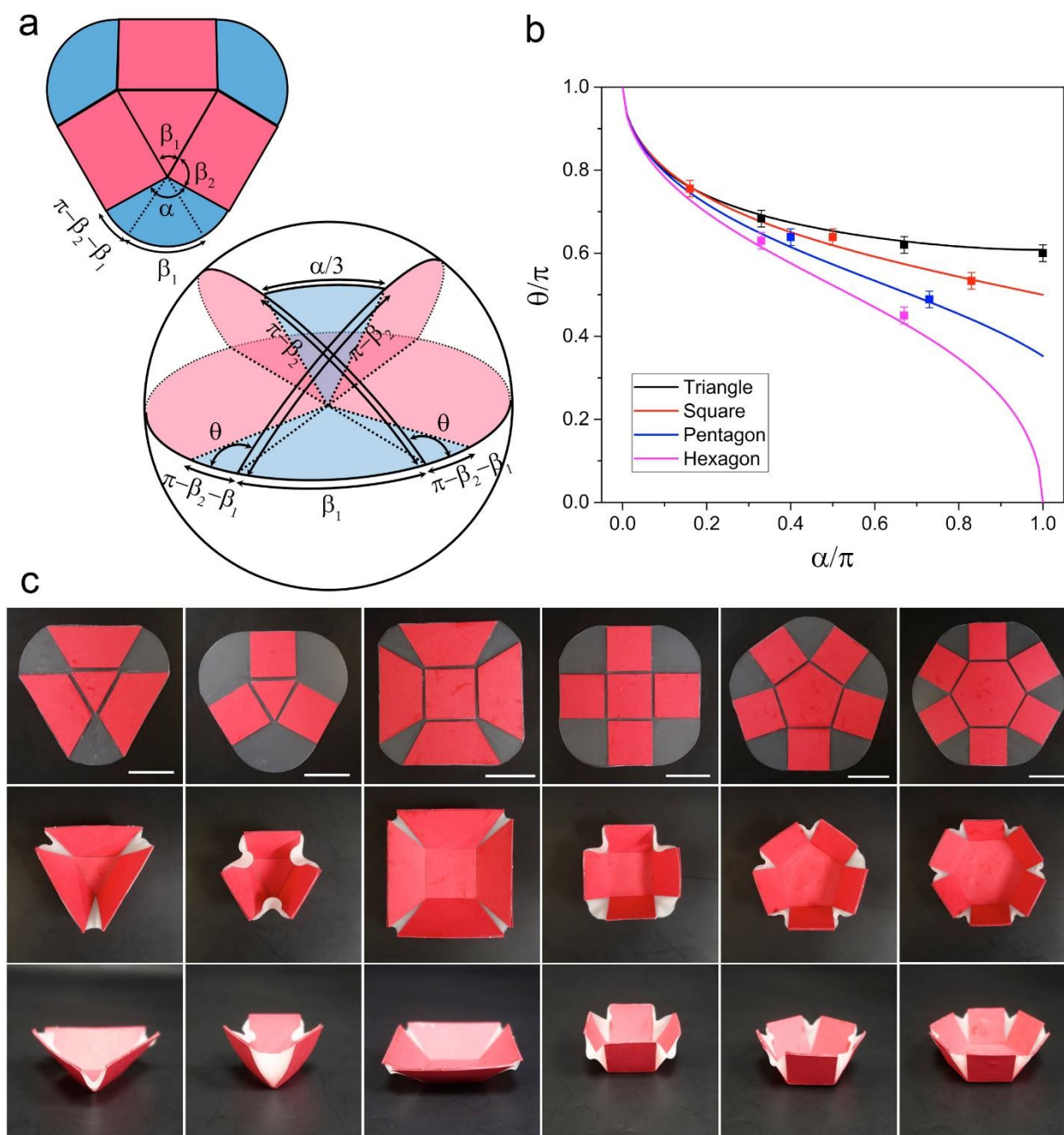


Figure 5.3 Folding truncated pyramids using multiple angular shrinkage gadgets. (a) Schematic of the folding and related parameters. (b) Plot of the dihedral angle (θ) as a function of the sector angle (α). Four cases (triangle, square, pentagon, hexagon) are shown. (c) Images showing folding results. Top: before heating; middle: after heating (top view); bottom: after heating (perspective view). Scale bars: 30 mm.

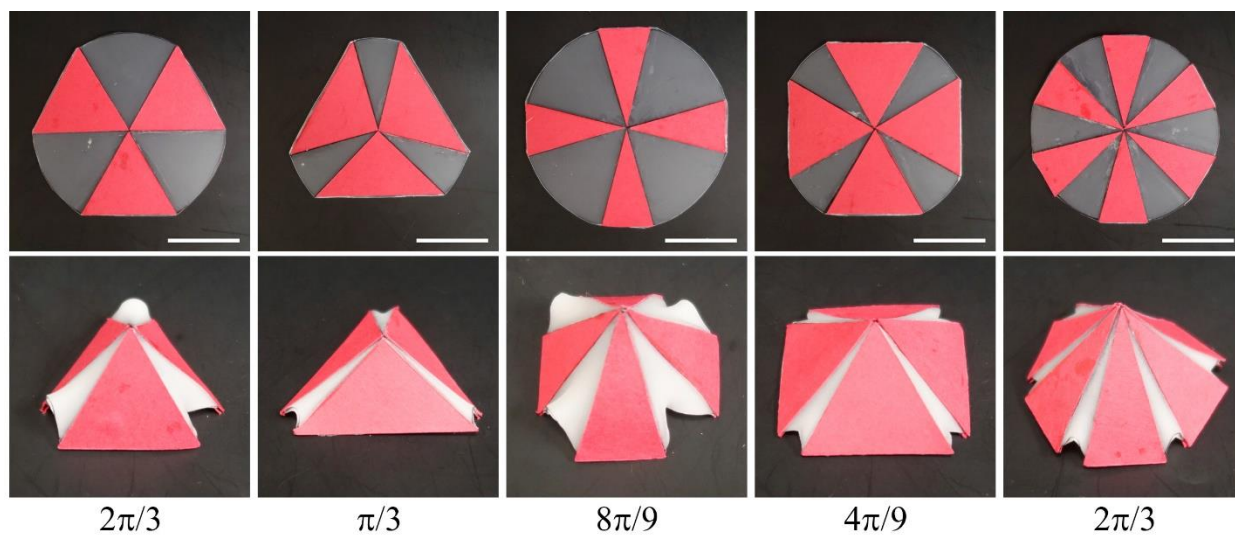


Figure 5.4 Folding of cones with different angular defect. Top: before heating; middle: after heating; bottom: angular defect value of the folded structures. Scale bars: 30 mm.

We have shown that a flat composite sheet can be shaped into a surface with positive Gaussian curvature by creating angular defect. One commonality shared by the abovementioned structures is that shrinkage occurs in the peripheral areas, while the central area is constrained. One question would be how the shape changes under the opposite condition, i.e. central area shrinks while periphery is constrained. A closely related situation is a constrained center with an expanding periphery. In that case, the periphery is wrinkled, generating a saddle surface (negative Gaussian curvature).^[18, 30] Here a shrinking center with constrained periphery is similar to a constrained center with expanding periphery. Thus, we expect the sheet to be shaped into a saddle surface.

Figure 5.5 shows the shape transformation when the periphery of PS sheet was constrained by origami structure. **Figure 5.5a** shows three motifs (square, rhombic and square twist). The structures were inspired by the kirigami pattern developed by Sussman et al.^[31] In the central area, there was a PS panel. In the peripheral area, there were eight paperboard panels, which were arranged into a ring and hinged with eight creases. The PS panel was a square or a rhombic, with its four sides constrained by rigid paperboard panels. Upon heating, the central PS panel tended to shrink its area. However, the sides cannot shrink or bend. The only way to reduce the area of PS panel was to bring opposite vertices toward each other by rotating the sides about the vertices, as the sides are free to rotate. Since the shrinkage in PS was isotropic, both pairs of opposite vertices were brought together. **Figure 5.5b** shows perspective view of the structure after transformation. The structure was flipped over and rotated 90 degrees from top panel to bottom panel. From the two images, the PS sheet curved upward in the horizontal direction. This meant that the PS sheet curved in opposite directions

along perpendicular directions. In other words, the PS sheet was shaped into a saddle surface with negative Gaussian curvature.

As the central area was shaped into a saddle surface, the origami structure in the peripheral area was wrinkled/buckled. **Figure 5.5c** shows top view of the folded structures, illustrating degeneracy in the folding modes. As can be seen from **Figure 5.5b** and **5.5c**, after folding, paperboard panels located at one pair of opposite vertices popped up, while those at the other pair popped down. For an individual motif, there are two degenerate folding states, as each pair of vertices can pop up or pop down. The two configurations are symmetrically equivalent to each other, i.e. one configuration can be converted to the other via symmetric operation. For square and square twist motifs, one configuration can be converted to the other by 90 degrees rotation. Two successive rotations bring it coincident with the initial state. For the rhombic motif, a reflection through the flat surface (mirror plane) can convert one state to the other. Again, two successive reflections bring it coincident with the initial state.

Next, the motifs were tessellated into a square or tilted square array, as shown in **Figure 5.5d**. Every motif had four neighbors surrounding it, each of which shared a side (three paperboard panels) with it. Upon heating, the motifs were folded in a parallel manner. The shared side required two adjacent motifs to fold in different modes. Thus, after the folding mode of one motif was determined, that of its four neighbors can be determined. This can propagate to the whole array. Since there were two degenerate folding modes for the initial motif, the whole array also had two degenerate configurations, which are symmetrically equivalent to each other. **Figure 5.5e** and **5.5f** shows the folded structure. A 2D pattern was transformed into 3D checkboard pattern upon heating. This is very similar to the checkboard

wrinkle pattern. We believe that similar structure can be used to guide the wrinkling process of a thin film.

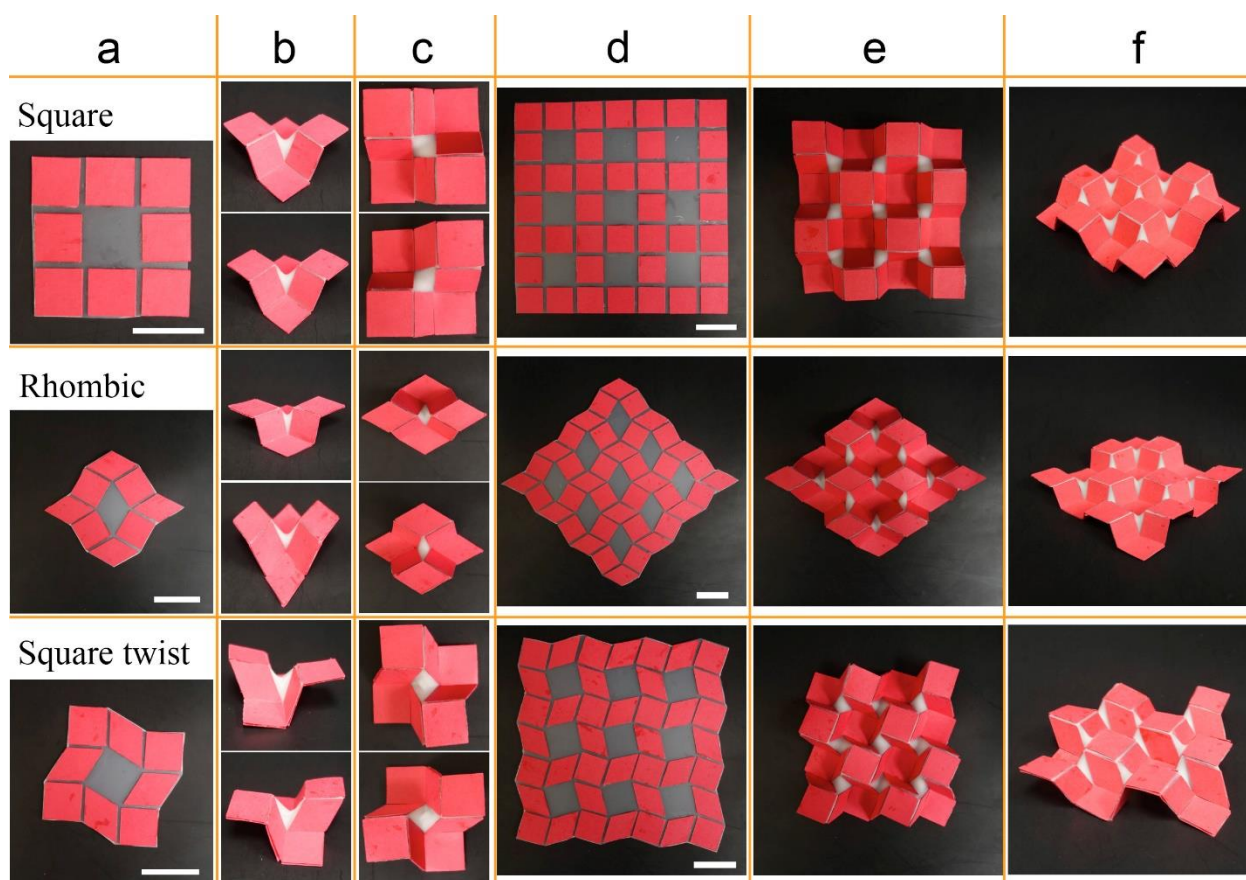


Figure 5.5 Folding results with central PS sheet surrounded by a ring of unfold flat origami structure. (a) Flat motif. (b) Perspective view of the folded structure (after taken the top image, sample was flipped over and rotated 90 degrees). (c) Top view illustrating two degenerate folding modes (images were taken from the same sample but different orientation as indicated in the main text). (d) Square lattice of the motif. (e) Top view of the folded 3D checkboard pattern. (f) Perspective view of the folded 3D checkboard pattern.

5.4 Conclusion

We have demonstrated a new approach to fold origami structures, which is based on changing Gaussian curvature. Flat unfold origami structures are embedded into a heat shrinkable polymer sheet, making a composite sheet. The composite sheet experiences non-uniform in-plane shrinkage upon heating, since polymer shrinks and the origami structure does not. This non-uniform shrinkage can change the Gaussian curvature of the sheet and convert a flat surface (zero Gaussian curvature) into a spherical (positive Gaussian curvature) or a saddle surface (negative Gaussian curvature). The shape changing is guided by the embedded origami mechanism. When origami structure is located at the center and surrounded by PS sheet, the result is surface with positive Gaussian curvature. The folded origami structures include truncated pyramids and cones. When PS is located at the center and surrounded by a ring of origami structure, surfaces with negative Gaussian curvature can be obtained. The flat origami is folded into a stepped structure. When the rings are tessellated into array (with overlapped sides), 3D checkboard pattern can be obtained. The method reported in this work is a combination of shape morphing in soft materials and origami folding in rigid structures. It can be potentially used to design shape reconfigurable structures with programmable stiffness.

Supplementary Information (SI)

5.S1 Calculate the dihedral angle from the sector angles

As shown in **Figure 5.S1**, the dihedral angle (θ) can be calculated from the sector angles using spherical trigonometry. Considering two spherical triangles in green, two equations can be obtained from the spherical law of cosines:

$$\cos(\beta_1) = \cos^2(\lambda) + \sin^2(\lambda)\cos(\phi) \quad (5.S1)$$

$$\cos(\alpha/3) = \cos^2(\pi - \beta_2 - \lambda) + \sin^2(\pi - \beta_2 - \lambda)\cos(\phi) \quad (5.S2)$$

λ and ϕ can be obtained by solving **Equations 5.S1** and **5.S2** simultaneously. Then θ can be solved using spherical law of sines:

$$\frac{\sin(\beta_1)}{\sin(\phi)} = \frac{\sin(\lambda)}{\sin(\pi - \theta)} \quad (5.S3)$$

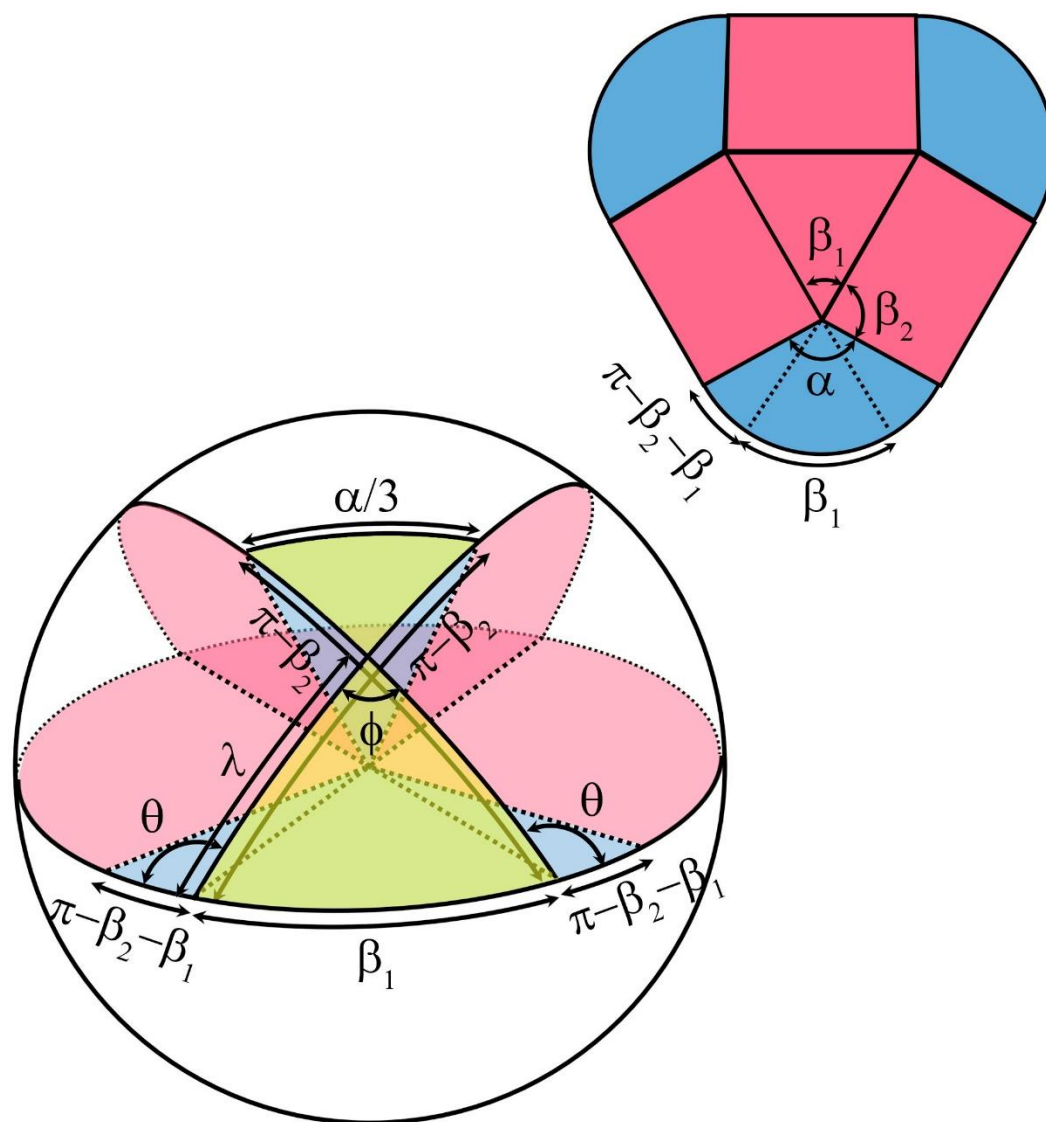


Figure 5.S1 Schematic of the folding of a truncated triangular pyramids

References

- [1] H. Kobayashi, B. Kresling, J. F. Vincent, Proceedings of the Royal Society of London B: Biological Sciences 1998, 265, 147.
- [2] H. Liang, L. Mahadevan, Proceedings of the National Academy of Sciences 2011, 108, 5516.
- [3] S. Armon, E. Efrati, R. Kupferman, E. Sharon, Science 2011, 333, 1726.
- [4] Y. Forterre, J. M. Skotheim, J. Dumais, L. Mahadevan, Nature 2005, 433, 421.
- [5] D. W. Thompson, On growth and form. 1942.
- [6] M. Zarek, M. Layani, I. Cooperstein, E. Sachyani, D. Cohn, S. Magdassi, Advanced Materials 2016, 28, 4449.
- [7] S. Xu, Z. Yan, K.-I. Jang, W. Huang, H. Fu, J. Kim, Z. Wei, M. Flavin, J. McCracken, R. Wang, Science 2015, 347, 154.
- [8] J. F. Vincent, in *Deployable structures*, Springer, 2001, 37.
- [9] R. F. Shepherd, F. Ilievski, W. Choi, S. A. Morin, A. A. Stokes, A. D. Mazzeo, X. Chen, M. Wang, G. M. Whitesides, Proceedings of the National Academy of Sciences 2011, 108, 20400.
- [10] F. Ilievski, A. D. Mazzeo, R. F. Shepherd, X. Chen, G. M. Whitesides, Angewandte Chemie 2011, 123, 1930.
- [11] M. W. Han, S. H. Ahn, Advanced Materials 2017, 29.
- [12] J. Hu, H. Meng, G. Li, S. I. Ibekwe, Smart Materials and Structures 2012, 21, 053001.
- [13] R. Fernandes, D. H. Gracias, Advanced drug delivery reviews 2012, 64, 1579.
- [14] S. Timoshenko, JOSA 1925, 11, 233.
- [15] A. S. Gladman, E. A. Matsumoto, R. G. Nuzzo, L. Mahadevan, J. A. Lewis, Nature materials 2016, 15, 413.
- [16] M. Finot, S. Suresh, Journal of the Mechanics and Physics of Solids 1996, 44, 683.
- [17] J. Kim, J. A. Hanna, M. Byun, C. D. Santangelo, R. C. Hayward, Science 2012, 335, 1201.
- [18] Y. Klein, E. Efrati, E. Sharon, Science 2007, 315, 1116.

- [19] Z. L. Wu, M. Moshe, J. Greener, H. Therien-Aubin, Z. Nie, E. Sharon, E. Kumacheva, *Nature communications* 2013, 4, 1586.
- [20] P. Froeter, X. Yu, W. Huang, F. Du, M. Li, I. Chun, S. H. Kim, K. J. Hsia, J. A. Rogers, X. Li, *Nanotechnology* 2013, 24, 475301.
- [21] A. M. Hubbard, R. W. Mailen, M. A. Zikry, M. D. Dickey, J. Genzer, *Soft Matter* 2017, 13, 2299.
- [22] J. L. Silverberg, A. A. Evans, L. McLeod, R. C. Hayward, T. Hull, C. D. Santangelo, I. Cohen, *science* 2014, 345, 647.
- [23] S. Felton, M. Tolley, E. Demaine, D. Rus, R. Wood, *Science* 2014, 345, 644.
- [24] S. Heimbs, in *Dynamic failure of composite and sandwich structures*, Springer, 2013, 491.
- [25] Y. Liu, B. Shaw, M. D. Dickey, J. Genzer, *Science Advances* 2017, 3, e1602417.
- [26] E. A. Peraza-Hernandez, D. J. Hartl, R. J. Malak Jr, D. C. Lagoudas, *Smart Materials and Structures* 2014, 23, 094001.
- [27] J. Cui, S. Yao, Q. Huang, J. G. Adams, Y. Zhu, *Soft Matter* 2017, 13, 3863.
- [28] Y. Zhang, Z. Yan, K. Nan, D. Xiao, Y. Liu, H. Luan, H. Fu, X. Wang, Q. Yang, J. Wang, *Proceedings of the National Academy of Sciences* 2015, 112, 11757.
- [29] D. A. Huffman, *IEEE Transactions on computers* 1976, 1010.
- [30] T. Mora, A. Boudaoud, *The European Physical Journal E: Soft Matter and Biological Physics* 2006, 20, 119.
- [31] D. M. Sussman, Y. Cho, T. Castle, X. Gong, E. Jung, S. Yang, R. D. Kamien, *Proceedings of the National Academy of Sciences* 2015, 112, 7449.